GEOLOGICAL SURVEY OF CANADA
CURRENT RESEARCH 1995-F

RADIOGENIC AGE AND ISOTOPIC STUDIES: REPORT 9

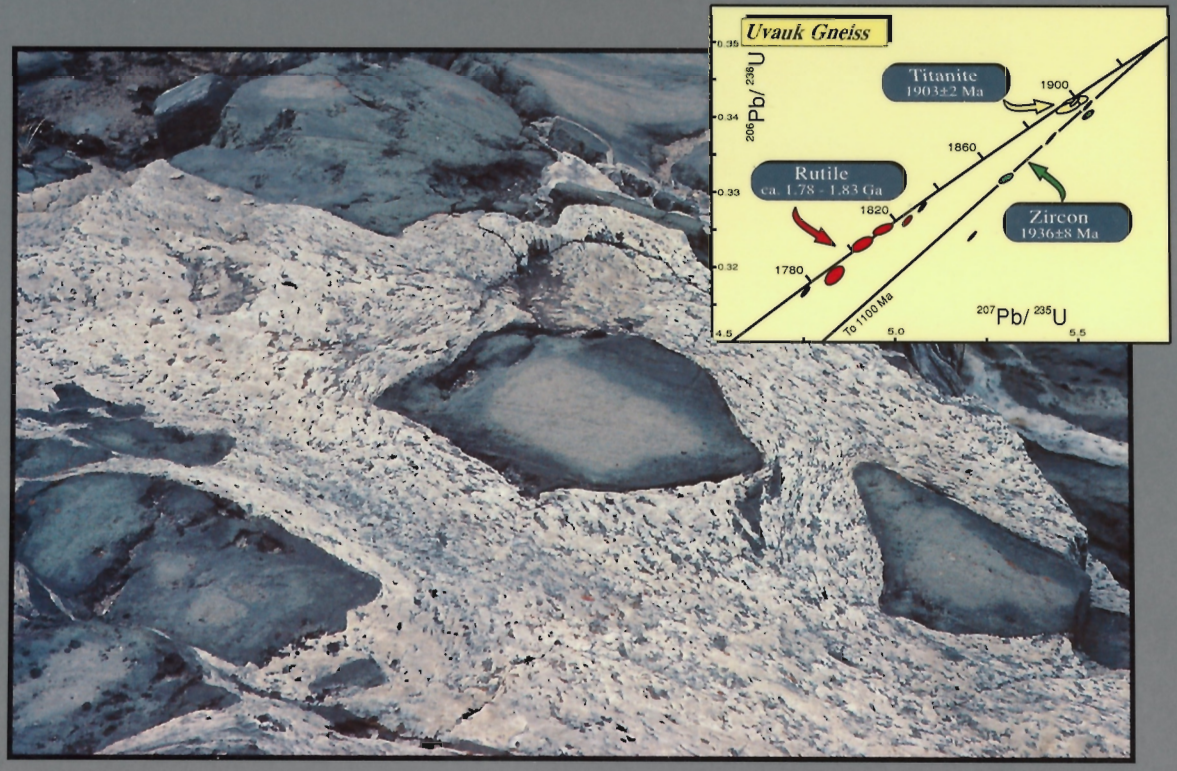

1996

Natural Resources Canada Ressources naturelles Canada

Canada

STAFF, GEOCHRONOLOGY SECTION
GEOLOGICAL SURVEY OF CANADA

Research Scientists:	Otto van Breemen Randal R. Parrish Richard Stern
Visiting Scientists:	Bill Davis
Professional Scientists:	Patricia A. Hunt Vicki J. McNicoll Réginald J. Thériault Mike Villeneuve Natasha Wodicka Mike Gerasimoff
Technical Staff:	Diane Bellerive Jack L. Macrae Fred B. Quigg Klaus Santowski

GEOLOGICAL SURVEY OF CANADA
CURRENT RESEARCH 1995-F

RADIOGENIC AGE AND ISOTOPIC STUDIES: REPORT 9

1996

Catalogue No. M44-1995/6E
ISBN 0-662-16431-0

Available in Canada from
Geological Survey of Canada offices:

601 Booth Street
Ottawa, Ontario K1A 0E8

3303-33rd Street N.W.,
Calgary, Alberta T2L 2A7

100 West Pender Street
Vancouver, B.C. V6B 1R8

or from

Canada Communication Group – Publishing
Ottawa, Ontario K1A 0S9

and through authorized bookstore agents and other bookstores

A deposit copy of this publication is also available for reference
in public libraries across Canada

Price subject to change without notice

Cover description

Photograph of a dismembered mafic dyke in anorthositic gabbro, Uvauk Complex, District of Keewatin, Northwest Territories. The complex, located 100 km northwest of Chesterfield Inlet, is comprised of an Archean layered gabbro-mafic granulite-anorthosite suite which was deformed and metamorphosed at mid-crustal levels during Late Archean and Paleoproterozoic events. It forms a rootless, triangular segment (30 x 20 km) of straight gneisses, the boundaries of which are marked by granulite grade ultramylonites.
Photo by S. Tella, GSC 1992-253 DD

The concordia plot displays the geochronology, carried out by Chris Roddick, on a representative sample from the anorthositic gabbro ultramylonite. The data suggests that the 1936 ± 8 Ma zircon age records a Paleoproterozoic, granulite grade, ductile event that overprinted an Archean (ca. 2.59 Ga), granulite grade mylonitic event. Titanite and rutile ages record post-mylonite, uplift and cooling events. Thermobarometric data suggests that the Paleoproterozoic event occurred at pressures in excess of 10 kbar, (30 km).

CONTENTS

RADIOGENIC AGE AND ISOTOPIC STUDIES: REPORT 9

INTRODUCTION

"Radiogenic Age and Isotopic Studies" is an annual collection of research presentations containing U-Pb, Sm-Nd, Rb-Sr, and ^{40}Ar-^{39}Ar data generated by the Geochronology Laboratory under the auspices of the of the Continental Geoscience Division, Geological Survey of Canada. Report 9 contains 5 papers from regions across Canada (see back cover), followed by a compilation of ^{40}Ar-^{39}Ar and K-Ar ages. Authors herein present data, relate results to field settings, and make brief interpretations. Readers are thus reminded that much of the research encompassed represents "work-in-progress" and that more extensive publications may follow at a later date. Listed at the end of the report are additional publications containing data produced by the CGD lab, mostly in outside journals.

For the Geochronology Laboratory, 1995 was a year of expectations and tragedy. On February 23, 1995, Chris Roddick's accidental death left not only a scientific legacy which has been profound for the Geological Survey of Canada and scientists around the world, but also an expertise that will be deeply missed in the Geochronology Laboratory.

Chris Roddick made a substantial mark on isotope geoscience. He contributed consistently careful and meticulous scientific work to the literature, particularly in the fields of ^{40}Ar-^{39}Ar, Rb-Sr, and U-Pb geochronology, and to the art of isotopic measurement using modern mass spectrometers. Chris conceived the use of the argon correlation diagram, which allows identification of extraneous argon components within step-heated mineral samples, a method of argon data analysis that is a standard procedure today. During the last few years, efforts by Chris and colleagues in the argon laboratory were focused on modernizing first the K-Ar, and later the ^{40}Ar-^{39}Ar methodologies using a low-blank double vacuum furnace and spot fusion analyses with a laser. Chris was also the backbone of computation and data management within the laboratory, designing and writing computer code not only to efficiently collect and store isotopic data in ^{40}Ar-^{39}Ar, U-Pb, Rb-Sr, and Sm-Nd methods, but also to facilitate tabulation and presentation of isotopic analytical data in a system that ranks among the best. He was also the source of definitive advice and information on principles of measurement and interpretation of radiogenic

INTRODUCTION

La publication intitulée *Radiogenic age and isotope studies* est un recueil annuel d'articles scientifiques contenant des résultats de datations U-Pb, Sm-Nd, Rb-Sr et ^{40}Ar-^{39}Ar, effectuées par le personnel du laboratoire de géochronologie, sous les auspices de la Division de la géologie du continent (Commission géologique du Canada, CGC). Le rapport 9 contient cinq articles sur des régions d'un peu partout au Canada (voir la couverture arrière), suivis d'une compilation d'âges déterminés au moyen des méthodes ^{40}Ar-^{39}Ar et K-Ar. Les auteurs présentent des données, établissent des liens entre les résultats et les milieux établis à l'aide des travaux sur le terrain, en plus de donner de courtes interprétations. Les lecteurs doivent cependant garder en mémoire qu'une bonne partie des recherches citées sont «en cours» et que des publications plus détaillées pourraient suivre. À la fin du rapport se trouve une liste de publications, pour la plupart dans des revues scientifiques ne relevant pas de la CGC, dans lesquelles on fait référence à des données produites par le laboratoire de géochronologie.

L'année 1995 en a été une d'attentes et de tragédie pour le laboratoire de géochronologie. Chris Roddick est décédé accidentellement le 23 février 1995. Du point de vue scientifique, il a fourni un apport qui a marqué profondément la Commission géologique du Canada et des collègues de partout dans le monde. Son départ représente une perte de compétences qui sera fortement ressentie au laboratoire de géochronologie.

Chris Roddick a beaucoup apporté à la méthode isotopique. Il a contribué de façon continue aux ouvrages scientifiques par son travail soigné et méticuleux, en particulier dans le domaine de la géochronologie basée sur les méthodes ^{40}Ar-^{39}Ar, Rb-Sr et U-Pb, sans oublier son apport aux techniques de mesure isotopique faisant appel aux spectromètres de masse modernes. Chris a conçu l'utilisation du diagramme de corrélation avec l'argon, qui permet l'identification de composantes étrangères contenant de l'argon à l'intérieur d'échantillons de minéraux chauffés par étapes, une méthode d'analyse des données relatives à cet élément qui est d'usage courant aujourd'hui. Au cours des quelques dernières années, les efforts de Chris et de ses collègues du laboratoire ont visé à moderniser d'abord la méthode K-Ar, puis la méthode ^{40}Ar-^{39}Ar, en utilisant un four à double vide et à faible degré de contamination et en effectuant des analyses par fusion ponctuelle à l'aide du laser. Chris a aussi joué un rôle de pilier dans le domaine des calculs et de la gestion des données au sein du laboratoire, concevant et écrivant des programmes informatiques, non seulement pour recueillir et stocker efficacement des données isotopiques d'analyse par les méthodes ^{40}Ar-^{39}Ar, U-Pb, Rb-Sr et Sm-Nd, mais aussi pour faciliter la mise en tableaux et la présentation de données isotopiques dans un système qui figure parmi les meilleurs. Il était aussi une source d'avis formel et d'informations concernant les principes de mesure et d'interprétation pour ce qui est de la méthode basée

isotope science and its related uncertainties. For these contributions and his generosity and enthusiasm, he will be dearly missed.

Other transitions include the retirements of Robert W. Sullivan and Jean-Claude Bisson after long careers with the Geochronology Laboratory; on behalf of the staff, I want to thank these individuals for their efforts and attention to detail. Their legacy has made our work more fruitful and productive.

Expectations during the 1996 year include the commissioning of both the laser-fusion ^{40}Ar-^{39}Ar laboratory into routine operation, a task which has been accomplished by laboratory staff after Chris Roddick's passing, and the installation and commissioning of the GSC SHRIMP (sensitive high resolution ion microprobe) ion microprobe. Both Chris Roddick and Bob Sullivan, in addition to others in the laboratory, played integral roles in these analytical initiatives, and without their ideas and efforts the bringing of these new methodologies into routine operation at the GSC could not have occurred.

Report 9, though shorter this year, because of the time required to implement the massive changes to the laboratory caused by retirements and Chris Roddick's passing away, nevertheless continues the tradition of an annual publication of recent work of the staff.

sur les isotopes radiogéniques et des incertitudes qui s'y rattachent. Son absence sera profondément ressentie pour toutes ces raisons, mais aussi parce qu'il savait être généraux et transmettre son enthousiasme.

D'autres transitions ont eu lieu, notamment les départs de Robert W. Sullivan et de Jean-Claude Bisson, qui ont pris leur retraite après une longue carrière au laboratoire de géochronologie. Au nom du personnel, je tiens à les remercier pour leurs efforts et leur souci du détail. Grâce à leur contribution, notre travail a été plus fructueux et productif.

Pendant l'année 1996, on prévoit notamment amener le laboratoire d'analyse ^{40}Ar-^{39}Ar par fusion laser à un mode d'utilisation régulière, une tâche qui a été accomplie par le personnel du laboratoire après le décès de Chris Roddick; quant à la microsonde ionique SHRIMP de la CGC, elle a été installée en décembre 1995 et est donc prête pour une utilisation régulière. Le sigle SHRIMP est formé à partir de l'expression anglaise *sensitive high resolution ion microprobe*, c'est-à-dire microsonde ionique sensible à haute résolution. Chris Roddick, Bob Sullivan et d'autres membres du laboratoire ont joué des rôles essentiels dans ces projets et, sans leurs idées et leurs efforts, ces nouvelles méthodes ne seraient pas du quotidien de la CGC.

Le rapport 9 est plus court cette année, principalement en raison du temps qu'il a fallu consacrer à l'instauration de changements massifs au sein du laboratoire à la suite des départs susmentionnés et du décès de Chris Roddick. Il maintient néanmoins la tradition d'une publication annuelle des travaux récents dans ce domaine.

Randall R. Parrish

Efficient mass calibration of magnetic sector mass spectrometers

J.C. Roddick[1]

Roddick, J.C., 1996: Efficient mass calibration of magnetic sector mass spectrometers; in Radiogenic Age and Isotopic Studies: Report 9; Geological Survey of Canada, Current Research 1995-F, p. 1-9.

Abstract: Magnetic sector mass spectrometers used for automatic acquisition of precise isotopic data are usually controlled with Hall probes and software that uses polynomial equations to define and calibrate the mass-field relations required for mass focusing. This procedure requires a number of reference masses and careful tuning to define and maintain an accurate mass calibration. A simplified equation is presented and applied to several different magnetically controlled mass spectrometers. The equation accounts for nonlinearity in typical Hall probe controlled mass-field relations, reduces calibration to a linear fitting procedure, and is sufficiently accurate to permit calibration over a mass range of 2 to 200 amu with only two defining masses. Procedures developed can quickly correct for normal drift in calibrations and compensate for drift during isotopic analysis over a limited mass range such as a single element. The equation is:

$$\text{Field} = A \cdot \text{Mass}^{1/2} + B \cdot (\text{Mass})^{p}$$

where A, B, and p are constants. The power value p has a characteristic value for a Hall probe/controller and is insensitive to changing conditions, thus reducing calibration to a linear regression to determine optimum A and B.

Résumé : Les spectromètres de masse à secteur magnétique fonctionnent habituellement avec des sondes Hall et un logiciel qui se sert d'équations polynomiales pour définir et étalonner les relations masse-champ requises pour la focalisation de masse. Ces appareils sont utilisés pour l'acquisition automatique de données isotopiques précises. Ils nécessitent plusieurs masses de référence et un ajustement précis pour définir et maintenir un étalonnage exact de la masse. Une équation simplifiée est présentée et appliquée à plusieurs spectromètres de masse contrôlés magnétiquement. Cette équation tient compte de la non linéarité des relations typiques entre la masse et le champ qui sont contrôlées par la sonde, réduit l'étalonnage à un ajustement linéaire et est suffisamment exacte pour permettre un étalonnage sur un intervalle de masse de 2 à 200 amu en n'utilisant que deux masses de définition. Les procédés élaborés servent à corriger rapidement l'écart normal observé dans les étalonnages et à compenser l'écart durant l'analyse isotopique sur un intervalle de masse limité comme dans le cas d'un seul élément. L'équation est la suivante :

$$\text{champ} = A \cdot \text{masse}^{1/2} + B \cdot (\text{masse})^{p}$$

où A, B et p sont des constantes. La valeur de la puissance (p) est caractéristique pour une sonde Hall et ne varie pas avec les conditions changeantes, ce qui réduit l'étalonnage à une régression linéaire visant à déterminer les valeurs optimales de A et de B.

[1] Deceased

INTRODUCTION

Mass spectrometer manufacturers now provide sophisticated computer software to control the various functions of, and data collection from, their instruments. To control the magnet for focusing the required masses on ion beam detectors, it is usual for the software to use a third degree or higher polynomial equation to define the mathematical relation between the mass and magnetic field as measured by a Hall probe. Calibration of this polynomial relation requires the determination of the intensity of the magnetic field for at least three masses over the mass range of interest. Because of the nonlinearity of the relation of mass to field intensity, a larger number of calibrating masses over the complete mass range will provide a more precise calibration. This requirement of a number of defining masses over a large mass range results in a calibration needing special samples with the appropriate range of isotopes to encompass the mass range. Defining each isotope for calibration involves varying the magnetic field in the appropriate mass range for an element and then confirming the correct isotope by identifying the relative abundances of the isotopes for that element. With changes in operating parameters or drift in instrument conditions a new calibration must be carried out. Therefore significant amounts of time may be spent in maintaining a precise and accurate calibration of the mass scale of the instrument. Here, an alternative algorithm to the polynomial equation is presented. Using this algorithm, calibration of the magnetic field is significantly simplified and maintenance can be reduced to a re-calibration using a single mass. The procedure appears to have general applicability to magnetic sector instruments controlled with Hall probes and is demonstrated for several different mass spectrometers.

DEVELOPMENT OF A MASS-FIELD ALGORITHM

The development of improved mass calibration of mass spectrometers was first carried out on a Finnigan-MAT 261 thermal ionization instrument at the Geological Survey of Canada. Application of the algorithm to several other MAT 261 machines confirmed the general applicability of calibration to this type of machine. Subsequently the algorithm was used to calibrate a VG 3600 gas mass spectrometer and a NBS Shields design 12", 90 magnetic sector thermal ionization mass spectrometer controlled with Teslameters recently developed by the National Institute of Standards and Technology (NIST). All these instruments use Hall probes to measure and control the magnetic field. Calibration of the VG 3600 is used for development of the algorithm and the applicability to other instruments demonstrates the usefulness of the algorithm in the calibration of different mass spectrometers.

The equation relating mass (m) to magnetic flux density (F) for mass spectrometers which use magnetic field switching of a magnet (radius r) to accelerate particles of charge q through an electric field of V volts is

$$2 \cdot m \cdot V = F^2 \cdot q \cdot r^2 \qquad (1)$$

The high voltage is normally maintained at a constant value and for particles of mass to charge ratio M (=m/q) the basic relation simplifies to

$$F = A \cdot M^{1/2} \qquad (2)$$

where A is a constant. Therefore the field required to focus an isotope on a detector should be a linear function of the square root of mass and determination of the field at a single mass will define the constant A and thus the field values at all other masses. If the observed relation of mass to field, as measured and controlled by a Hall probe, follows this relation calibration is a trivial exercise. Unfortunately, this is not the case and thus polynomial fits have been applied to the calibration of mass spectrometers. In some cases these fits may use the mass versus observed field and not the root mass versus field data which are relatively linear (Fig. 1).

Table 1 presents measured magnetic field intensity of a VG 3600 mass spectrometer over the mass range ^{2}H to ^{186}W. A number of masses are multiple charge W isotopes from the filament in the mass spectrometer. The observed magnetic field values are expressed as volts of output from

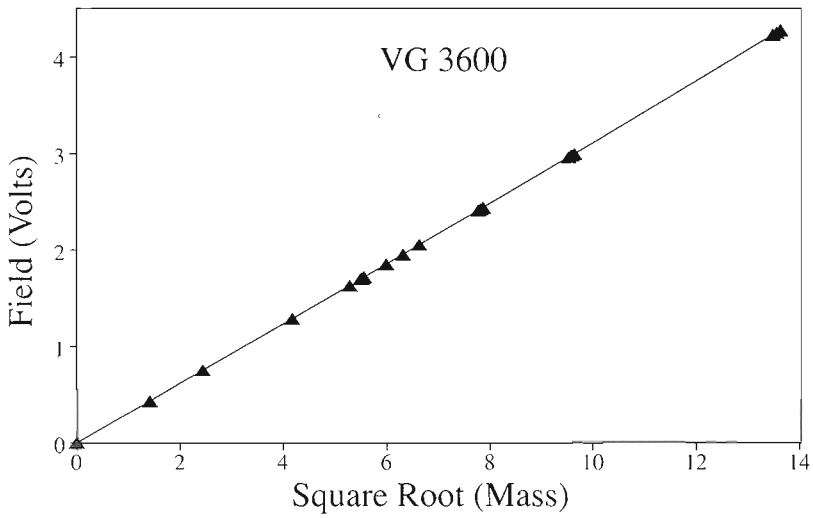

Figure 1.

A plot showing the apparent linearity of the variation of magnetic field intensity with the square root of mass for a VG 3600 mass spectrometer as expected from Equation 2. The field is expressed as a voltage output from a Hall probe. The data are from Table 1.

Table 1. Measured magnetic field in volts from a Hall probe versus mass for a VG 3600 mass spectrometer.

Isotope	Charge	Mass M	Measured Field F in Volts	A= F/M
---		0		0.3074*
$^{1}H_2$	+	2.0157	0.43657	0.3075
^{12}C	2+	6.0000	0.75444	0.3080
^{35}Cl	2+	17.484	1.29062	0.3087
^{28}N	+	28.006	1.63461	0.3089
^{182}W	6+	30.325	1.70181	0.3090
^{184}W	6+	30.659	1.71140	0.3091
^{186}W	6+	30.992	1.72098	0.3091
^{36}Ar	+	35.968	1.85449	0.3092
^{40}Ar	+	39.962	1.95544	0.3093
$^{12}C^{16}O_2$	+	43.990	2.05320	0.3096
^{182}W	3+	60.649	2.41470	0.3101
^{184}W	3+	61.317	2.42820	0.3101
^{186}W	3+	61.985	2.44150	0.3101
^{182}W	2+	90.974	2.96647	0.3110
^{184}W	2+	91.976	2.98321	0.3111
^{186}W	2+	92.977	2.99990	0.3111
^{182}W	+	181.948	4.22808	0.3135
^{184}W	+	181.951	4.25222	0.3135
^{186}W	+	181.954	4.27611	0.3136

*Extrapolated value

the instrument's Hall probe. Figure 1, a mass versus field plot for these data, displays an apparently linear relation as expected from the theoretical equation (Equation 2). Table 1, however, shows that the relation is not precisely linear as the ratio of F/M (= A) ranges from 0.3075 to 0.3136, a variation of about 2% over the tabulated mass range. A precise mass calibration must correct for this small deviation from the theoretical relation. An estimate of a limiting value of A may be made by extrapolating the variation of A in Table 1 to zero mass. Using this zero mass value of A, Figure 2A shows that the deviation of the observed field from the theoretical field based on Equation 2 is a regular positive variation with mass. Addition of a function to Equation 2 which corrects for this deviation from the theoretical function will better define the observed mass-field relation tabulated in Table 1 and provide a linear calibration procedure.

The correcting function must model the curve of Figure 2A which shows an increasing field deviation with increasing mass, and can be accommodated for by making the correction proportional to mass raised to a power p that is greater than 1.0. Therefore the correcting function approximating the curve of Figure 2 can be written as $B \cdot M^p$ where B is a constant. The power factor p will account for any curvature of the correcting function and simplifies to a linear correction with mass if p = 1.0. Modelling this relation to

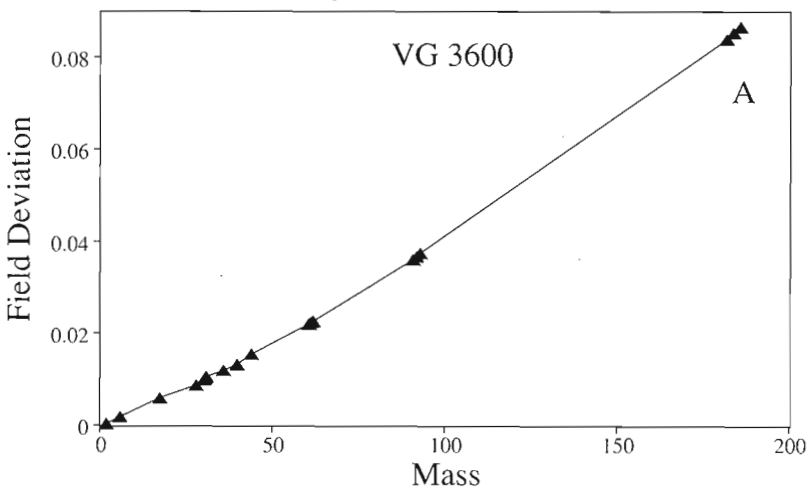

Figure 2A.

The deviations of observed magnetic field intensity (Table 1) from theoretical values defined by the relation of Equation 2 (F = A·M) for a VG 3600 mass spectrometer. The deviations, in units of volts, are slightly nonlinear with mass with increasingly positive values of up to 2.0% greater than the theoretical field at mass 186.

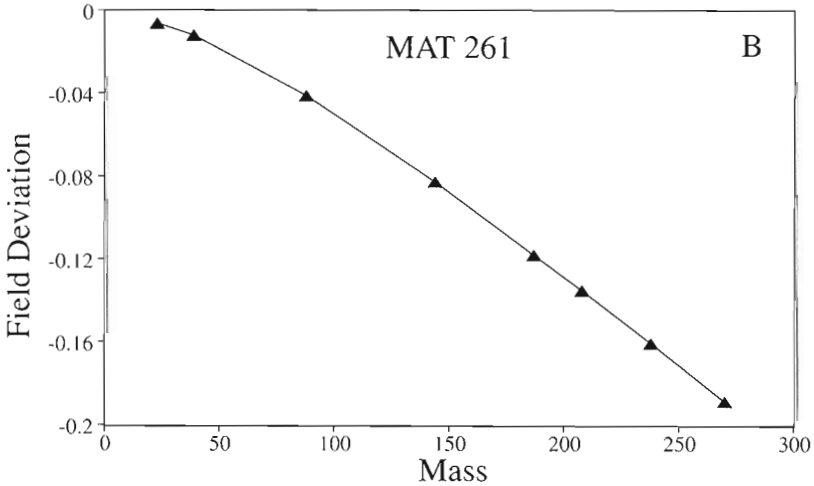

Figure 2B.

A plot similar to Figure 2A for a Finnigan-MAT 261 mass spectrometer at eight field values at masses 23, 39, 88, 144, 187, 208, 238, and 270. The field intensity is scaled to the same units and intensity as the VG 3600 data at mass 186 to permit comparison of deviations of the different mass spectrometers. In this case the deviations (in volts) are increasingly negative with -2.7% deviation from the theoretical field at mass 187.

determine the appropriate B and p which fit the curve of Figure 2A shows that values of B = 0.00016 and p = 1.25 are best but the sensitivity to p is not great and p can have values ranging from 1.15 to 1.30 with appropriate compensating values of A and B. Finnigan-MAT 261 mass spectrometers show a similar nonlinear deviation but with an increasingly negative deviation from the theoretical field with increasing mass (Fig. 2B). The appropriate power factor p, however, is similar to the VG 3600 data with values from 1.0 to 1.3, and typically 1.2.

The general equation defining the observed mass-field relation is therefore:

$$F = A \cdot M^{1/2} + B \cdot M^{p} \quad (3)$$

where p = 1.2 (typical).

The second term is a correction to restore linearity in the F versus M relation. This equation can be rearranged to define a linear function and regression analysis applied to a set of calibration data to determine the best values of the parameters A and B with p at a suitable fixed value. Rewriting Equation 3 as

$$F/M^{1/2} = A + B \cdot M^{p-0.5} \quad (4)$$

an equation of a straight line is defined with a slope of B and an intercept of A. Figure 3A presents the results of applying regression analysis to the VG 3600 data in Table 1 with the per cent deviations of the observed field from the regression line plotted against mass. The deviations are generally less than 0.03% over the mass range from 2 to 186 amu, with a ±0.002% reproducibility of field values using a beam centring routine. These deviations can be compared to the precision necessary to focus an ion beam in the detector. The VG3600 has a resolution of 300 at 5% peak height which is equivalent to requiring the field to be within ±0.085% of the correct value to collect 5% of the peak. Collector slit width is set to permit collection of all the ion beam arriving at the slit for a ±0.040% variation of the field and this results in a flat topped region of the peak. Therefore over the mass range 2-186 amu the algorithm can focus on 5% of a peak and in most cases focus on the maximum or flat topped region of a peak. The masses with field deviations of 0.05-0.06% will be positioned on >50% of a peak and can be subsequently centred. Magnet hysteresis may be responsible for some of the observed scatter as no attempt was made to determine the mass-field values in a systematic manner (i.e. with increasing field). Note that if mass is to be determined the equivalent per cent deviations of mass from the regression line are double the field deviations because mass is dependent on the square of the field (Equation 1). Sensitivity to the power factor p is shown in Figure 3B where the same analysis is applied using p = 1.25. There is a slight improvement in the fit of most masses over the mass range defined.

Figure 4 presents the same analysis as above to data from two Finnigan-MAT 261 mass spectrometers. The plot with a power factor p = 1.25 is the same data as displayed in Figure 2B. The fit of the data is similar to that of the VG 3600 with the three lowest masses deviating by ±0.03-0.06% (with ±0.001% reproducibility) but the remaining masses are in

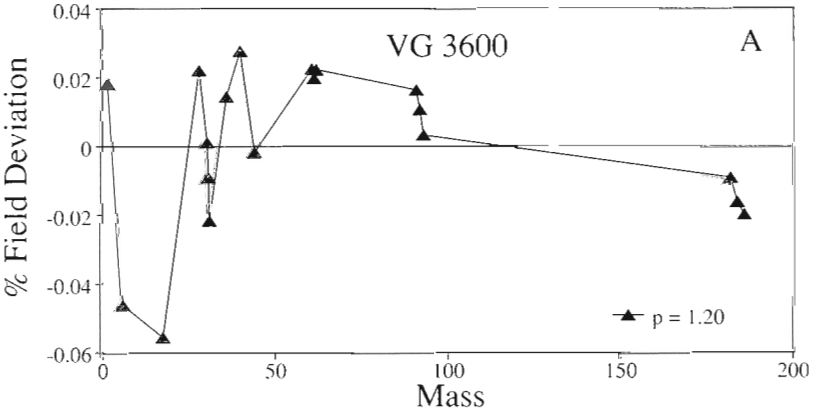

Figure 3A.

A plot of deviations of observed magnetic field intensities from calculated values based on applying Equation 3 to VG 3600 data of Table 1. Reproducibility of the field values is about 0.002% using a beam centring routine. Deviations of <±0.040% will accurately focus a mass in the ion detector. The deviations are derived from regression of the data calculated using Equation 4 with p = 1.2 and result in parameters of A = 0.30729, B = 0.000160.

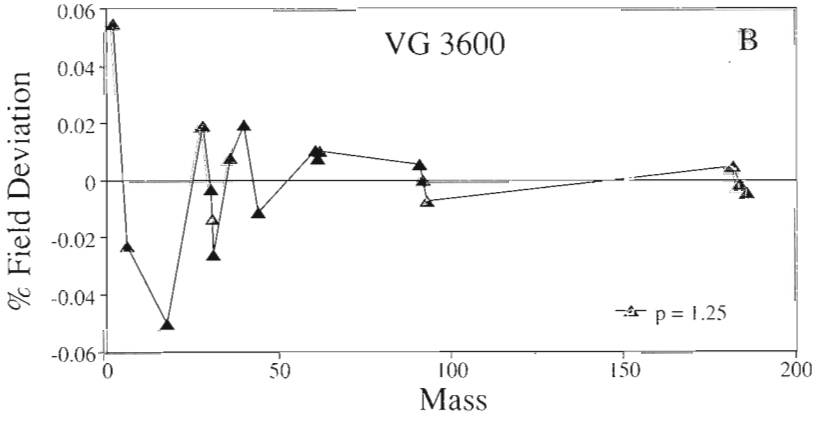

Figure 3B.

Plot of the same data as Figure 3A but with a regression using p = 1.25. This regression results in parameters of A = 0.30746, B = 0.000121.

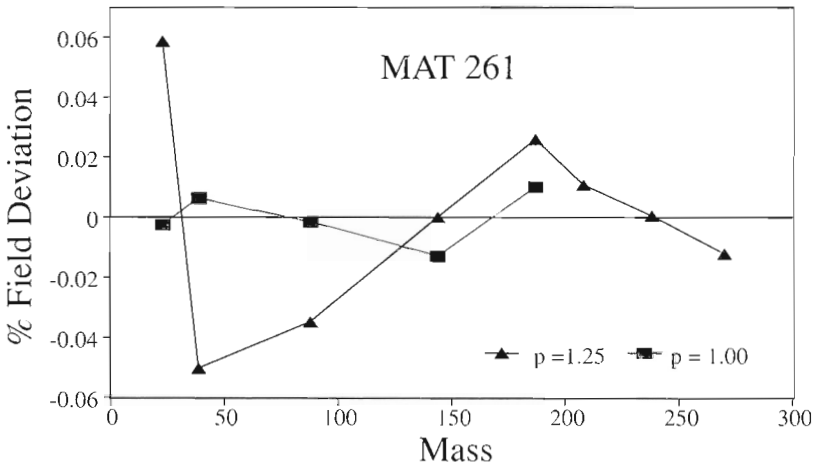

Figure 4.

A similar plot to Figure 3 for data from two Finnigan-MAT 261s. The per cent deviations for the data with p = 1.25 are derived from a regression of the eight observations in Figure 2B, calculated using Equation 4 with p = 1.25 and result in parameters of A = 0.32303, B = -0.000185. The second data set is from another MAT 261 with an optimum power factor p = 1.0 for the mass range 23 to 187 amu. Regression results are A = 0.33138 and B = -0.00130.

better agreement. This instrument has a 5% resolution of 500, equivalent to a field uncertainty of ±0.050% for detecting 5% peak intensity and a peak flat topped region of ±0.018% of field. Therefore over the mass range 23-270, the mass calibration will focus on 5% of a required mass, and for masses 100-270 on or near the optimum region of a peak. The second data set with a mass range of 23 to 187 is from another MAT 261 with an optimum power factor of p = 1.0, indicating a linear deviation with mass from the ideal relation. In this case all field values are within the range required to focus on the flat topped peak region.

Figure 5 presents similar results for a NBS Shields 12" mass spectrometer controlled with two different Hall probe based NIST Teslameters. In the case of Teslameter #1 the magnitude of the observed deviations from the theoretical relation (Fig. 5A) are similar to the MAT 261 (Fig. 2B) but with greater curvature of the relation. For this instrument a larger power factor p of 1.7 is required to correct for the curvature. Figure 5B shows that regression analysis of the mass-field values fit to within 0.06% for all but masses 23 and 39 which deviate by ±0.10%. In contrast, calibration with Teslameter #2 shows about 18 times less deviation from the theoretical relation (Fig. 5A) and very little curvature to the correcting relation (optimum p = 0.35). The fit of the data also is improved with calculated field values within ±0.020% of the observed values (Fig. 5B). The relation is insensitive to the power factor for Teslameter #2 and for a regression using p = 1.0 the deviations remain within ±0.020% of observed values. This instrument, with a 5% resolution of 315, is similar to the VG3600, and therefore requires a field uncertainty of ±0.085% for detecting 5% peak intensity. The peak flat topped region is ±0.040% of field. Therefore over the mass range 23-270, a calibration using Teslameter #2 can focus on the optimum field for all masses. In contrast, for Teslameter #1 the mass calibration will focus on 5% intensity of a required mass for masses greater than 50 but at masses 23 and 39 the deviations are significant enough that a peak could be missed.

APPLICATION OF THE ALGORITHM TO MASS CALIBRATION AND ANALYSES

The use of the mass-field calibration algorithm for routine analyses can be applied in several ways. If the magnet and electronics are very stable there will be little or no change of calibration with time and a detailed mass-field reference table, such as Table 1 for the VG 3600, can be established. The parameters A and B of Equation 3 could be determined once and a recalibration carried out if any mass is found to be drifting significantly from the calculated field value. Minor drift can be corrected in a simple manner. Because of the nearly linear relation of field with square root of mass (Fig. 1), to a very good approximation field drift arising from electronic drift, or minor magnet repositioning for optimum peak shape, involves a small change of slope of the curve and a change in all calibrated field values by the same fractional or percentage amount. Thus a small fractional drift correction determined from one mass can be applied to the field values of other calibration masses and new parameters A and B determined and a precise recalibration can be done using only one measurement. This recalibration procedure is quite general and also could be applied to polynomial calibrations.

Experience with Finnigan-MAT 261 instruments shows that field drift of 0.02 to 0.1% in a calibration is typical over a week and over 2.0% in six months. The weekly variations are sufficient to compromise centring on a desired mass but a detailed multi-mass calibration curve is not practical because of the time and different elements required to maintain it. A procedure has been developed that utilizes the advantages of the new algorithm and minimizes the maintenance of an accurate mass-field reference table. Because only two masses are required to define the parameters A and B for the mass calibration curve, the simplified procedure utilizes only two mass-field calibration values and no detailed calibration is required. Although a minimum of two masses is adequate, additional masses can be included in the mass-field reference table to minimize the interpolation for the field of a required mass. The procedure searches the table for the two

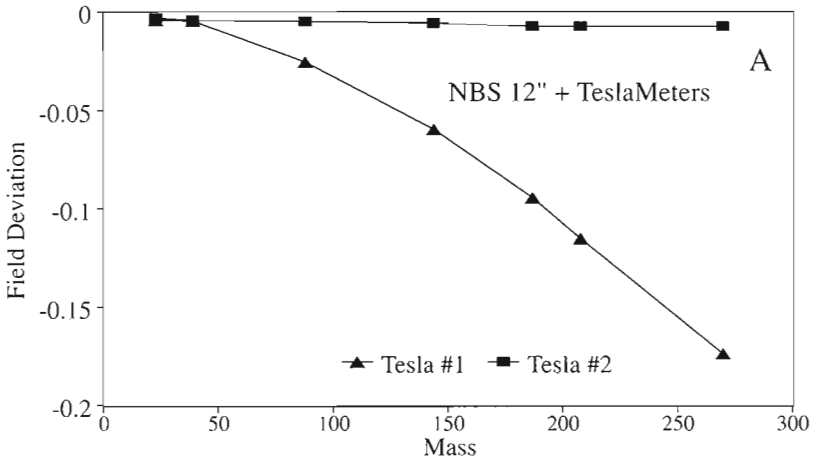

Figure 5A.

Deviations of observed magnetic field intensity at masses 23, 39, 88, 144, 187, 208, and 270 from theoretical values defined by the relation of Equation 2 for a NBS Shields 12" mass spectrometer using two different NIST Teslameters. The field intensity is scaled to the same units and magnitude as the VG 3600 data at a mass of 187. The magnitude and sign of the deviations for Teslameter #1 are similar to the Finnigan-MAT 261 (Fig. 2B) but with greater nonlinearity to the curve.

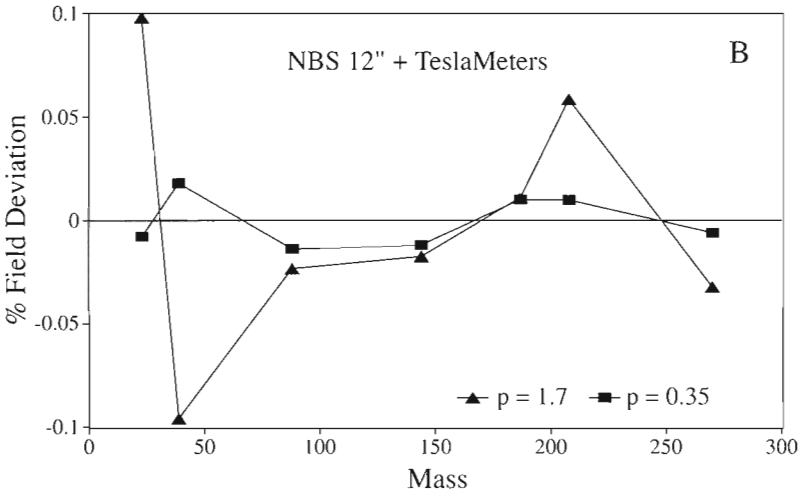

Figure 5B.

A similar plot to Figure 3 for data given in Figure 5A. The deviations are derived from a regression of the field observations using Equation 4. Teslameter #1 has an optimum fit with p = 1.7 and results in parameters of A = 0.32404, B = -0.0000129. Teslameter #2 has an optimum fit with p = 0.35 and results in parameters of A = 0.31410, B = -0.00107, although similarly good fits are attained for p up to 1.0 (excluding p = 0.5).

masses nearest the required mass and uses the associated fields to calculate optimum A and B parameters and then the field of the required mass. Field drift can be corrected in the same manner as outlined above: fractional drift determined from one calibrating mass can be used to correct and update the other calibrated masses in the mass-field reference table.

Routine analyses usually involves measuring intensities of isotopes of a single element (i.e. Pb, Sr, Ar) or a range of elements within a limited mass range (i.e. rare-earth elements). One isotope of an element under analysis is included in the mass-field reference table and the isotopes of interest are analyzed by sequentially focusing ion beams on a detector and repeating the sequence many times. Magnet hysteresis arising from cycling in a limited mass range will result in small divergences from the expected field positions derived from the standard calibration performed over a large mass range. These deviations can be minimized by including another nearby calibrated mass of the same element in the mass-field reference table. The fields of the two reference masses then can be used to determine A and B parameters and thus the field values at other nearby masses in the analysis.

This inclusion of another calibrating mass can be modified slightly to provide additional flexibility. Rather than actually adding an additional nearby or local mass to the mass-field reference table, this mass can be used to establish local A and B parameters which are then retained in a second level calibration. These parameters can then be used to calculate nearby mass positions by difference from a mass in the reference table near the local calibrating mass. The field for this mass is not stored, only the local A and B parameters determined at the time of calibration using the local mass. This local calibration can be optimized to the hysteresis loop actually used during data collection by cycling through the masses to be measured to establish the hysteresis and performing a mass calibration at two calibrating masses (one in the reference table and the local calibrating mass) to establish the local A and B parameters. Other nearby masses in the data sequence then use these local A and B parameters and the field of the nearest mass in the reference table to determine the optimum mass positions. In practise local masses are defined as within ±12 amu of the mass used to establish the local parameters. This technique is particularly useful for establishing precise field positions of a baseline measurement, or a mass with an ion beam intensity which is too small to accurately determine the appropriate field value with a beam centring routine.

There are two reasons for not including the local calibrating mass in the reference table but only retaining the calculated local A and B parameters. First, it is an additional mass to maintain as an up-to-date reference. Second, once established the local calibration parameters A and B are quite

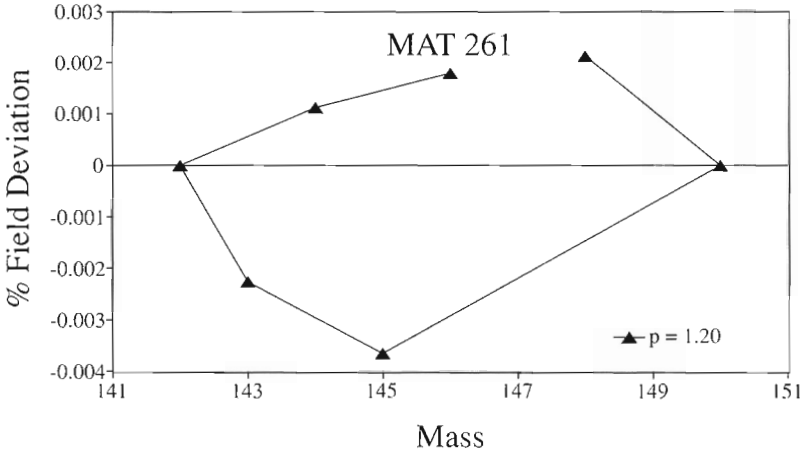

Figure 6.

A plot of deviations of observed magnetic field intensities from calculated values for a Finnigan-MAT 261 in the Nd mass range. The switching sequence loops through masses 146, 144, etc. as shown. The deviations are derived from a two point solution to Equation 3 using observed fields at masses 150 and 142 with p = 1.2 and result in local parameters A = 0.29639, B = -0.000200. Reproducibility of the field values is about ±0.001% using a beam centring routine. This is a different instrument to those used to display results in Figure 4.

insensitive to changes of calibration due to drift. It can be shown (Appendix 1) that the error in field position of an uncalibrated mass, arising from using previously established local A and B parameters, can be expressed as

$$\%\ Field\ Error = (\sqrt{M_2} - \sqrt{M_1}) / \sqrt{M_2} \cdot (\%\ drift) \quad (5)$$

where M_1 and M_2 are a currently calibrated mass in the reference table, and the required uncalibrated mass, respectively, and per cent drift is the long term drift in the field since the last local mass calibration. The function strongly demagnifies the field error. For example if the calibrated mass is ^{40}Ar and the field at ^{36}Ar is calculated, the error is 0.051 (% drift) and a 0.1% drift error results in an error in the mass 36 field of 0.005%. At heavier masses the error is smaller and for masses 204 and 208 the error is 0.010 (% drift).

Figure 6 demonstrates the application of this local calibration technique and the levels of error in determining the positions of seven Nd and one Sm isotope analyzed in a Finnigan-MAT 261 instrument. A hysteresis loop was established for the mass sequence 146, 144, 142, 143, 145, 150, 148 and the masses 142 and 150 were used to determine the local A and B parameters. The fields of the other masses, were also precisely determined using a beam centring routine and the plot shows the deviations of the calculated field values from the observed values as a result of using the local calibration parameters to determine their field positions.

DISCUSSION

The algorithm presented as Equation 3 can successfully model the deviation of the mass-field calibration from the theoretical equation (Equation 2) over the mass range of interest for all isotopic analyses. Reasons for deviation from the theoretical relationship can be ascribed to several possibilities. Magnet hysteresis certainly plays a part in some of the small deviations observed and minor magnet saturation could be responsible for the overall divergence from the theoretical value. Saturation could account for the Finnigan-MAT 261 calibrations, however, the VG 3600 calibration shows higher magnet fields at higher masses – the reverse of a saturation effect. Therefore saturation may only be a minor component.

Hall probe linearity is a more likely source of apparent deviation as two different probes (NIST Teslameters) used to control the same NBS 12" mass spectrometer produce different calibrations. In addition, the same Teslameter used on a different Shields NBS mass spectrometer (6") produces a similar calibration to the 12" machine. Calibration for Teslameter #1 is significantly nonlinear and requires a power factor p = 1.7 for optimum fit, whereas the second Teslameter closely approximates the ideal relation (Fig. 5A) and is insensitive to the power factor, with excellent fits for p ranging from 0.35 to 1.0 (excluding the singularity at p = 0.5). This second Teslameter was developed to improve on the first probes characteristics by minimizing the minor intrinsic nonlinearities of Hall probes (R. Schideler, pers. comm., 1994) and clearly measures the magnetic field with greater accuracy and linearity than the first Teslameter. One characteristic of the calibrations of three of the five probe units used is a correlation of significant deviations at the low end of the mass range with greater deviations from the ideal mass spectrometer relation. The VG 3600 shows maximum deviation at masses 2 and 17; a MAT 261 deviates at masses 23 and 39, and the NBS 12" with Teslameter #1 deviates at masses 23 and 39. These calibrations have the largest power factors (p = 1.2, 1.2 and 1.7). In contrast, the better fitting calibrations have more linear deviations (p = 1.0). The two Teslameters on the NBS 12" instrument most clearly demonstrate this correlation and suggest that Hall probes that can accurately and linearly measure magnetic fields will provide the most accurate calibrations of the mass-field relations of magnetic sector mass spectrometers.

Despite the exact source of the deviation from the ideal equation, the algorithm defining the mass-field relation for mass spectrometers controlled with Hall probes appears to have general applicability. In addition to the three types of instruments calibrated here the procedure has also been applied to mass-field data from SHRIMP II, a large radius double focusing ion microprobe (Clement and Compston, 1994). The algorithm is also able to improve on linear and

quadratic calibrations of this instrument. The ability to define an essentially linear relationship results in an efficient technique of calibrating mass spectrometer magnets and maintaining a calibration.

CONCLUSIONS

These calibrations for several different instruments with different electronics for controlling the magnetic field show that the algorithm of Equation 2 has a general application to Hall probe controlled mass spectrometers. There are several advantages of this algorithm over usual polynomial fits:

1. The value of p has a limited range, even for different Hall probe/controllers, and once determined for a probe it can be a fixed value.
2. A fixed p reduces the algorithm to a linear relation with only two unknowns (A, B in Equation 3) and any two widely spaced masses are adequate to define the calibration. This is a significant advantage as a single calibrating standard with two elements of widely differing atomic weight can be used to check and maintain the calibration.
3. Because the mass-field relation has been reduced to a linear relationship extrapolation outside the defined mass range is precise, in contrast to polynomial fits in which extrapolation produces increasing uncertainty in obtaining the desired mass with increasing extrapolation.
4. As the algorithm will yield zero field at zero mass, extrapolation to low masses is similarly precise.
5. The algorithm can be used to assess a calibration because the A and B parameters, once established, have consistent values with little variation. For example, if a recalibration is attempted on the wrong mass (i.e. ^{207}Pb mistaken for ^{206}Pb) the parameters will differ significantly from the expected values and the calibration can be rejected with a warning to the operator.
6. The algorithm can be further refined by the introduction of second level of local calibrating masses to increase the flexibility of the procedure and account for the hysteresis loop. As such, precise field positions for baseline measurement or small mass intensities can be precisely determined.

ACKNOWLEDGMENTS

The staff of the GSC Geochronology laboratory is thanked for assistance and patience during the development of this work. S. Hemming and T. Rasbury of SUNY, Stony Brook generously provided calibration data for the NBS Shields mass spectrometers and J. Blenkinsop, Carleton University for another MAT 261 instrument. R. Schideler, NIST, is thanked for discussions on characteristics of Hall probes. W. Compston of the Australian National University provided mass calibration data for SHRIMP II ion microprobe. S. Hemming and T. Rasbury critically reviewed the manuscript. Patricia Hunt is thanked for assisting with drafting of the diagrams.

REFERENCE

Clement, S.W.J. and Compston, W.
1994: Ion probe parameters for very high resolution without loss of sensitivity; in Abstracts of the Eighth International Conference on Geochronology, Cosmochronology and Isotope Geology, (ed.) M.A. Lanphere, G.B. Dalrymple, and B.D. Turrin; United States Geological Survey Circular 1107, p. 62.

APPENDIX 1

Effects of field drift on use of local parameters

From Equation 3 with

$$p = 1.2: F = A \cdot \sqrt{M} + B \cdot M^{1.2}$$

The field at one mass position can be expressed in terms of the field at another mass and the A and B parameters. The field F_2 at an uncalibrated mass M_2 in terms of the field F_1 at M_1, a calibrated mass is

$$F_2 = F_1 + A \cdot (\sqrt{M_2} - \sqrt{M_1}) + B \cdot (M_2^{1.2} - M_1^{1.2})$$

For analysis in a limited mass range (±12 amu) the A and B parameters can be calibrated locally in this mass range to provide precise field positions. If the field has drifted and a recalibration of the local A and B parameters carried out a new F_2' is

$$F_2' = F_1' + A' \cdot (\sqrt{M_2} - \sqrt{M_1}) + B' \cdot (M_2^{1.2} - M_1^{1.2})$$

Suppose that the field of calibrated mass M_1 is corrected for the drift (to F_1') but the old local A and B parameters are used for calculating the field of M_2, then

$$F_2'' = F_1'' + A \cdot (\sqrt{M_2} - \sqrt{M_1}) + B \cdot (M_2^{1.2} - M_1^{1.2})$$

The error in the field of M_2 because of the use of the old local parameters is therefore:

$$F_{err} = F_2' - F_2'' = (\sqrt{M_2} - \sqrt{M_1}) \cdot (A' - A) + (B' - B) \cdot (M_2^{1.2} - M_1^{1.2})$$

For the calibration data in Table 1 the second term in the above equation is only 1% of the first term in the region of mass 40 and about 3.9% near mass 207, corrections small enough to ignore the last term. This approximation is equivalent to assuming B = 0 and the theoretical relation in Equation 2 applies.

Thus the % error in the field of M_2 can be simplified to

$$\%F_{err} = (\sqrt{M_2} - \sqrt{M_1}) / \sqrt{M_2} \cdot (A' - A) / A \cdot 100$$

Since % drift in field can be approximated by (A' – A)/A·100 then

$$\%F_{err} = (\sqrt{M_2} - \sqrt{M_1}) / \sqrt{M_2} \cdot (\%\ drift)$$

This relation shows that error in the field is demagnified by the mass terms. For example if the correct mass is ^{40}Ar and the field at ^{36}Ar is calculated the error is 0.051 (% drift) and a 0.1% drift in field results in an error in the field of mass 36 of 0.005%. At heavier masses the error is smaller and for masses 204 and 208 the error is reduced to 0.010 (% drift). Therefore errors in field positions resulting from field drift are generally less than 1/20 of the drift for masses greater than 35 when local calibration parameters are used. This demagnification can be demonstrated graphically by considering that drift in the mass-field relation in Figure 1 rotates the calibration curve about the origin. This shifts the field values but the local slope of the line at any point is relatively insensitive to this shift of field and changes by a much smaller amount.

U-Pb zircon age for a volcanic suite in the Rankin Inlet Group, Rankin Inlet map area, District of Keewatin, Northwest Territories[1]

Subhas Tella[2], J.C. Roddick[3], and Otto van Breemen[2]

Tella, S., Roddick, J.C., and van Breemen, O., 1996: U-Pb zircon age for a volcanic suite in the Rankin Inlet Group, Rankin Inlet map area, District of Keewatin, Northwest Territories; in Radiogenic Age and Isotopic Studies: Report 9; Geological Survey of Canada, Current Research 1995-F, p. 11-15.

Abstract: U-Pb zircon analyses from a felsic band within dominantly mafic volcanics of the Rankin Inlet Group yields a U-Pb upper concordia intercept age of 2663 ± 3 Ma. These supracrustals at Rankin Inlet appear to be 15-20 Ma younger than volcanics of the Kaminak Group in the Tavani area, 70 km to the southwest. The 2.68-2.66 Ga volcanism in the Tavani and Rankin Inlet areas coincided with the last stage of the main phase of magmatism in the Slave Structural Province.

Résumé : Les analyses U-Pb sur zircon d'une bande felsique dans des volcanites surtout mafiques du Groupe de Rankin Inlet indiquent un âge de 2 663 ± 3 Ma (intercept supérieur avec la Concordia). Ces roches supracrustales observées à l'inlet Rankin semblent plus récentes de 15 à 20 Ma que les volcanites du Groupe de Kaminak dans la région de Tavani, à 70 km au sud-ouest. Dans les régions des inlets Tavani et Rankin, l'épisode volcanique qui s'est produit entre de 2,68 et 2,66 Ga coïncide avec le dernier stade de la principale phase de magmatisme dans la Province structurale des Esclaves.

[1] Contribution to the Canada-NWT Mineral Initiatives 1991-96, a subsidiary Canada-Northwest Territories Economic Development Agreement. Project funded by the Geological Survey of Canada
[2] Geological Survey of Canada, 601 Booth Street, Ottawa, Ontario K1A 0E8
[3] Deceased

INTRODUCTION

The Rankin Inlet map area (Fig.1) encompasses a portion of an Archean and Paleoproterozoic granite-greenstone-gneiss terrane within the western Churchill Structural Province of the Canadian Shield. The results of most recent regional bedrock mapping in the map area were reported by Armitage et al. (1993), Tella (1994), Tella and Schau (1994), and Tella et al. (1986), and the reader is referred to these publications for a comprehensive overview of the geology and structure of this region. In this study we report on an age from the felsic volcanics of the Rankin Inlet Group (Fig. 1, 2) and compare these to previously reported U-Pb zircon ages of the Kaminak Group in the Tavani area 70 km southwest of Rankin Inlet (Tella et al., 1990; Parker and Ralser, 1992) and with igneous ages in the Slave Structural Province, District of Mackenzie.

GEOLOGICAL SETTING

The Rankin Inlet area is underlain by an Archean polydeformed metavolcanic-metasedimentary supracrustal sequence, the Rankin Inlet Group (RIG). The sequence is composed of massive and pillowed mafic volcanic flows, felsic volcanics, interflow sediments, quartz-magnetite iron-formation, and minor mafic and felsic tuffs, pyroclastics, volcanic breccia, and gabbro sills (Tella et al., 1986). The main rock types are sheared and carbonatized mafic metavolcanics (chlorite schist, amphibolite), minor intercalated mafic and felsic tuffs, and greywacke. They are fine- to medium-grained, well layered, and massive to well cleaved. Altered metamafic rocks contain blue-green amphibole, chlorite, biotite, and carbonate. Chemically the volcanic rocks and associated gabbroic rocks are tholeiitic basalts (unpublished data of Tella) and they show similar geochemical signatures to those reported from the Tavani region (Park and Ralser, 1992). Ultramafic (komatiitic) sills, in part containing Cu-Ni mineralization, occur within the mafic volcanic sequence. Neoarchean ages of 2748 ± 92 Ma and 2776 ± 88 Ma were determined using the Re-Os method on Ni-Cu-PGE ores from ultramafic rocks of the Rankin Inlet Group (Hulbert and Gregoire, 1993).

Two major cycles of volcanism with intervening conglomerate deposition are present within the mafic volcanic sequence. The ultramafic rocks containing ores dated by the Re-Os method are in the upper cycle of the Rankin Inlet Group (Hulbert and Gregoire, 1993). Felsic volcanics, intercalated with the mafic volcanic rocks of which they make up less than 10%, occur only within the lower volcanic cycle.

Previous stratigraphic and structural studies (Tella et al., 1986; Borradaile et al., 1989) in the Rankin Inlet Group established that the sequence forms an F_1 homocline that is folded into a southeast-plunging F_2 syncline. Strain estimates based on deformed lava pillows reveal that the Rankin Inlet Group stratigraphy is locally thinned, up to 12-23% of its original thickness on the flanks of the major F_2 fold (Tella et al., 1986; Borradaile et al., 1989). The metamorphic grade of the Rankin Inlet Group is greenschist facies and both deformation and metamorphism are considered to be Archean, because the structurally overlying Proterozoic rocks were unaffected by penetrative deformation and metamorphism.

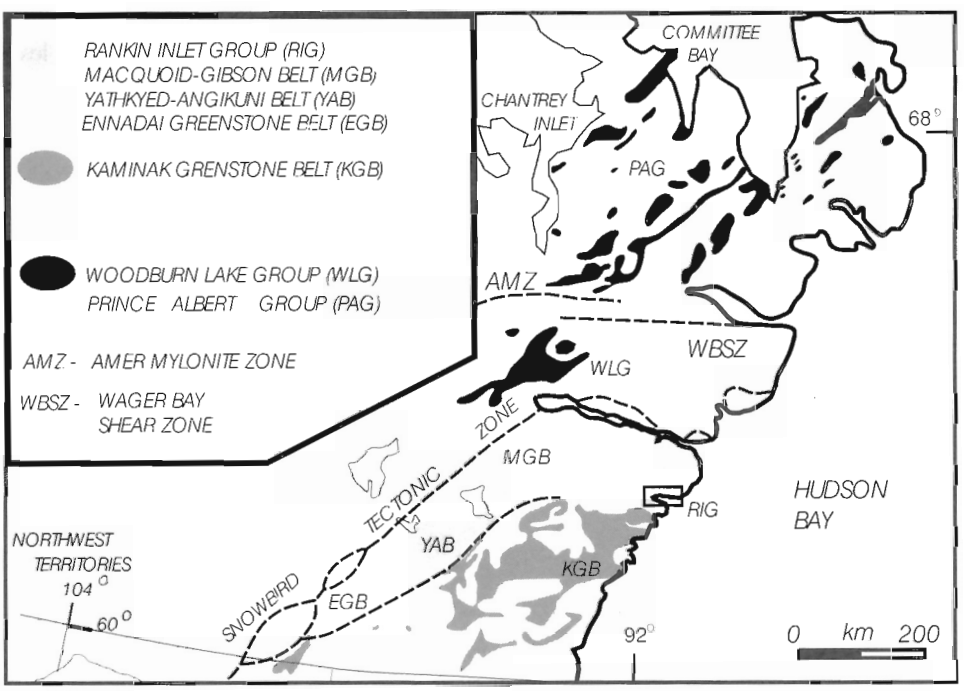

Figure 1. *Sketch map showing the distribution of Archean supracrustal belts in the Churchill Structural Province and the location of the Rankin Inlet Group (RIG).*

ANALYTICAL PROCEDURES AND RESULTS

Felsic sample 92TXA-410B, selected for the U-Pb dating, contains a few quartz eyes within the sheared felsic matrix, suggesting a protolith of rhyolite porphyry (Fig. 2). Zircons are clear and colorless and consist mostly of euhedral to subhedral prisms with length to breadth ratios of 2:1. There are, however, a significant number of more equidimensional grains, some of which manifest igneous overgrowths on distinct cores, which were avoided during crystal selection. Mineral extraction and isotope dilution techniques for U-Pb analysis are detailed in Parrish et al. (1987). Analytical results are listed in Table 1 and displayed on a concordia plot with 2 sigma uncertainties (Fig. 3). Errors reflect propagation of all analytical uncertainties (Roddick, 1987).

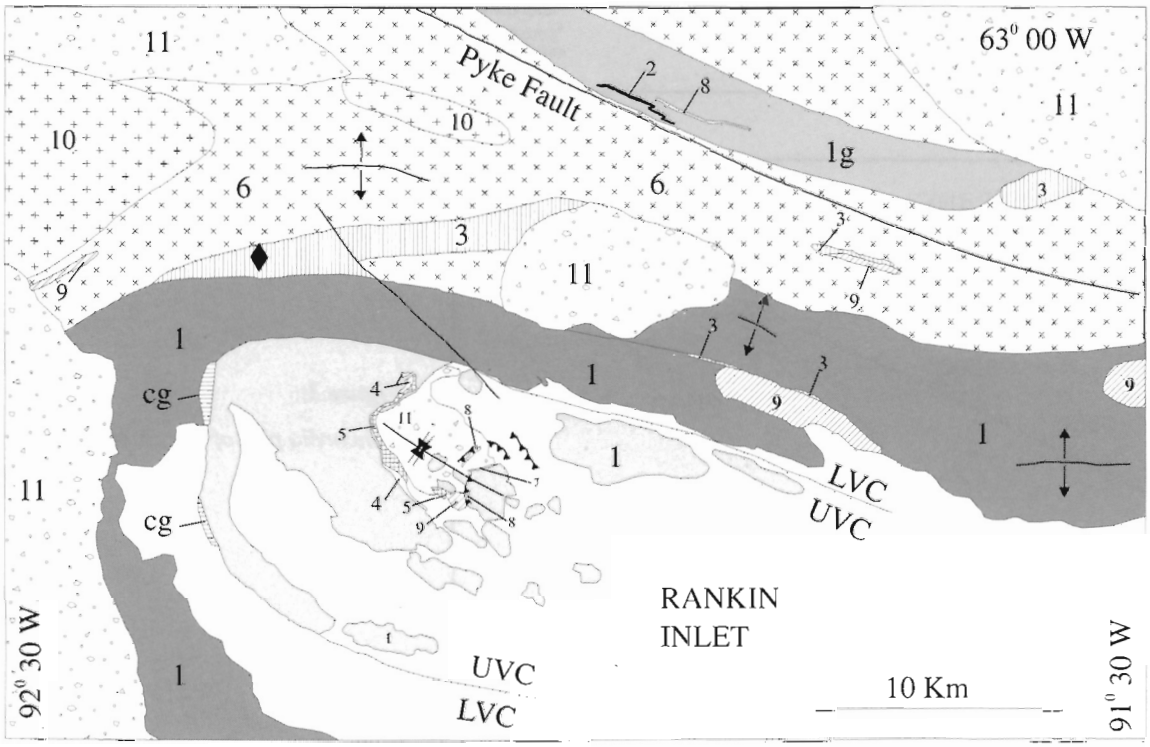

LEGEND

11 Quaternary cover

PROTEROZOIC
10 granite
9 orthoquartzite

ARCHEAN
RANKIN INLET GROUP
8 gabbro
7 ultramafics
6 mafic volcanic schist and tuffs (derived from 1)
5 impure quartzite
4 carbonate
3 felsic volcanics
2 banded iron formation
1 mafic volcanics, greywacke (1g), mafic and felsic tuffs, pyroclastics and conglomerate (cg)

Geochron Sample Locality
UVC - Upper Volcanic Cycle
LVC - Lower Volcanic Cycle
Axial trace F1-Anticline
Axial trace F2-Anticline
Fault
Thrust Fault

Figure 2. *Simplified geological sketch map, Rankin Inlet area, showing sample location.*

Table 1. U-Pb isotopic data, zircon fractions from sample 92TXA-410B.

Fraction[1]	Wt. (µg)	U (ppm)	Pb^2 (ppm)	$^{206}Pb/^{204}Pb^3$ (meas.)	Pb_c^4 (pg)	$^{208}Pb^2$ (mole %)	$^{206}Pb/^{238}U^5$ (± 1σ, %)	$^{207}Pb/^{238}U^5$ (± 1σ, %)	Disc. (%)	$^{207}Pb/^{206}Pb^5$ (± 1σ, %)	Age[6] (± 2s, Ma)
Felsic volcanic, Rankin Inlet Group (92-TXA-410b; #3269; UTM 15 E 544972 N 6976287)											
A, > 74	10	44	27	459	28	11.4	0.5247 ± .19	13.735 ± .72	0.76	0.18985 ± .59	2740.9 ± 19.3
B, > 74	10	48	25	1687	8	9.7	0.4625 ± .13	11.586 ± .13	0.90	0.18169 ± .06	2668.4 ± 1.9
C, < 74	14	78	44	1913	17	9.5	0.4997 ± .10	12.476 ± .11	0.92	0.18107 ± .04	2662.7 ± 1.4
D, < 74	13	73	40	2919	10	9.7	0.4933 ± .10	12.326 ± .11	0.91	0.18120 ± .05	2663.9 ± 1.5
E, > 74	11	88	49	3309	9	10.4	0.4905 ± .41	12.240 ± .41	1.00	0.18097 ± .04	2661.8 ± 1.2
F, < 74	4	50	28	593	11	9.4	0.5047 ± .22	12.688 ± .24	0.85	0.18232 ± .13	2674.1 ± 4.3

[1] average breadths in microns; fractions are non-magnetic at a side slope of 1 degree and 1.7 A.
[2] radiogenic Pb
[3] measured ratio, corrected for spike and fractionation;
[4] total common Pb in analysis corrected for fractionation and spike
[5] corrected for blank Pb and U, common Pb
[6] $^{207}Pb/^{206}Pb$ model age.

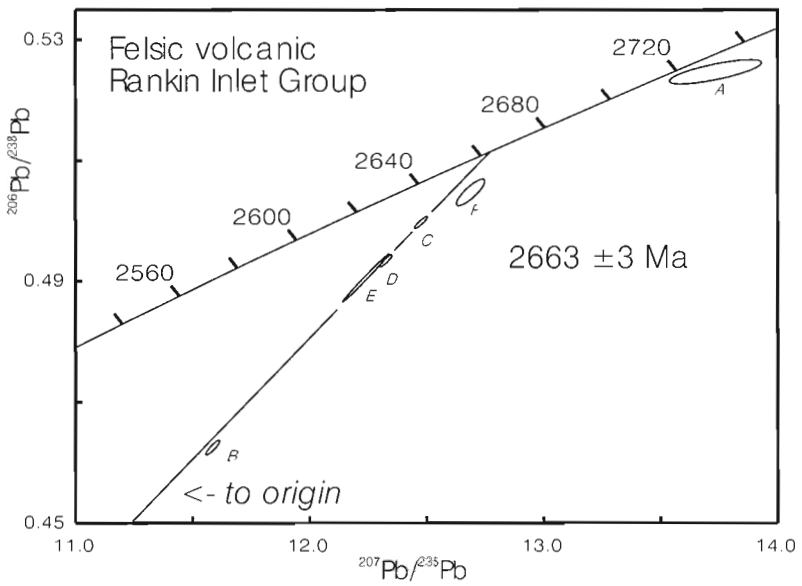

Figure 3.
Concordia plot of zircon data.

Uranium contents range from 40-90 ppm (Table 1). Low U concentrations notwithstanding, analyses are significantly discordant, except fraction A that reflects a significantly older Pb component (Fig. 3). Fraction A consisted of four small grains in which it was difficult to establish the absence of cores; the 270Pb/206Pb model age of 2741 ± 20 Ma is taken as a minimum for the inherited component. Discordant fraction F plots slightly to the right of an apparent alignment of the remaining data points (Fig. 3) suggesting that it contains minor inheritance. Regression analysis of the remaining four data points yields an upper intercept age of 2660 ± 3 Ma, a slightly negative lower intercept of -209 ± 158 Ma and a level of scatter (MSWD = 3.94) that is slightly beyond what could be attributed to analytical uncertainties alone. Because of the negative lower intercept, it is suspected that fraction B may also contain minor inheritance, and as such, the assigned age was calculated by forcing a line through clustered points C, D, E, and the origin, yielding a time of emplacement of 2663 ± 3 Ma.

DISCUSSION

The U-Pb age of 2663 ± 3 Ma establishes a precise Neoarchean age for the Rankin Inlet supracrustal sequence near Rankin Inlet. In the Tavani region syntectonic to late tectonic granites and porphyry that intrude the metavolcanic Kaminak Group yield precise U-Pb zircon ages of 2672 ± 2 Ma, 2666 ± 2 Ma, and 2666 ± 9 Ma, respectively (unpublished U-Pb data, J.C. Roddick in Parker and Ralser,1992). Tella et al. (1990) summarized the magmatic history in the Tavani area as: 2.68 Ga, felsic volcanics; 2.67-2.66 Ga, syntectonic granites; and 2.66-2.65 Ga post-tectonic granites. The younger age obtained from the felsic volcanics of the Rankin Inlet Group suggests that the volcanism and subsequent deformation of the Rankin Inlet Group postdates that of the Kaminak Group by 15-20 Ma.

The Rankin-Kaminak belts appear to be significantly younger than supracrustal sequences north of the Snowbird Tectonic Zone, such as the Woodburn Group dated at 2798+24/-21 Ma (Tella et al., 1985), and the Prince Albert Group dated at ca. 2.7-3.0 Ma (Schau, 1982). However, identical U-Pb zircon ages have been documented from felsic volcanic rocks in the Slave Structural Province west of the Thelon Tectonic Zone: e.g. Russell Lake, 2658 ± 1 Ma and Clan Lake, 2661 ± 2 Ma (Mortensen et al., 1992). These ages are at the younger end of the main 2.73-2.66 Ga 'Yellowknife Supergroup' phase of volcanism and turbidite deposition that is recorded throughout the Slave Province (Mortensen et al., 1988; van Breemen et al., 1992; Villeneuve et al., 1994). Volcanism of this age is clearly widespread in the Northwest Territories; whether the magmatism in the Rankin-Kaminak belts and the Slave Province are genetically related requires further study.

ACKNOWLEDGMENTS

The paper was critically read by M.E. Villeneuve.

REFERENCES

Armitage, A.E., Tella, S., and Miller, A.R.
1993: Iron-formation hosted gold mineralization and its geological setting, Meliadine Lake area, District of Keewatin, Northwest Territories; in Current Research, Part C; Geological Survey of Canada, Paper 93-1C, p. 187-195.

Borradaile, G., Tella, S., and McArthur, J.
1989: Magnetic fabric as a kinematic indicator of faults: a test case; Annales Tectonicae, v. III, no.1, p. 3-11.

Hulbert, L.J. and Gregoire, D.C.
1993: Re-Os isotope systematics of the Rankin Inlet Ni ores: an example of the application of ICP-MS to investigate Ni-Cu-PGE mineralization and the potential use of Os isotopes in mineral exploration; The Canadian Mineralogist, Journal of the Mineralogical Association of Canada, v. 31, pt. 4, p. 861-876.

Mortensen, J.K., Henderson, J.B., Jackson, V.A., and Padgham, W.A.
1992: U-Pb geochronology of Yellowknife Supergroup felsic volcanic rocks in the Russell lake and Clan Lake area, southwestern Slave Province, N.W.T.; in Radiogenic Age and Isotopic Studies: Report 5; Geological Survey of Canada, Paper 91-2, p. 1-7.

Mortensen, J.K., Thorpe, R.I., Padgham, W.D., King, J.E., and Davis, W.J.
1988: U-Pb ages for felsic volcanism in the Slave province, N.W.T.; in Radiogenic Age and Isotopic Studies: Report 2; Geological Survey of Canada, Paper 88-2, p. 85-95.

Park, A.F. and Ralser, S.
1992: Precambrian geology of the southwestern part of the Tavani map area, District of Keewatin, Northwest Territories; Geological Survey of Canada, Bulletin 416, 81 p.

Parrish, R.R., Roddick, J.C., Loveridge, W.D., and Sullivan, R.W.
1987: Uranium-lead analytical techniques at the Geochronology Laboratory, Geological Survey of Canada; in Radiogenic Age and Isotopic Studies: Report 1; Geological Survey of Canada, Paper 87-2, p. 3-7.

Roddick, J.C.
1987: Generalized numerical error analysis with application to geochronology and thermodynamics; Geochemica et Cosmochemica Acta, v. 51, p. 359-362.

Schau, M.
1982: Geology of the Prince Albert Goup in parts of Walker Lake and Laughland Lake map areas, District of Keewatin; Geological Survey of Canada, Bulletin 337, 62 p.

Tella, S.
1994: Geology, Rankin Inlet (55K/16), Falstaff Island (55J/13), and Marble Island (55J/11), District of Keewatin, Northwest Territories; Geological Survey of Canada, Open File 2968, scale 1:50 000.

Tella, S. and Schau, M.
1994: Geology, Gibson Lake east-half, District of Keewatin, Northwest Territories; Geological Survey of Canada, Open File 2737, scale 1:250 000.

Tella, S., Annesley, I.R., Borradile, G.J., and Henderson, J.R.
1986: Precambrian geology of parts of Tavani, Marble Island and Chesterfield Inlet map areas, District of Keewatin, N.W.T.; Geological Survey of Canada, Paper 86-13, 20 p.

Tella, S., Heywood, W.W., and Loveridge, W.D.
1985: A U-Pb age on zircons from a dacite porphyry, Amer Lake map area, District of Keewatin; in Current Research, Part B; Geological Survey of Canada, Paper 85-1B, p. 371-374.

Tella, S., Roddick, J.C., Park, A.F., and Ralser, S.
1990: Geochronological constraints on the evolution of the Archean and Early Proterozoic terrane in the Tavani-Rankin Inlet region, District of Keewatin, N.W.T.; Geological Society of America, Abstracts with Programs, v. 22, no. 7, p. A174.

van Breemen, O., Davis, W.J., and King, J.E.
1992: Temporal distribution of granitoid plutonic rocks in the Archean Slave Province, northwest Canadian Shield; Canadian Journal of Earth Sciences, v. 29, p. 2186-2199.

Villeneuve, M.E., Relf, C., Hrabi, B., and Jackson, V.
1994: Geochronology of supracrustal sequences in the Slave Province, N.W.T., Canada: implications for age of basement; Abstracts of the Eighth International Conference on Geochronology, Cosmochronology and Isotope Geology, ICOG 8, Berkely, California, United States Geological Survey, Circular 1107, p. 342.

Archean crustal evolution in the central Minto block, northern Quebec

T. Skulski[1], J.A. Percival[1], and R.A. Stern[1]

Skulski, T., Percival, J.A., and Stern, R.A., 1996: Archean crustal evolution in the central Minto block, northern Quebec; in Radiogenic Age and Isotopic Studies: Report 9; Geological Survey of Canada, Current Research 1995-F, p. 17-31.

Abstract: The central Minto block contains three volcano-sedimentary successions. Near Lake Qalluviartuuq, an isotopically primitive ($^{2.83\ Ga}\varepsilon_{Nd}$ +3.8 to +2.3) 2.83 Ga volcano-plutonic sequence comprises depleted tholeiitic basalts, anorthositic gabbro, and diorite-granodiorite that is unconformably overlain by <2.77 Ga conglomerates. Overlying the conglomerate is a more evolved ($^{2.76\ Ga}\varepsilon_{Nd}$ +1.8) calc-alkaline sequence of pillow basalts, andesites, and peridotite cut by 2.73 Ga diorite. To the west, and in inferred tectonic contact, the sediment-dominated Kogaluc sequence includes both isotopically evolved calc-alkaline rocks ($^{2.76\ Ga}\varepsilon_{Nd}$ +1.6 to -0.1) including <2.76 Ga rhyolitic tuff, pillowed andesites, and 2.76 Ga quartz-feldspar porphyry, and less abundant, depleted tholeiitic basalts ($^{2.76\ Ga}\varepsilon_{Nd}$ +2.4). These are interlain with sedimentary rocks including banded iron-formation, quartzite, and metagreywacke. Calc-alkaline batholiths include 2.78 Ga pyroxene-bearing intermediate and felsic plutons ($^{2.78\ Ga}\varepsilon_{Nd}$ <+2.7) and younger, peraluminous tonalites (ε_{Nd} <+1.3). Late, 2.73 Ga peraluminous granitoids are isotopically evolved ($^{2.725\ Ga}\varepsilon_{Nd}$ -1.6).

Résumé : La partie centrale du bloc de Minto contient trois successions volcano-sédimentaires. Près du lac Qalluviartuuq, une séquence volcano-plutonique isotopiquement primitive ($^{2,83\ Ga}\varepsilon_{Nd}$ +3,8 à +2,3) de 2,83 Ga comprend des basaltes tholéiitiques appauvris, du gabbro anorthositique et un mélange de diorite et de granodiorite, laquelle séquence est recouverte en discordance de conglomérats de < 2,77 Ga. Au-dessus du conglomérat, on observe une séquence calco-alcaline plus évoluée ($^{2,76\ Ga}\varepsilon_{Nd}$ +1,8) de basaltes en coussins, d'andésites et de péridotites recoupés par de la diorite de 2,73 Ga. À l'ouest, la séquence principalement sédimentaire de Kogaluc, que l'on suppose en contact tectonique, se compose de roches calco-alcalines isotopiquement évoluées ($^{2,76\ Ga}\varepsilon_{Nd}$ +1,6 à -0,1) et, en moindre abondance, de basaltes tholéiitiques appauvris ($^{2,76\ Ga}\varepsilon_{Nd}$ +2,4). Parmi les roches calco-alcalines, il y a un tuf rhyolitique (< 2,76 Ga), des andésites en coussins et un porphyre quartzo-feldspathique (2,76 Ga). Ces lithologies sont intercalées de roches sédimentaires (formation de fer rubanée, quartzite et grauwacke métamorphisé). Les batholites calco-alcalins consistent en des plutons intermédiaires et felsiques à pyroxène de 2,78 Ga ($^{2,78\ Ga}\varepsilon_{Nd}$ < +2,7) et de tonalites hyperalumineuses plus récentes (ε_{Nd} < +1,3). Les granitoïdes hyperalumineux tardifs de 2,73 Ga sont isotopiquement évolués ($^{2,725\ Ga}\varepsilon_{Nd}$ +1,6).

[1] Geological Survey of Canada, 601 Booth Street, Ottawa, Ontario K1A 0E8

INTRODUCTION

Geological mapping was initiated in 1994 in the central Minto block to establish the distribution, geological and tectonic setting, and economic potential of Archean granite-greenstone belts (Percival et al., 1995a, b; Lin et al., 1995; Winsky et al., 1995). The Minto block comprises a number of lithologically distinct crustal domains with prominent northwest-trending structural and magnetic fabrics (Percival et al., 1992). Goudalie domain forms a central, north-northwest-trending spine of granite-greenstone terranes characterized by regional magnetic lows, in contrast to the plutonic-dominated Lake Minto and Utsalik domains (Fig. 1b). Percival et al. (1994) proposed that Utsalik and Lake Minto domains represent protocratonic blocks, and the suture separating the two lies in deformed rocks of the Goudalie domain that include depleted mantle-derived oceanic rocks (Skulski et al., 1994).

Geochronological (U/Pb and reconnaissance Sm/Nd) and geochemical data, primarily from metavolcanic and plutonic units from the central Minto block, are used here to define the age of volcanic and plutonic sequences, to examine the relative contribution of mantle and continental crust in their development, and to decipher their tectonic setting. The structural and geological setting of these rocks are discussed in Lin et al. (1995), Percival et al. (1995a), and Percival et al. (1996).

GEOLOGICAL SETTING

The geology of Minto block at the latitude of the Leaf River has been summarized by Percival et al. (1992), Percival and Card (1994), and Percival et al. (1994). The southern Goudalie domain contains the Vizien greenstone belt (Fig. 1b; Percival and Card, 1992; Percival et al., 1993; Skulski et al., 1994; Lin et al., 1995; Skulski and Percival, in press). The oldest unit in the Vizien belt is a 2786 Ma mafic-ultramafic sequence with primitive ε_{Nd} values that is interpreted to have formed in an oceanic plateau environment (Skulski and Percival, in press). This sequence is in fault contact with a 2724 Ma calc-alkaline volcanic arc sequence, and a 2722 Ma bimodal continental tholeiitic sequence which may have formed during marginal basin development (Skulski and Percival, in press). The youngest Vizien rocks consist of <2718 Ma sedimentary rocks that rest unconformably on 2942 Ma tonalite and are overlain by 2697 Ma tholeiitic mafic rocks and a depositional mélange associated with overthrusting of the mafic-ultramafic sequence. Polyphase deformation of the Vizien belt, documented by Lin et al. (1995), affected the <2718 Ma sediments, and was largely over by 2693 Ma.

The southern Lake Minto domain (Fig. 1) consists of largely undeformed sheets of calc-alkaline, arc-related, 2725 Ma pyroxene±hornblende granodiorite and associated mafic plugs (Stern et al., 1994). Peraluminous diatexites were intruded at 2713 Ma. Magmatism ended with the emplacement of late granites at ~2690 Ma. Enclaves of granulite paragneiss, banded iron-formation, and mafic gneiss occur within the various plutonic units (Percival et al., 1992).

Qalluviartuuq belt

The Qalluviartuuq belt (Fig. 1b; Percival et al., 1995a; Winsky et al., 1995) is a north-striking, amphibolite facies, volcanic-dominated belt exposed between northern Lake Qalluviartuuq and southern Payne Lake, with several major branches (Fig. 1b). The Qalluviartuuq belt contains two volcanic sequences. North of Lake Qalluviartuuq, the older sequence includes a volcano-sedimentary sequence of basalts, pelite, and conglomerate intruded by hypabyssal diorite-granodiorite with minor anorthositic gabbro. A zoned diorite-granodiorite pluton whose upper part is cut by hornblende-plagioclase dioritic dykes intrudes the upper part of the older sequence. Resting unconformably on the granodiorite are clastic sediments comprising the base of the younger volcano-sedimentary sequence (Percival et al., 1995a). The sediments are overlain by a sequence of andesitic lapilli tuff and pillowed, epidotized basalts, and ultramafic layers crosscut by a foliated diorite dyke. Northward, along strike, a massive, serpentinized peridotite body of 300 m diameter is in abrupt (intrusive?) contact with the younger greenstones. Winsky et al. (1995) proposed that the volcanic package may be allochthonous with respect to underlying sediments. However, recent mapping of the contact shows no evidence of localized shear at the contact (Percival et al., 1996).

On Payne Lake (Fig. 1b) the greenstone belt contains a volcanic sequence of pillow basalts including aphyric and plagioclase glomeroporphyritic flows that are locally amygdaloidal and interbedded with pillow breccia. These are intruded by equigranular gabbro, and local plagioclase megacrystic sills that grade into anorthositic gabbro. The presence of anorthositic gabbro in both the older sequence north of Lake Qalluviartuuq, and at Payne Lake, suggests that the Payne Lake basalts and gabbros belong to the older sequence. North of Payne Lake, a foliated tonalite is unconformably overlain by monomict and polymict conglomerate and quartz-rich sandstone intruded by gabbro.

Kogaluc-Tasiat belt

The Kogaluc-Tasiat greenstone belt and Payne Lake gneiss belt (Percival et al., 1995a) were originally considered to be part of the Goudalie domain but are now recognized as a northern extension of the Lake Minto domain (Fig. 1; Percival et al., 1995b). Mid-amphibolite schists of the less than 2 km wide Kogaluc belt extend northwards from Lake Canadé to Lake Tasiat (Fig. 1). The Kogaluc-Tasiat belt is sediment-dominated and local preservation of facing criteria indicate that the metasediments locally overlie intermediate metavolcanic rocks. The southern Kogaluc volcanic rocks include plagioclase-phyric andesite interbedded with semi-pelite, and pillowed andesite intruded by diorite sills. These are overlain by pelite, grit, pebble conglomerate, and a lens of quartz-phyric rhyolitic tuff. The central and northern parts of the Kogaluc belt contain silicate- and oxide-facies banded iron-formation. A thick, oxide-facies banded iron-formation lies locally at the interface between metavolcanic and metasedimentary units and is overlain by quartz-rich siltstone.

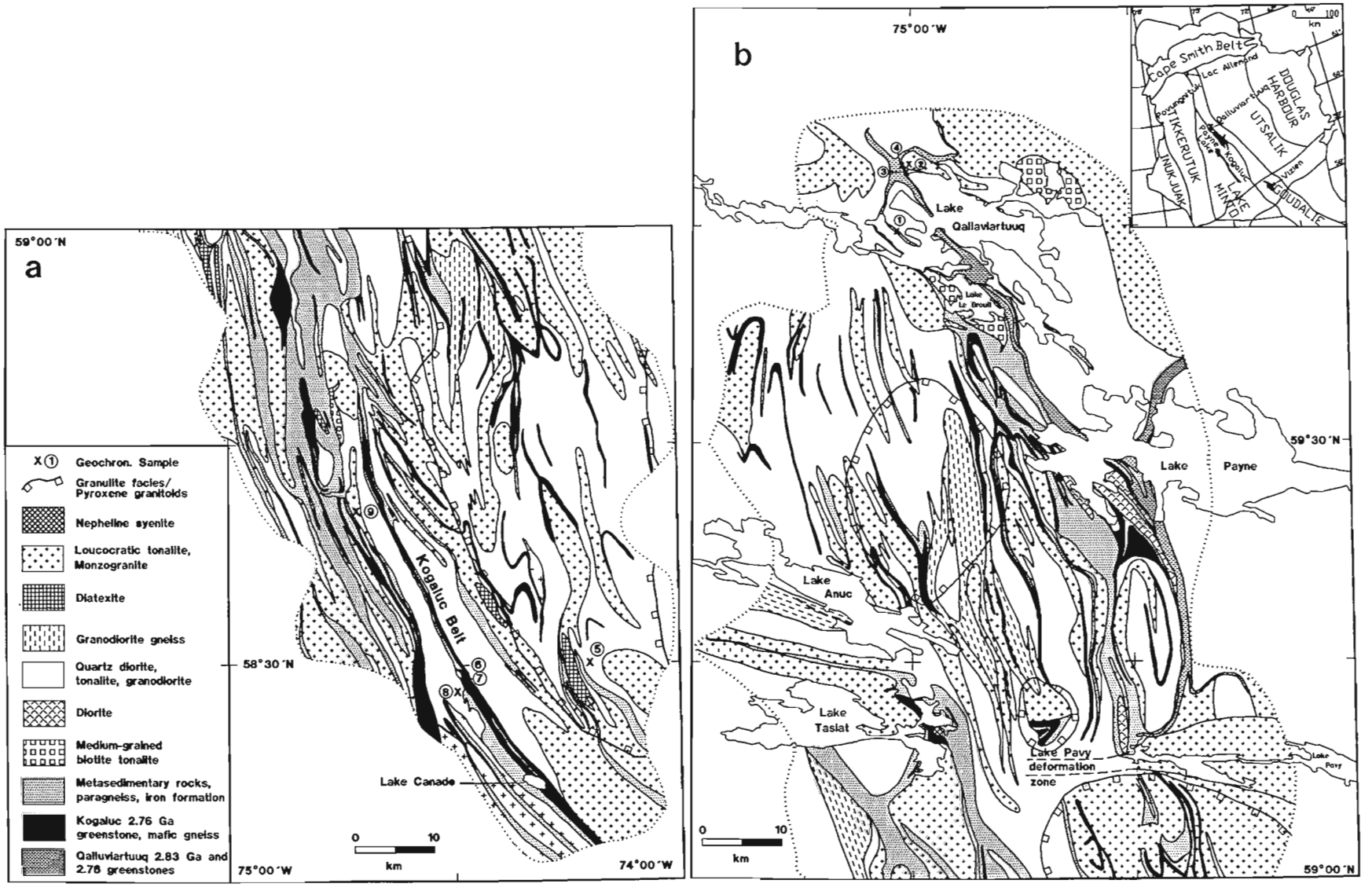

Figure 1. *Compilation map of the central Lake Minto domain and Goudalie domain.* ***a****) southern region (NTS 34J), showing the Kogaluc-Tasiat belt;* ***b****) northern region (NTS 34O) showing the Payne Lake and Qalluviartuuq belts. Geochronological samples are keyed numerically to Tables 1 and 2.*

Granulite to upper amphibolite gneisses and schists that are correlative with lower grade Kogaluc schists flank the Kogaluc belt and extend northwards as the Payne Lake gneisses (Percival et al., 1995a). An inferred tectonic contact separates the Payne Lake gneisses of the eastern Lake Minto domain, from the Qalluviartuuq belt in the Goudalie domain. Relative to the adjacent Qalluviartuuq belt, the Payne Lake gneisses are distinguished by positive aeromagnetic anomalies and the presence of thick silicate-facies banded iron-formation. A small layered intrusion within the gneiss terrane (Percival et al., 1995a) contains a thin, plagioclase-megacrystic gabbro overlain by magnetite-ferrogabbro, norite, and a thick upper sequence of anorthositic gabbro.

Plutonic rocks

Plutonic rocks in the region are subdivided on the basis of crosscutting relationships, presence of tectonic fabrics, petrography, and normative corundum content (where peraluminous rocks have >0.4% normative corundum CIPW). Many parts of the map area contain metaluminous, medium grained, weakly foliated to gneissic, biotite± orthopyroxene±clinopyroxene±hornblende tonalites and quartz diorites and less abundant pyroxene-bearing monzodiorite, granodiorite, and monzogranite. Microcline is rare in the tonalites and quartz diorites, but antiperthite is present and commonly weathers pink-red. Percival et al. (1995a) interpret the pyroxene in this suite as having an igneous origin because pyroxene-bearing plutons crosscut amphibolites, hornblende and biotite commonly overgrow pyroxene, and pyroxene can occur as subhedral phenocrysts. The foliation in these plutons defines the regional tectonic fabric. The plutons contain xenoliths of mafic gneiss, tonalitic gneiss, and rare anorthositic gabbro with discordant fabric, and enclose narrow belts of mafic granulite gneiss, paragneiss±banded iron-formation. Neodymium model ages of three samples of tonalite gneiss vary between 2.86 Ga and 3.1 Ga.

Large enclaves (up to 300 m) of pyroxenite, orthopyroxenite, clinopyroxenite, hornblendite, and hornblende pyroxenite are associated with metaluminous pyroxene-bearing plutons and peraluminous tonalites. A small composite ultramafic body east of the Kogaluc belt contains an orthopyroxenite core comprising orthopyroxene (En 82) megacrysts with anhedral olivine inclusions (Fo 82) and interstitial phlogopite, dolomite, hornblende, magnetite, pyrrhotite, and secondary tremolite. Crosscutting this unit is a pegmatitic vein of megacrystic hornblendite (PBAS-94-150B; see Table 3 below) containing clinopyroxene cores in hornblende megacrysts, and interstitial patches of plagioclase (An 33), biotite, quartz, and magnetite. The outer part of the plug is a hornblende pyroxenite with hornblende megacrysts enclosing clinopyroxene and orthopyroxene (En 75) and interstitial biotite and magnetite. The pyroxenites have similar mafic mineralogy as the metaluminous pyroxene-bearing tonalite-quartz diorite suite and may represent mafic cumulate enclaves (see below).

The biotite±pyroxene-bearing metaluminous plutons are commonly associated with younger, red feldspar tonalites. This suite of peraluminous plutons is weakly foliated, medium- to coarse-grained, and distinguished in the field as leucocratic rocks with red-weathering antiperthite, along with biotite±muscovite±hornblende±clinopyroxene. A suite of foliated peraluminous granodiorites and monzogranites intrude Kogaluc schists and can be traced northward to southern Lake Qalluviartuuq. The major mineral constituents are quartz, microcline, plagioclase, biotite, muscovite, and in pegmatites, garnet and tourmaline. Foliated, metaluminous hornblende+biotite±epidote granodiorites are a minor component of the map area. These plutons are distinguished by the presence of microcline phenocrysts and megacrysts. In places the megacrysts are aligned parallel to the regional tectonic fabric.

A nepheline syenite plug measuring 2 x 3 km occurs in the eastern Lake Tasiat area. The pluton intrudes foliated granodiorite and is cut by a Proterozoic diabase dyke. The nepheline syenite is medium- to coarse-grained and locally shows magmatic layering and a younger tectonic foliation defined by nepheline and biotite. Phases of the pluton vary from leucocratic nepheline syenites and pegmatites with biotite, microcline, plagioclase, nepheline, ilmenite, and apatite, to more melanocratic nepheline syenites containing biotite, aegerine-augite, nepheline, microcline, perthite, plagioclase, with accessory zircon, sphene, apatite, ilmenite, and fluorite.

Massive peraluminous biotite+muscovite monzogranite plutons throughout the map area range from pegmatitic pods to circular plutons 4-5 km in diameter. Some of the larger plutons show a weak igneous foliation along their margins that is locally discordant to the regional tectonic fabric.

GEOCHRONOLOGY

Zircon U-Pb and Pb-Pb ages are presented for nine samples from the central Minto block (Tables 1 and 2; Fig. 2). The zircons were separated from the rock matrix using standard heavy liquid and magnetic methods. Zircons were selected using the light microscope, and then air-abraded following the method of Krogh (1982). Analytical procedures used for U-Pb zircon analysis have been summarized by Parrish et al. (1987), and the treatment of analytical errors follows Roddick (1987) with regression analysis modified after York (1969) and Davis (1982). Isotopic data have been corrected for the measured U and Pb blanks of 0.5-2 pg and 4-20 pg, respectively. Samarium-neodymium data are also presented and the analytical methodology, accuracy, and precision are summarized in Skulski et al. (1994).

Many of the zircon fractions analyzed had low U contents (<100 ppm), which limited our success in analyzing single grains as opposed to multiple grain fractions. Some of the data to be presented below reveal complex discordance patterns, and it is possible that much of the complexity could be due to the mixing of inherited components with magmatic components in the analyses. Complex discordance could also result from multiple episodes of Pb loss. For example, some of the zircons displayed thin rims, interpreted as metamorphic in origin, that are undated in this study but which are possibly 2.67-2.71 Ga based on studies in the southern Minto block (Percival et al., 1992; Stern et al., 1994). Lower intercepts in

many of the plutonic rocks in the Minto block are 1-1.8 Ga, possibly indicative of a Proterozoic metamorphic event that (Percival et al., 1992; Stern et al., 1994). Lower intercepts in affected the rocks. Thus, the complexity in discordance could in some cases be due to the combined effect of Archean, Proterozoic, and younger Pb-loss events.

In this study, in which we present preliminary results and interpretations, we have yet to conduct the detailed grain-scale studies (e.g. backscattered imaging, cathodoluminescence) that would permit a better understanding of the discordance patterns, and allow greater confidence to be placed in the age interpretations. For the difficult samples, we have tried to offer alternative interpretations of the data. The reader is cautioned that in some cases there is no unique age interpretation possible.

Lake Qalluviartuuq geochronology

Four samples of plutonic rocks from the Lake Qalluviartuuq area were collected for U-Pb geochronology (Table 1 and 2; Fig. 1b). These include anorthositic gabbro and biotite granodiorite associated with the early Qalluviartuuq volcanic sequence, a granodiorite cobble from sediments at the base of the younger sequence that unconformably overlie biotite granodiorite, and a diorite dyke that cuts pillowed basalts belonging to the younger sequence.

A sample of anorthositic gabbro was collected from an irregularly shaped pluton (ca. 1 x 2 km) on the northern shore of Lake Qalluviartuuq (QAN-92; Tables 1 and 2; Fig. 2, #1). The pluton is part of a suite of plagioclase-phyric rocks that

Table 1. Description of zircon fractions.

Fract.	Length max.(μm)	Form	Clarity	Colour	Zoning	Inclusions	Cores	Fracture
1) Qalluviartuuq anorthositic gabbro (QAN-92)								
2	300	prism/broken	cloudy	pale pink-brown	yes	opaque	none	many
3	200	equant/broken	moderate	pink-brown	yes	opaque	none	few
2) Qalluviartuuq biotite granodiorite (PBAW-94-290)								
1	<100	equant	clear	colourless-yellow	yes	apatite	none	few
2	<110	equant	moderate	colurless-grey	yes	apatite	none	few
3	<110	prism 1:1.5	moderate	colurless-grey	yes	apatite	yes	few
4	<150	equant	moderate	pink-yellow	yes	apatite	none	few
3) Qalluviartuuq granodiorite cobble (PBAW-94-292)								
1	150	prism 1:2.5	moderate	pale brown	yes	apatite	none	rare
3	110	prism/broken	clear	pale yellow-brown	no	apatite	none	few
4	110	equant	clear	pale yellow-brown	yes	clear	none	few
5	100	prism 1:2	clear	pale yellow	yes	opaque	none	rare
4) Qalluviartuuq diorite dyke (PBAW-94-293)								
1	80	equant	clear	pale pink-tan	yes	apatite	none	few
3	150	prism/broken	clear	colourless-pink	no	apatite	none	few
4	200	rounded	moderate	tan	no	apatite	none	rare
5) Kogaluc tonalite (PBAC-94-113)								
1a	300	prism 1:2.5	clear	colourless-yellow	no	apatite	none	none
1b	350	prism 1:3	clear	colourless-pink	no	apatite	thin rim	rare
1c	230	prism 1:2.5	clear	colourless-yellow	weak	apatite	none	none
2a	200	prism 1:2	clear	colourless-pink	yes	apatite	none	none
2b	200	prism 1:2	clear	colourless-pink	yes	apatite	thin rim	none
6) Kogaluc quartz feldspar porphyry sill (PBAC-94-158)								
1	250	prism/broken	clear	pink-brown	yes	none	thin rim	many
2	250	prism 1:2	clear	pale pink	yes	opaque	none	rare
3	300	prism/broken	moderate	brown-pink	yes	opaque	yes	few
4	250	dipyramidal	moderate	pink-brown	yes	none	thin rim	few
5	150	equant	moderate	colourless-pink	yes	none	none	rare
7) Kogaluc rhyolitic tuff (SNB-93-94)								
1b	200	prism 1:4	clear	pale pink	yes	opaque	none	rare
2b	200	prism 1:2	moderate	pale pink-brown	no	none	none	rare
3b	175	prism/broken	moderate	pink-brown	weak	small	none	none
4b	140	prism 1:2	clear	pink-brown	yes	none	none	few
8) Kogaluc granodiorite (SNB-93-95)								
1c	200	prism/broken	clear	pale pink	yes	apatite	thin rim	none
5a	200	prism/broken	moderate	pink core	yes	apatite	clear rim	few
8a	150	equant 1:1.5	moderate	reddish-brown	yes	fluid	large	rare
9) Kogaluc monzogranite (SNB-93-240)								
1	290	prism 1:2.5	clear	pale mauve	no	opaque	large	none
2	150	prism 1:2	clear	pale mauve	no	none	none	none
3	180	equant	moderate	pale mauve	no	opaque	none	few
A	300	prism 1:3	cloudy	pale yellow	yes	opaque	none	none

includes glomeroporphyritic sills and pillow basalts found in the Lake Qalluviartuuq-western Payne Lake area. The anorthositic gabbro sample is a mesocumulate containing unaltered cumulus plagioclase (~An 65; up to 2 cm in length), and intercumulus magnetite and secondary hornblende, and epidote after pyroxene. The hornblende defines a prominent stretching lineation. Accessory intercumulus zircon occurs as inclusions in hornblende and is surrounded by pleochroic radiation halos. Two multi-grain zircon fractions were abraded and these include broken, pale pink-brown fractured prisms (up to 300 µm; fraction 2, Table 1, #1), and broken, pale yellow-brown, equant zircon (up to 200 µm; fraction 3). Fraction 2 is slightly reversely discordant and has a $^{207}Pb/^{206}Pb$ age of 2832 ± 1.7 Ma (Table 2; Fig. 2, #1). Fraction 3 is discordant (1.6%) and a chord passing through fractions 2 and 3 has a lower intercept age of 1766 Ma, possibly reflecting episodic lead loss. With the few data available at present, the age of the anorthositic gabbro is interpreted to be 2.83 Ga.

A sample of medium grained biotite granodiorite was collected from the older sequence beneath the northern Lake Qalluviartuuq unconformity (PBAW-94-290; Tables 1 and 2; Fig. 2, #2). The sample was collected from the upper part of a zoned diorite-granodiorite hypabyssal pluton that intrudes the upper part of the older sequence. The foliated pluton contains biotite, epidote, quartz, plagioclase, microcline, and accessory apatite, sphene, and zircon. Four multi-grain fractions of zircon were abraded and include <110 µm clear, colourless to yellow equant and stubby prisms (fractions 1-3), and a fourth fraction of pink-yellow, <150 µm equant crystals (Table 1). Possible inherited cores were observed in fraction 3. Fractions 1 and 2 are concordant and overlap within error. The $^{207}Pb/^{206}Pb$ age of fraction 1 is 2831 ± 1.2 Ma and

Table 2. U-Pb zircon analytical data and interpretation of results.

Fraction[a]	Weight µg	U ppm	Pb[b] ppm	Pb[c] pg	$^{206}Pb/^{204}Pb$[d]	^{206}Pb %	$^{206}Pb/^{238}U$[e] (±1σ)	$^{207}Pb/^{235}U$[e] (±1σ)	$^{207}Pb/^{206}Pb$[e] (±1σ)	$^{207}Pb/^{206}Pb$ (±2σ Ma)	Disc %
1) Qalluviartuuq anorthositic gabbro (QAN-92; z3800; 59°44'6.4"N 75°1'26.4"W)											
2: 7, NM5°	14	76	59	25	1421	26.2	0.5531±.10	15.308±.12	0.20073±.05	2832 ± 1.7	-0.3
3: 11, NM5°	11	58	40	7	2806	19.8	0.5342±.13	14.467±.14	0.19640±.04	2797 ± 1.4	1.6
2) Qalluviartuuq biotite granodiorite (PBAW-94-290; z3819; 59°48'52.2"N 75°1'32.7"W)											
1: 10, NM2°	10	74	49	12	2193	15.0	0.5510±.12	15.235±.13	0.20053±.04	2831 ± 1.2	0.1
2: 2, NM2°	6	48	32	30	332	15.6	0.5535±.26	15.281±.36	0.20023±.24	2828 ± 7.7	-0.5
3: 6, NM2°	7	80	54	5	3800	15.6	0.5497±.14	15.225±.14	0.20086±.04	2833 ± 1.5	0.4
4: 7, M2°	5	72	49	6	1983	16.1	0.5494±.19	15.262±.19	0.20147±.05	2838 ± 1.5	0.7
3) Qalluviartuuq granodiorite cobble (PBAW-94-292; z3943; 59°48'52.2"N 75°1'32.7"W)											
1: 5, M0°	9	116	69	5	6674	10.2	0.5224±.09	13.740±.10	0.19077±.03	2749 ± 1.0	1.8
3: 5, NM0°	5	57	38	8	1267	15.0	0.5462±.17	14.881±.17	0.19760±.06	2806 ± 1.8	-0.1
4: 3, NM0°	7	125	78	10	2910	12.1	0.5367±.10	14.297±.11	0.19320±.03	2770 ± 1.1	0.0
5: 4, NM0°	4	141	87	6	3354	10.8	0.5364±.12	14.267±.13	0.19291±.04	2767 ± 1.1	-0.1
4) Qalluviartuuq diorite dyke (PBAW-94-293; z3818; 59°48'58"N 75°2'0.4"W)											
1: 34, NM5°	5	79	49	9	1433	11.9	0.5316±.14	13.820±.15	0.18853±.05	2729 ± 1.6	-0.9
3: 5, NM5°	5	40	26	5	1284	12.8	0.5511±.25	15.197±.25	0.20000±.06	2826 ± 1.9	-0.1
4: 1, NM5°	5	83	54	6	2344	13.1	0.5539±.14	15.369±.14	0.20123±.05	2836 ± 1.5	-0.2
5) Kogaluc tonalite (PBAC-94-113; z3683; 58°29'46.7"N 74°12'46.5"W)											
1a: 5, NM2°	12	56	35	11	1997	10.8	0.5425±.12	14.711±.12	0.19667±.06	2799 ± 1.9	0.2
1b: 3, NM2°	11	61	38	9	2665	10.6	0.5419±.12	14.610±.12	0.19553±.04	2789 ± 1.3	-0.1
1c: 10, NM2°	25	57	35	9	5491	10.3	0.5400±.10	14.574±.11	0.19573±.04	2791 ± 1.2	0.3
2a: 11, NM2°	17	91	56	16	3238	9.6	0.5380±.09	14.443±.10	0.19468±.04	2782 ± 1.2	0.3
2b: 17, NM2°	8	79	49	17	1243	10.3	0.5390±.12	14.496±.12	0.19506±.05	2785 ± 1.8	0.3
6) Kogaluc quartz feldspar porphyry sill (PBAC-94-158; z3815; 58°28'30"N 74°29'30"W)											
1: 5, NM-1°	5	173	101	10	2914	7.6	0.5248±.10	13.856±.12	0.19150±.03	2755 ± 1.1	1.6
2: 10, NM-1°	5	152	86	5	4419	7.1	0.5152±.11	13.536±.12	0.19058±.04	2747 ± 1.3	3.0
3: 2, NM-1°	9	88	52	5	5138	8.7	0.5306±.10	13.991±.11	0.19124±.03	2753 ± 1.1	0.4
4: 4, NM-1°	6	57	33	6	1616	6.5	0.5325±.18	14.093±.18	0.19194±.05	2759 ± 1.6	0.3
5: 3, NM-1°	7	65	38	8	2067	7.8	0.5252±.14	13.826±.14	0.19093±.05	2750 ± 1.3	1.3
7) Kogaluc rhyolitic tuff (SNB-93-94; z3263; 58°28'30"N 74°29'30"W)											
1b: 12, NM2°	4	205	122	5	4698	8.0	0.5326±.10	14.094±.11	0.19191±.03	2759 ± 1.1	0.3
2b: 5, NM2°	3	92	54	5	1753	5.3	0.5439±.13	14.521±.13	0.19362±.05	2773 ± 1.7	-1.2
3b: 11, NM2°	3	173	104	7	2928	8.6	0.5364±.10	14.297±.11	0.19332±.04	2771 ± 1.2	0.1
4b: 9, NM2°	5	102	63	7	2122	9.9	0.5403±.12	14.476±.13	0.19432±.04	2779 ± 1.4	-0.2
8) Kogaluc granodiorite (SNB-93-95; z3270; 58°28'19.9"N 74°28'50"W)											
1c: 2, M2°	5	68	43	7	1512	15.5	0.5250±.13	13.675±.14	0.18890±.05	2733 ± 1.6	0.5
5a: 1, M2°	7	151	91	2	1617	14.9	0.5007±.15	13.016±.15	0.18855±.05	2730 ± 1.6	5.0
8a: 1, M2°	2	230	134	2	880	7.7	0.5244±.22	13.664±.21	0.18899±.08	2733 ± 2.6	0.7
9) Kogaluc monzogranite (SNB-93-240; z3323; 58°39'52.6"N 74°58'16.4"W)											
1: 1, NM1°	2	294	143	15	1163	3.5	0.4645±.45	11.478±.48	0.17922±.09	2646 ± 2.9	8.5
2: 3, NM1°	1	68	40	8	311	11.6	0.5134±.49	13.267±.49	0.18742±.26	2720 ± 8.6	2.2
3: 2, NM1°	2	102	65	18	470	15.6	0.5256±.17	13.625±.25	0.18800±.16	2725 ± 5.2	0.1
A: 3, NM1°	8	2301	1147	54	10900	0.9	0.4877±.10	11.982±.11	0.17819±.03	2636 ± 0.9	3.5

notes: a: fraction, number of abraded grains analyzed, NM nonmagnetic and M magnetic at side slope indicated; b: radiogenic Pb; c: total common Pb in analysis in picograms d: corrected for Pb spike and fractionation; e: corrected for blank Pb and U, common Pb and mass fractionation. Samples are located in Figure 1.

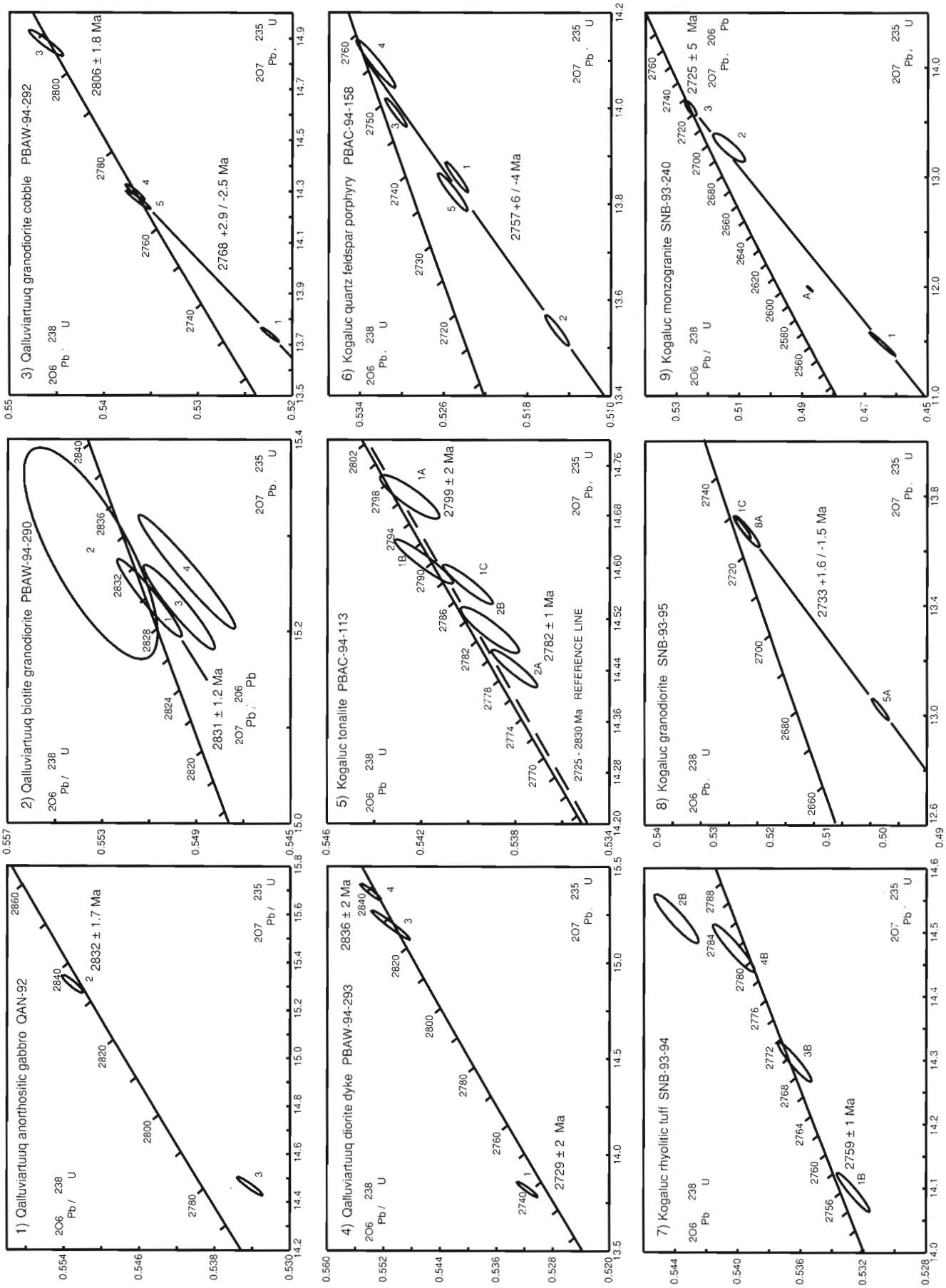

Figure 2. *Concordia diagrams showing U-Pb zircon data from plutons and volcanic rocks in the central Minto block. Error ellipses are at the 2σ level.*

relative to fraction 2, provides a relatively precise estimate of the crystallization age of the pluton (Fig. 2, #2). Fraction 3 is slightly discordant and overlaps the error ellipse of fraction 2. Fraction 4 is discordant and has a $^{207}Pb/^{206}Pb$ age of 2838 ± 1.5 Ma. A slightly older age for fraction 4 could be the result of a small amount of inherited cores, although these were not visible through the optical microscope. The small spread in $^{207}Pb/^{206}Pb$ ages of fractions 1, 3, and 4 (2831-2838 Ma) does not correlate with their radiogenic Pb contents (Table 1). Therefore, notwithstanding the fortuitous case in which inherited and magmatic zircons have similar Pb contents, the spread in $^{207}Pb/^{206}Pb$ ages of all three fractions does not appear to reflect a mixing relationship between inherited and magmatic zircon components. The crystallization age of the pluton is interpreted to be 2831 ± 1.2 Ma, the $^{207}Pb/^{206}Pb$ age of fraction 1, and is similar to the preliminary age estimate of the anorthositic gabbro.

Polymict orthoconglomerate overlies the 2832 Ma biotite granodiorite, and a clast (20 cm in length) of medium grained granodiorite (PBAW-94-292; Tables 1 and 2; Fig. 2, #3) was collected to constrain the age of the younger sequence. The foliated granodiorite contains biotite, hornblende, plagioclase, K-feldspar, and accessory apatite and zircon. Four multi-grain fractions of zircon were abraded and include equant yellow-brown zircons (~110 μm; fraction 4, Table 1) and prismatic pale yellow to pale brown zircons (100-150 μm, fractions 1 and 5). Fraction 3 consists of pale yellow-brown, broken prisms (about 100 μm fragments) and has notably lower U content (57 ppm) than fractions 1, 4, and 5 (116-141 ppm; Table 2). Fractions 4 and 5 are concordant and along with fraction 1 (1.8% discordant) define a discordia with an upper intercept crystallization age of 2768 +2.9/-2.5 Ma (MSWD = 2.3) and a lower intercept age of 1395 Ma (Fig. 2, #3). Fraction 3 is concordant and has a $^{207}Pb/^{206}Pb$ age of 2806 ± 1.8 Ma likely reflecting inclusion of inherited zircons. The age of clastic sediments resting unconformably on 2831 Ma granodiorite and overlying pillowed volcanic rocks of the younger sequence is less than 2768 Ma.

A foliated, fine grained diorite dyke cuts the younger sequence north of Lake Qalluviartuuq (PBAW-94-293; Tables 1 and 2, Fig. 2, #4). The diorite contains secondary hornblende, cummingtonite, plagioclase, quartz, and accessory magnetite, zircon, and apatite. Three fractions of zircon were separated from a sample of the dyke. Fraction 1 consists of small (80 μm), equant, euhedral, clear pale pink zircons with colour zoning (Table 1). Fraction 3 consists of broken, clear, colourless prisms and fraction 4 is a single 200 μm rounded, tan coloured zircon. Fractions 3 and 4 are concordant and have $^{207}Pb/^{206}Pb$ ages of 2826 ± 2 Ma and 2836 ± 2 Ma and are interpreted to be inherited grains possibly derived from underlying 2832 Ma granodiorite (Table 2; Fig. 2, #4). Fraction 1 is slightly discordant and has a $^{207}Pb/^{206}Pb$ age of 2729 ± 2 Ma. Since it is possible that fraction 1 included a small amount of inherited cores, this result is interpreted as the maximum crystallization age. A suite of chemically similar mafic to felsic, weakly foliated dykes cut late granitoid plutons (Percival et al., 1995a). The age of the younger Qalluviartuuq sequence is constrained by the granodiorite cobble and the diorite dyke to be <2.768 Ga and >2.73 Ga.

Geochronology of the Kogaluc greenstone belt and adjacent plutons

Five samples were collected from the Kogaluc greenstone belt and surrounding plutons (Tables 1 and 2; Fig. 1a). These include: orthopyroxene tonalite east of the Kogaluc belt, rhyolitic tuff and quartz-feldspar porphyry from the southern Kogaluc belt, foliated two-mica granodiorite that cuts the western margin of the Kogaluc belt, and massive monzogranite that cuts foliated two-mica granodiorite.

A sample of weakly foliated orthopyroxene tonalite was collected southeast of the Kogaluc belt (PBAC-94-113; Tables 1 and 2; Fig. 2, #5). The pluton forms part of the regionally extensive metaluminous pyroxene-bearing tonalite-quartz diorite suite. The rock is medium grained and contains quartz, plagioclase, antiperthite, trace amounts of orthopyroxene and biotite, secondary epidote and chlorite, and accessory zircon and apatite. Five multi-grain fractions of zircon were abraded (Table 1). These zircons range in size from 200 to 350 μm and share common prismatic habit, high clarity, apatite inclusions, and colourless to pale yellow-pink colour. Fractions 1b and 2b have thin rims developed on the tips of zircon that were subsequently removed during abrasion. Fractions 1a, 1b, and 2b are concordant and fractions 2a and 1c are only slightly discordant (0.3%; Table 2; Fig. 2, #5). The zircon fractions encompass a range of ages from 2799 ± 2 Ma (1a) to 2782 ± 1 Ma (2a). Fractions 1a and 1b include larger crystals (300-350 μm) with slightly lower U contents (56-61 ppm) relative to fractions 2b and 2a (200 μm; 79-91 ppm U).

The spread in ages can be explained in number of ways. Pyroxene-bearing granodiorites in the Lake Minto domain near Leaf River have zircon ages of 2725 ± 5 Ma (Percival et al., 1992; Stern et al., 1994). Mixing between zircons of this age and inherited zircons as old as 2830 Ma (Qalluviartuuq biotite granodiorite) could account for the spread in zircon ages (reference line in Fig. 2, #5). However, inherited zircon cores are neither obvious under the optical microscope, nor do the data plot near either of the end members. The spread in $^{207}Pb/^{206}Pb$ ages of fractions 1b, 2b, and 2a could also record a Paleoproterozoic lead-loss event. For example, fractions 1b, 2b, and 2a lie on a chord with a lower intercept age of 1882 Ma. This lower intercept is just outside of the range of lower intercept ages calculated for central Minto plutons (176-1766 Ma; this study). The preferred interpretation is that the tonalite has a maximum crystallization age of 2.78 Ga and contains small amounts of inherited zircons that are 2.80 Ga or older. This interpretation is supported by Sm-Nd isotopic data on the tonalite and other members of the metaluminous suite. The tonalite has a $^{2.78\ Ga}\varepsilon_{Nd}$ value of +2.5 and depleted mantle Nd model age (T_{DM}; DePaolo, 1980) of 2.78 Ga (Table 3) reflecting the juvenile nature of its source. Four widely-spaced samples from the metaluminous suite (including pyroxene tonalite and granodiorite), with $\varepsilon_{Nd} \geq +1.9$ have T_{DM} ages that range from 2.82 Ga to 2.75 Ga indicating abundant juvenile metaluminous plutonism with a mean age of 2.79 Ga.

A 10 x 10 m ultramafic body east of the Kogaluc belt associated with metaluminous pyroxene-bearing plutons was sampled for Sm-Nd age dating. Mineral separates of plagioclase and hornblende were obtained from a pegmatitic hornblendite at the margins of the ultramafic body. A five point isochron including orthopyroxenite, hornblende pyroxenite, and pegmatitic hornblendite whole rock samples (PBAS-94-150A, -150B, and -150C; Table 3) and hornblende and plagioclase separates from the pegmatite, result in an imprecise age of 2700 ± 87 Ma (MSWD = 10). This age, while imprecise, is barely within error of the maximum age estimate of orthopyroxene tonalite (2782 Ma) and supports the conclusion that the pyroxenite bodies may represent ultramafic cumulate enclaves derived from the pyroxene-bearing tonalite and quartz diorite suite.

A less than 50 m thick quartz-feldspar porphyry (QFP) sill from the central Kogaluc belt intrudes intermediate volcanic rocks. A sample for U-Pb dating (PBAC-94-158; Tables 1 and 2, Fig. 2, #6) contains recrystallized quartz and plagioclase phenocrysts in a foliated groundmass of secondary muscovite, biotite, microcline, plagioclase, tourmaline, and accessory zircon. Five fractions of zircon were abraded and

Table 3. Representative chemical analyses.

	PBAW 94290 GDI	PBAW 94293 DIO	PBAC 94113 TON	PBAC 94158 QFP	SNB 93094 RHY	SNB 93095 MGDI	SNB 93240 MGNT	PBAS 94150A OPX	PBAS 94150B HNB	PBAS 94150C PYR	PBAS 94502 NESYE	SNB 93131 AND	PBAS 94763 BAS
SiO_2	66.62	57.63	67.68	74.99	73.29	72.93	79.25	40.67	44.84	49.59	58.06	56.34	48.02
TiO_2	0.73	0.54	0.50	0.11	0.24	0.22	0.03	0.30	0.83	0.33	0.37	0.80	1.02
Al_2O_3	15.16	18.38	17.17	13.68	15.59	14.88	12.32	4.55	10.38	5.34	21.56	15.95	15.73
Fe_2O_3	0.77	1.05	0.46	0.31	0.31	0.31	0.04	2.96	1.82	1.21	0.60	0.85	2.19
MgO	1.92	4.16	0.67	0.17	1.11	0.44	0.00	30.11	14.36	16.00	0.53	2.30	5.29
FeO	3.93	5.38	2.33	1.59	1.58	1.58	0.21	15.07	9.27	6.19	3.06	4.32	11.19
MnO	0.07	0.10	0.02	0.02	0.02	0.04	0.00	0.24	0.17	0.16	0.09	0.08	0.24
CaO	3.18	7.31	4.21	1.20	2.18	1.80	1.58	2.70	12.27	17.31	0.40	13.36	11.96
Na_2O	4.06	4.55	5.17	4.55	0.99	4.23	3.32	0.87	1.58	1.06	8.90	1.94	2.42
K_2O	2.64	0.14	0.84	2.61	2.78	3.32	3.32	0.54	1.47	0.38	5.30	0.41	0.40
P_2O_5	0.18	0.12	0.10	0.04	0.11	0.10	0.04	0.06	0.73	0.14	0.10	0.11	0.08
LOI	0.60	0.37	0.83	0.59	1.71	0.27	0.15	1.50	1.06	1.28	0.86	3.20	1.07
Th	7.0	1.6	0.35	12	3.6	9.7	2.5	0.73	2.9	0.74	0.26	2.7	0.25
Sc	15	16	7	1	4	5	7	15	56	68	0	20	48
Cr	14	40	0	18	6	8	0	50	318	2196	0	54	116
Ni	27	75	10	43	26	34	0	351	109	134	0	54	138
Co	27	31	55	36	5	4	1	166	69	45	17	16	70
V	84	122	66	8	34	28	26	100	260	171	15	146	305
Y	23	11	2.9	9.6	3.3	7.8	2.6	5.2	16	9.0	0.48	3.3	26
Zr	270	100	110	110	120	120	44	44	71	54	200	90	51
Hf	6.8	2.4	2.3	3.2	3.1	3.4	1.4	1.0	2.0	1.2	3.7	2.2	1.4
Nb	8.3	3.1	2.7	9.3	2.8	7.8	0.68	0.99	2.3	0.82	43	4.6	2.2
La	38	12	12	39	15	17	10	6.7	22	9.3	0.89	14	2.6
Ce	85	28	24	73	30	36	14	17	53	23	2.5	31	7.6
Pr	11	3.4	2.6	7.5	3.4	3.7	1.2	2.2	7.3	3.3	0.37	3.9	1.2
Nd	40	14	9.8	24	13	14	3.8	9.8	33	15	1.3	16	6.3
Sm	7.0	2.7	1.5	3.3	2.1	2.3	0.53	1.9	6.6	3.3	0.23	3.4	2.1
Eu	1.1	0.80	0.71	0.61	0.51	0.44	0.64	0.55	1.8	0.90	0.02	1.0	0.80
Gd	5.2	2.4	1.0	2.2	1.3	1.6	0.40	1.6	5.3	2.7	0.14	3.5	3.5
Tb	0.73	0.35	0.12	0.29	0.14	0.24	0.06	0.19	0.64	0.34	<0.02	0.52	0.63
Dy	4.0	1.9	0.57	1.5	0.64	1.3	0.36	0.97	3.1	1.7	0.09	2.9	4.0
Ho	0.76	0.37	0.09	0.28	0.10	0.25	0.06	0.18	0.55	0.30	<0.02	0.56	0.87
Er	2.0	0.99	0.23	0.76	0.24	0.72	0.20	0.45	1.3	0.73	0.06	1.5	2.4
Tm	0.34	0.14	0.02	0.13	0.04	0.13	0.04	0.06	0.18	0.11	<0.02	0.22	0.36
Yb	2.1	1.1	0.22	0.87	0.27	0.79	0.29	0.45	1.2	0.73	0.10	1.6	2.8
Lu	0.32	0.17	0.03	0.14	0.04	0.12	0.05	0.07	0.18	0.11	0.02	0.24	0.43
age(Ma)*	2830	2725	2780	2760	2760	2725	2725	2780	2780	2780	2725	2760	2830
ϵ_{Nd}	2.8	1.9	2.6	1.4	0.1	-1.5	0.1	1.9	1.1	1.1	2.0	-0.1	2.4
TDM	2793	2768	2778	2788	2934	3017	2871	2826	2907	2908	2760		
$\frac{147Sm}{144Nd}$	.1082	.1094	.0924	.0832	.1050	.0995	.0750	.1207	.1256	.1325	.0913	.1271	.2135
$\frac{143Nd}{144Nd}$**	.511128	.511166	.510850	.510676	.510974	.510809	.510454	.511337	.511383	.511515	.510844	.511366	.513075

* age used for calculating ϵ_{Nd}, ** measured.
note: analytical methods described in Skulski et al. (1994). Abbreviations are as follows: GDI granodiorite; DIO diorite dyke; TON orthopyroxene tonalite; QFP quartz feldspar porphyry; RHY rhyolitic tuff; MGDI muscovite granodiorite; MGNT muscovite granite; OPX orthopyroxenite; HNB megacrystic hornblendite; PYR hornblende pyroxenite; NESYE nepheline syenite; AND andesite; and BAS basalt.

include: 1) broken pink-brown prisms with thin clear rims; 2) small (≤100 μm) pale pink prisms; 3) two broken, brownish-pink prism fragments with thin rims; 4) pink-brown bipyramidal zircon with thin rims; and 5) pale pink bipyramidal zircons (Table 1). The thin clear rims found on zircons in fractions 1, 3, and 4 are interpreted to reflect the growth of zircon during amphibolite grade metamorphism, and were largely removed during abrasion. Fraction 4 is concordant and all five fractions are scattered around a chord (MSWD = 19) with a lower intercept age of 612 Ma and an upper intercept age of 2757+6/-4 Ma (Fig. 2, #6). The scatter in the data could reflect either multistage lead loss, or alternatively the range in $^{207}Pb/^{206}Pb$ ages from 2759 Ma to 2750 Ma (fractions 5 and 4; Table 2) could be the result of zircon inheritance. Since the rock has a relatively primitive Nd isotopic composition ($^{2.76\,Ga}\varepsilon_{Nd} = +1.4$; Table 3), it is unlikely that it recycled large amounts of older crust. Therefore, the range of $^{207}Pb/^{206}Pb$ ages from 2759 Ma to 2750 Ma provides a reasonable bracket of the crystallization age of the porphyry, and youngest Kogaluc volcanism.

A sample of quartz-phyric rhyolitic tuff was collected from the southern Kogaluc belt (SNB-93-94; Tables 1 and 2; Fig. 2, #7). The tuff comprises a 50 x 500 m lens within pelites and grits. It is foliated and contains recrystallized phenocrysts of quartz, in a matrix of secondary muscovite, biotite, sillimanite, andalusite, quartz, hornblende, tourmaline, pyrite, and accessory zircon. Four multi-grain fractions of zircon were extracted from the rock. These include pink-brown prismatic crystals with aspect ratios of 1:2 to 1:4, and lengths ranging from 140 μm to 200 μm (Table 1). Fractions 4b, 3b, and 1b are concordant and span a range of $^{207}Pb/^{206}Pb$ ages from 2779 ± 1 Ma (4b) to 2759 ± 1 Ma (1b; Table 2; Fig. 2, #7). This range of ages likely reflects various detrital zircon components, and therefore, deposition of the tuff must have been after 2759 ± 1 Ma. This maximum age estimate falls within the estimated range of values bracketing the crystallization age of the quartz-feldspar porphyry sill in the central Kogaluc belt.

A peraluminous biotite+muscovite granodiorite that intrudes the southwestern margin of the Kogaluc belt was sampled (SNB-93-95; Tables 1 and 2; Fig. 2, #8). The pluton is foliated, coarse grained, and composed of quartz, plagioclase, microcline, biotite, muscovite, and accessory magnetite, zircon, and apatite. Three fractions of zircon were abraded. Fraction 1c consists of a 200 μm prism with a thin rim. Fraction 8a is a single zircon with a thin rim that was abraded off. Fraction 5a is a single large broken prism tip with a thin clear rim. The thin zircon rims, eliminated from the analyzed grains, may have formed during amphibolite metamorphism accompanying development of a foliation in the pluton. The three abraded fractions lie on a chord with a lower intercept age of 176 Ma, and an upper intercept age of 2733 ± 2 Ma (MSWD = 0.3), interpreted to be the crystallization age of the granodiorite (Fig. 2, #8).

In the central Kogaluc belt, foliated peraluminous granodiorite is intruded by massive monzogranite. A sample of monzogranite was collected for zircon U-Pb dating (SNB-93-240; Tables 1 and 2; Fig. 2, #9). The monzogranite is composed of quartz, microcline, plagioclase, biotite, muscovite, and accessory zircon and apatite. Four fractions of zircon were abraded. Fractions 1 (single zircon) and 2 are clear, pale mauve prismatic crystals (150-290 μm). A thin rim on fraction 1 was removed during abrasion. Fraction 3 consists of equant zircons of moderate clarity and pale mauve colour. Fraction A consists of long prisms (1:3 aspect ratio, 300 μm length) that are cloudy and are pale yellow. Fraction A is discordant (3.5%), has a very high U content (2301 ppm; Table 3), and must have sustained lead loss at a different time than the other grains. Fractions 1, 2, and 3 define a chord with an imprecise U/Pb upper intercept age of 2727 +10/-9 Ma (MSWD = 2.0; Fig. 2, #9). Fraction 3 is concordant with a $^{207}Pb/^{206}Pb$ age of 2725 ± 5 Ma and is interpreted to be the best estimate of the crystallization age of the monzogranite consistent with field relations.

GEOCHEMISTRY OF VOLCANIC AND SEDIMENTARY ROCKS

The chemical and Nd isotopic composition of the volcanic rocks are used here to determine the extent of crustal reworking and to help constrain their tectonic settings. Aphyric basalts and plagioclase megacrystic pillow basalts from the older sequence at Payne Lake and metabasalts from northern Lake Qalluviartuuq are enriched in Fe and therefore tholeiitic (Fig. 3). The most primitive tholeiitic basalt analyzed has 8.1% MgO but has low Ni abundances (162 ppm), and is too Fe-rich to have been in equilibrium with upper mantle olivine. Trace element profiles reveal that tholeiitic basalts and Qalluviartuuq anorthositic gabbro are depleted in incompatible elements including La, Nb, and Th (Fig. 4). The Payne Lake tholeiites have positive $^{2.83\,Ga}\varepsilon_{Nd}$ values of +2.4 to +3.8 (Table 3) reflecting derivation from Archean depleted mantle. The 2831 Ma biotite granodiorite pluton within the older sequence is calc-alkaline, has a low $^{147}Sm/^{144}Nd$ value, positive $^{2.83\,Ga}\varepsilon_{Nd}$ of +2.3, and a depleted mantle Nd model age (T_{DM}; Table 3) of 2.79 Ga that is close to the U/Pb crystallization age (Table 3).

The Qalluviartuuq conglomerate is overlain by quartz-rich sandstone. A similar association of older tonalitic basement, conglomerate, and quartz-rich sandstone occurs around Payne Lake. Two samples of quartz-rich sandstone have low $^{147}Sm/^{144}Nd$ values, positive $^{2.83\,Ga}\varepsilon_{Nd}$ (+2.0 and +1.8), and T_{DM} ages of 2.86 Ga and 2.85 Ga. The Nd model age data suggest that the sources of the sediments were dominantly juvenile and similar in age and isotopic composition to biotite granodiorites described to the north.

The younger sequence includes peridotite, basalt, andesite, and diorite characterized by low Fe contents typical of calc-alkaline rocks (Fig. 3). With increasing differentiation the calc-alkaline sequence shows a progressive enrichment in light rare-earth elements (LREE) and Th relative to the heavy REEs (HREE) and Y (Fig. 4). The calc-alkaline rocks are depleted in Nb relative to both Th and La. The $^{2760Ma}\varepsilon_{Nd}$ values of cal-alkaline basalt and peridotite are +1.9 and +1.7, indicating derivation from an isotopically primitive mantle source (Table 3).

Kogaluc calc-alkaline volcano-plutonic rocks include diorite, andesite, and quartz-phyric rhyolite (Fig. 3). With increasing differentiation the sequence is characterized by progressive enrichment in LREEs and Th relative to the HREEs and Y (Fig. 4). All of the rocks show a prominent enrichment in La and Th relative to Nb. Epsilon Nd values at 2760 Ma range from -0.1 to +1.6 and do not vary systematically with SiO_2 content (Table 3). Kogaluc calc-alkaline rocks can be distinguished from those at Qalluviartuuq by their lack of mafic calc-alkaline rocks and their lower ε_{Nd} values. Samples of quartz-rich siltstone from the southern and northern Kogaluc belt have low $^{147}Sm/^{144}Nd$ values and T_{DM}

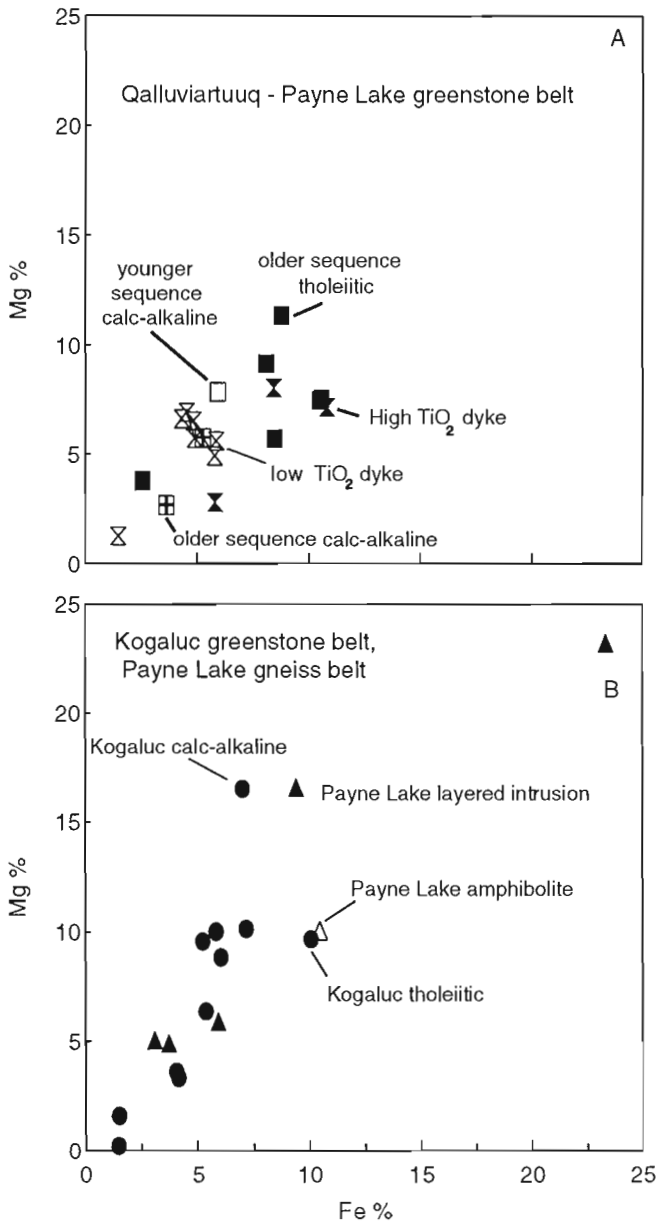

Figure 3. *Fe versus Mg (cation %) diagram of* ***A)*** *Qalluviartuuq-Lake Payne belts and* ***B)*** *Kogaluc-Payne Lake gneisses.*

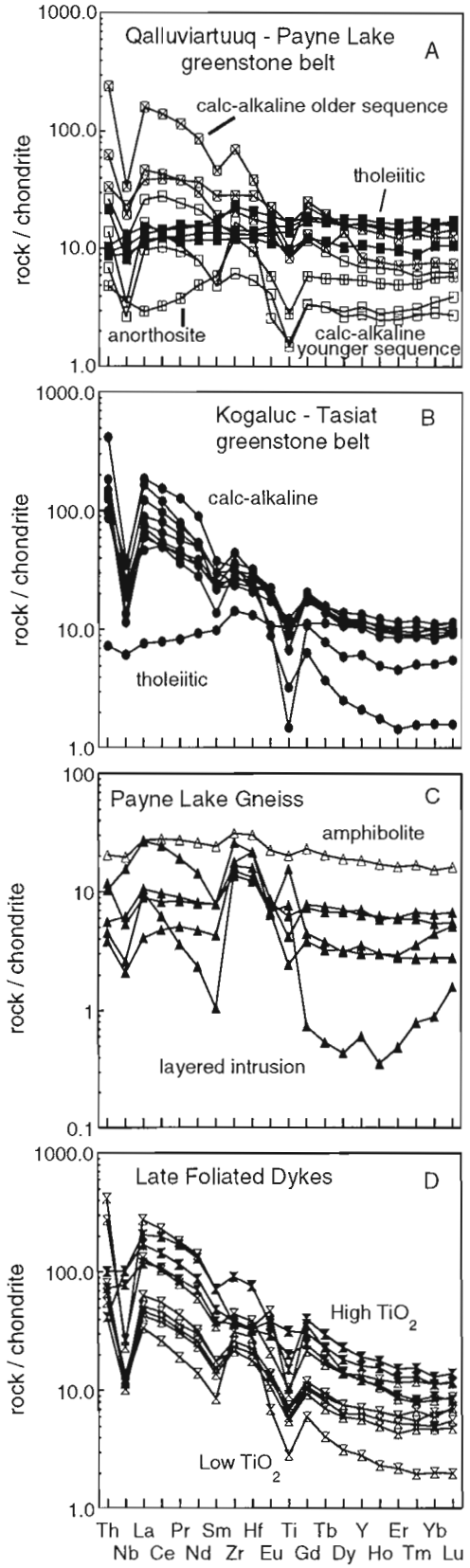

Figure 4. *Chondrite normalized trace element diagram of* ***A)*** *Qalluviartuuq-Payne Lake greenstone belt;* ***B)*** *Kogaluc greenstone belt;* ***C)*** *Payne Lake gneiss belt; and* ***D)*** *late foliated dykes.*

model ages of 2.93 Ga and 2.83 Ga respectively. These data indicate variable contributions from older crust either as intact source areas, or through the erosion of crustally-derived magmatic rocks.

A tholeiitic basalt from the northern Kogaluc belt, and an amphibolite from the Payne Lake gneiss belt are depleted in incompatible elements (La, Nb, and Th; Fig. 4) and the former has a high $^{2.76\ Ga}\varepsilon_{Nd}$ value of +2.3. The metabasalts are chemically and isotopically similar to Payne Lake depleted tholeiites. The layered intrusion from the Payne Lake gneiss belt contains tholeiitic anorthositic gabbros, magnetite-melagabbro, and norite. These are characterized by relatively flat incompatible element profiles with prominent peaks in Zr and Hf and slight depletion in Nb relative to La and Th (Fig. 4).

Some of the youngest Archean rocks in the map area are gabbro, diorite (e.g. PBAW-94-293; Table 3), and granodiorite dykes cutting Payne Lake-Qalluviartuuq greenstones and Payne Lake gneisses. Three of the dykes are plagioclase-phyric gabbros and diorite characterized by high Ti and Fe (TiO_2 1.-2.3%) contents (Fig. 3). High TiO_2 dykes (<0.8% TiO_2) are tholeiitic and show a slight enrichment in Fe and Ti. Both the low and high TiO_2 dykes are enriched in LREEs relative to HREEs and Y (Fig. 4). However, the high TiO_2 suite is enriched in La relative to both Th and Nb. Three low TiO_2 dykes (diorite and granodiorite) have highly variable $^{2.725\ Ga}\varepsilon_{Nd}$ values ranging between -1.7 in granodiorite to +1.9 in diorite (e.g. PBAW-94-293, Table 3). Since even the most primitive dyke contains inherited zircons derived from 2.83 Ga juvenile crust, the spread in ε_{Nd} values likely reflects the isotopic composition of the crust through which the dykes passed.

GEOCHEMISTRY OF MAJOR PLUTONIC SUITES

The 2.78 Ga metaluminous biotite±pyroxene±hornblende suite of tonalites and quartz diorites is calc-alkaline and characterized by parallel trace-element patterns showing enrichment in Th and LREEs relative to Y and the HREEs (e.g. chondrite-normalized La/Yb_n 13-44; Fig. 5) and depletion of Nb relative to Th and La. The HREEs and Y show relatively little fractionation, with Gd/Yb_n between 3 and 5. The majority of the samples analyzed have $^{2.78\ Ga}\varepsilon_{Nd}$ values between +0.8 and +2.5 with one at -0.2. The isotopic data suggest only limited recycling (e.g. assimilation, subduction zone recycling) of isotopically evolved crust. There is no systematic variation between SiO_2 content with ε_{Nd}. Tonalite gneiss inclusions with 3.1 Ga T_{DM} model ages would have had 2.78 GaeNd values of -1.3 and local assimilation of crust of this composition could account for the negative ε_{Nd} data.

Pyroxenites in the high grade terrane are characterized by less pronounced enrichment in LREEs and Th, and flatter HREE patterns relative to the metaluminous pyroxene-bearing suite (La/Yb_n 5-13; Gd/Yb_n 2-4; Fig. 5). Like the felsic rocks however, they also show Nb depletion relative to Th and La. The $^{2.780\ Ga}\varepsilon_{Nd}$ value of four samples varies

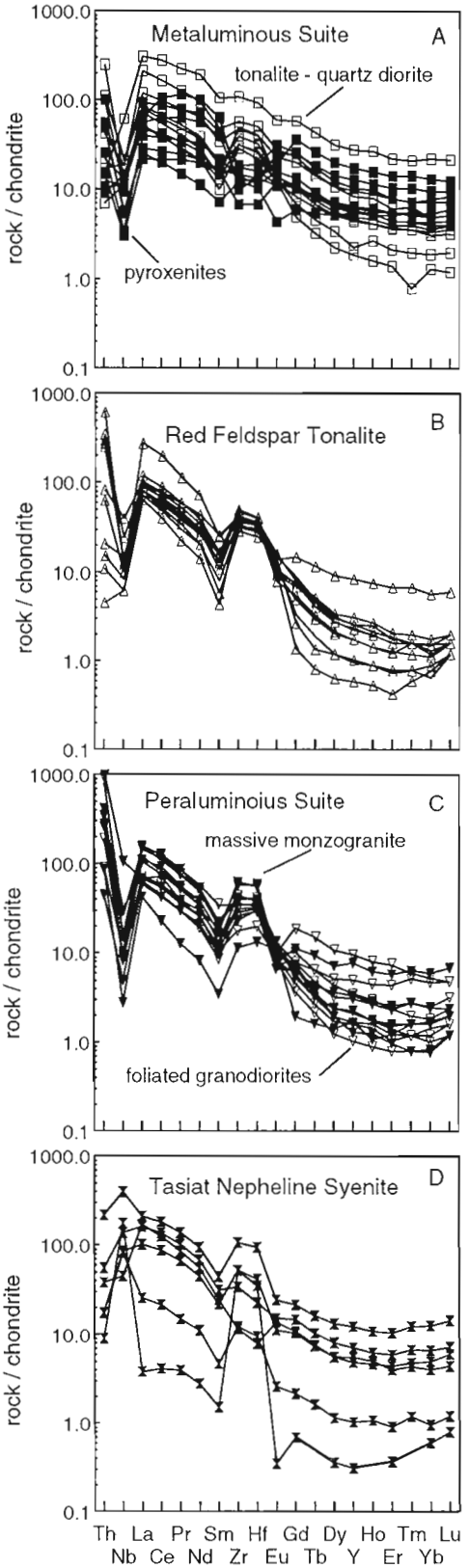

Figure 5. *Chondrite normalized trace element diagram of* ***A)*** *metaluminous, biotite±pyroxene quartz diorite-tonalite suite and related pyroxenites;* ***B)*** *peraluminous red feldspar tonalites;* ***C)*** *peraluminous foliated and massive granodiorites and monzogranites; and* ***D)*** *nepheline syenites.*

between +2.6 and +1.0, similar to the values of the metaluminous plutons. These data lend support to the earlier suggestion that the pyroxenites represent cumulate enclaves derived from metaluminous magmas.

The red feldspar tonalites are mildly peraluminous rocks with Shand index (molar Na+K+2Ca)/Al) ranging from 1 to 0.91. The tonalites are enriched in LREEs relative to HREEs (La/Yb_n 18-211) to a greater extent than that of the metaluminous suite (Fig. 5). They show a prominent depletion in Nb relative to Th and La (Fig. 5) and are similar to foliated peraluminous granodiorites. Two samples of tonalite have $^{2.78\ Ga}\varepsilon_{Nd}$ values of +0.8 and +1.3, overlapping values measured in metaluminous plutons.

The ~2733 Ma foliated peraluminous granodiorites have Shand indices of 0.97 to values as low as 0.83 in garnet-muscovite pegmatite. They are enriched in LREEs relative to HREEs (La/Yb_n 15-89) and show enrichment in Th and La relative to Nb (Fig. 5). The $^{2.725\ Ga}\varepsilon_{Nd}$ values of four samples varies from -1.6 to -1.0 for Kogaluc plutons, suggesting substantial involvement of evolved crust in the generation of Kogaluc plutons. A pluton from southern Payne Lake has an ε_{Nd} value of +2.0.

The ~2725 Ma massive peraluminous monzogranites have Shand indices of 0.97 to 0.88. These evolved plutons have variable trace element patterns, in part reflecting accessory mineral fractionation (Fig. 5). They are enriched in LREEs relative to HREEs (La/Yb_n 11-189), and include samples showing greater fractionation amongst middle- and heavy HREEs (Gd/Yb_n 1-9). All of the plutons show enrichment in Th (up to 1100 X chondrite) relative to Nb and to a lesser extent La. Two samples of monzogranite have $^{2.725\ Ga}\varepsilon_{Nd}$ values of 0.0 and +1.2.

The nepheline syenite pluton at Lac Tasiat is miaskitic (agpaitic indices (Na+K)/Al <1) and does not show extreme enrichment in incompatible trace elements (maximum Zr 410 ppm, Nb 97 ppm) as is typical of agpaitic nepheline syenites. The nepheline syenites are enriched in LREEs, but significantly, their trace element profiles peak at Nb (Fig. 5). The latter is a common feature of both continental and oceanic Phanerozoic alkaline suites. The trace element profiles show a prominent peak in Zr and Hf and some contain macroscopic zircon. The syenites also show a concave-up HREE profile (Ho/Lu_n <1). A sample of nepheline syenite has a low $^{147}Sm/^{144}Nd$ value, positive $^{2.725\ Ga}\varepsilon_{Nd}$ of +2, and a T_{DM} age of 2.77 Ma suggesting an Archean age for the pluton (Table 3). Two samples of nepheline syenite have $^{2.725\ Ga}\varepsilon_{Nd}$ values of +1.3 and +2.0.

CRUSTAL EVOLUTION OF THE CENTRAL MINTO BLOCK, 2.83-2.73 GA

Depleted tholeiitic basalts of the Payne Lake-Qalluviartuuq belt erupted before 2.83 Ga based on the maximum age of chemically correlative anorthositic gabbro (Table 4). The presence at Payne Lake of pillowed and amygdaloidal tholeiitic flows locally associated with sedimentary dolomites (Percival et al., 1996), argues for eruption under shallow marine conditions. Depletion in incompatible trace elements and high positive ε_{Nd} values indicate derivation of tholeiitic magmas from a depleted mantle source. The chemical and physical volcanological constraints are consistent with eruption on a continental shelf or oceanic plateau crust. Intrusion at 2.831 Ga of isotopically primitive, calc-alkaline diorite-granodiorite may reflect the onset of juvenile arc magmatism (Table 4).

The <2.768 Ga, >2.73 Ga younger Qalluviartuuq calc-alkaline volcanic sequence consists of locally emergent intermediate volcano-plutonic centres and submarine mafic extrusive rocks. The positive $^{2.76\ Ga}\varepsilon_{Nd}$ values of calc-alkaline basalts (+1.9) suggest that the observed enrichment in Th and La relative to Nb was acquired above a subduction zone, rather than by assimilation of continental crust. Furthermore, the low TiO_2 and Fe contents of the suite, in addition to the presence of andesites and pyroclastic rocks, are additional features common to modern arc environments. The <2.768 Ga calc-alkaline arc sequence may have formed on a composite oceanic plateau-juvenile arc crust represented by the older volcano-plutonic sequence.

The presence of depleted tholeiitic basalt and layered sills may be an early feature of the Kogaluc greenstone belt and Payne Lake gneiss belt. Anorthositic gabbro in the layered sill within the Payne gneisses may be a suitable target for U/Pb dating, and could test whether the tholeiites are coeval with Qalluviartuuq-Payne Lake tholeiitic basalts. The ~2.76 Ga Kogaluc sequence is likely to have formed in a continental setting since: 1) sedimentary and fragmental volcanic rocks are common; 2) mafic volcanic rocks are rare; 3) the belt contains rhyolite with low ε_{Nd} values; and 4) quartz-rich sediments have old T_{DM} ages. Eruption of Kogaluc pillowed andesites was followed by precipitation of locally thick banded iron-formation and later deposition of quartz-rich siltstones and immature clastic sediments. This suggests that shallow marine volcanism was initially followed by tectonic quiescence, and later renewed tectonic activity was accompanied by clastic sedimentation. Kogaluc calc-alkaline volcanic rocks have the chemical features of a continental margin arc sequence including enrichment in Th and La relative to Nb and abundance of andesites and felsic volcaniclastics.

The metaluminous biotite±pyroxene quartz diorites and tonalites are as old as 2.78 Ga (Table 4). Correlation of the Payne Lake gneisses with the 2.76 Ga Kogaluc sequence indicates that pyroxene-bearing plutons containing supracrustal screens of Payne Lake gneiss are younger than 2.76 Ga. The suite has continental arc affinities, including enrichment in Th and La relative to Nb, and the presence of both high ε_{Nd} values indicating mantle-derived magmas, and negative values consistent with local assimilation of continental crust. Ancient tonalite gneiss inclusions may be relics of an initially more widespread basement of ca. 3 Ga (c.f. Stern et al., 1994). The metaluminous suite may represent the older plutonic roots of a Kogaluc calc-alkaline arc. The metaluminous plutons differ from 2725 ± 5 Ma pyroxene± hornblende granodiorites-quartz monzodiorites in the Lake Minto domain near the Leaf River (Table 4; Stern et al., 1994),

Table 4. Summary of geochronology in the Lake Minto and goudalie domains.*

Lake Minto			Goudalie		
	south	north		south	north
late granites	2676 m 2688 z				
metamorphism	2671 z 2688 m 2693 z 2696 z 2699 z 2700 z 2707 m		 late pegmatite thol. volcanism late granodiorite ductile deformation	 2693 m 2697 z 2702 z ——	
diatexite	2713 z		unconformity granite boulder thol. volcanism	<2718 2718 z 2722 z	
granodiorite	2725 z		calc-alk. volcanism	2724 z	
monzogranite		2725 z			
ductile deformation		——	ductile deformation	 diorite	—— 2729 z
granodiorite		2733 z			
calc-alk. volcanism		2750-2759 z <2759 z	 calc-alk. volcanism unconformity granodiorite boulder thol. volcanism	 2786 z	 <2768 >2729 <2768 2768 z
tonalite		2782 z	 granodiorite thol. volcanism mafic dykes tonalite gneiss basement	 <2903 z 2903 z 2942 z	 2832 z >2832 z
tonalite gneiss		3100 TDM		3097 z	
enclaves	3125 z 3543 z				

* Notes: all ages in Ma. Abbreviations z – zircon, m – monazite, and TDM – Nd model age; data from Percival et al. (1992), Percival and Card (1994, references therein), this study.

in that the former lack positive Eu/Eu* anomalies and have lower $(La/Yb)_n$ values (13-44 versus 11-172). The mildly peraluminous red feldspar tonalites are commonly associated with the metaluminous plutons and dating in progress will test whether the two suites are coeval. The leucocratic tonalites may represent younger contaminated melts following a protracted history of Kogaluc arc magmatism.

Granodioritic and granitic magmatism between 2733 Ma and 2725 Ma (Table 4) involved significant recycling of upper crustal rocks as reflected in the peraluminous nature and negative ε_{Nd} values of plutons at this time. It is likely that the strongly peraluminous rocks reflect crustal stretching, deformation, and crustal melting.

ACKNOWLEDGMENTS

We are grateful to the staff of the Geochemical Laboratories (XRF; McGill University), analytical chemistry laboratories (ICP-MS; GSC), electron microprobe laboratory (GSC), and Geochronology Subdivision (U/PB and Sm/Nd; GSC) for their help in obtaining chemical and isotopic analyses. Reginald Theriault assisted with some of the Sm-Nd isotopic analyses. Ken Card, Shoufa Lin, Leopold Nadeau, Katherine Venance, and Pamela Winsky contributed to the mapping. We thank Pauline Orr, Eric Poirier, Allistair Still, and Lisa Tulk for field assistance and some independent mapping. Katherine Venance helped in the preparation of figures. The manuscript benefited from thoughtful reviews by Bill Davis and Randy Parrish.

REFERENCES

Davis, D.W.
1982: Optimum linear regression and error estimation applied to U-Pb data; Canadian Journal of Earth Sciences, v. 19, p. 2141-2149.

DePaolo, D.J.
1980: Crustal growth and mantle evolution: inferences from models of element transport and Nd and Sr isotopes; Geochimica et Cosmochimica Acta, v. 44, p. 1185-96.

Krogh, T.E.
1982: Improved accuracy of U-Pb ages by the creation of more concordant systems using an air abrasion technique; Geochimica et Cosmochimica Acta, v. 46, p. 637-649.

Lin, S., Percival, J.A., Winsky, P.A., Skulski, T., and Card, K.D.
1995: Structural evolution of the Vizien and Kogaluc greenstone belts in Minto block, northeastern Superior Province, northern Quebec; in Current Research 1995-C, Geology of Survey of Canada, p. 121-130.

Parrish, R.R., Roddick, J.C., Loveridge, W.D., and Sullivan, R.W.
1987: Uranium-lead analytical techniques at the Geochronology Laboratory, Geological Survey of Canada; in Radiogenic Age and Isotopic Studies: Report 1; Geological Survey of Canada, Paper 87-2, p. 3-7.

Percival, J.A. and Card, K.D.
1992: Vizien greenstone belt and adjacent high grade domains of the Minto block, Ungava Peninsula, Quebec; in Current Research, Part C; Geological Survey of Canada, Paper 92-1C, p. 69-80.
1994: Geology, Lac Minto-Rivière aux Feuilles, Québec; Geological Survey of Canada, Map 1854A, scale 1:500 000.

Percival, J.A., Card, K.D., and Mortensen, J.K.
1993: Archean unconformity in the Vizien greenstone belt, Ungava Peninsula, Quebec; in Current Research, Part C; Geological Survey of Canada, Paper 93-1C, p. 319-328.

Percival, J.A., Mortensen, J.K., Stern, R.A., and Card, K.D.
1992: Giant granulite terranes of northeastern Superior Province: the Ashuanipi complex and Minto block; Canadian Journal of Earth Sciences, v. 29, p. 2287-2308.

Percival, J.A., Skulski, T., Card, K.D., and Lin, S.
1995b: Geology of the Rivière Kogaluc-Lac Qalluviartuuq region (parts of 34J and 34O), Quebec; Geological Survey of Canada, Open File 3112, scale 1:250 000.

Percival, J.A., Skulski, T., Lin, S., and Card, K.D.
1995a: Granite-greenstone terrains of the northern Goudalie domain, northeastern Superior Province, Quebec; in Current Research 1995-C, Geological Survey of Canada, p. 141-150.

Percival, J.A., Skulski, T., and Nadeau, L.
1996: Granite-greenstone terrains of the northern Minto block, northeastern Superior Province, Quebec; in Current Research 1996-C.

Percival, J.A., Stern, R.A., Skulski, T., Card, K.D., Mortensen, J.K., and Bégin, N.J.
1994: Minto block, Superior Province: missing link in deciphering assembly of the craton at 2.7 Ga; Geology, v. 22, p. 839-842.

Roddick, J.C.
1987: Generalized numerical error analysis with application to geochronology and thermodynamics; Geochimica et Cosmochimica Acta, v. 51, p. 359-362.

Skulski, T. and Percival, J.A.
in press: Allochthonous 2.78 Ga oceanic plateau slivers in a 2.72 Ga continental arc sequence: Vizien greenstone belt, Northeastern Superior Province, Canada; Lithos.

Skulski, T., Percival, J.A, and Stern, J.A.
1994: Oceanic allochthons in an Archean continental margin sequence, Vizien greenstone belt, northern Quebec; in Current Research 1994-C, Geological Survey of Canada, p. 311-320.

Stern, R.A., Percival, J.A., and Mortensen, J.K.
1994: Geochemical evolution of the Minto block: a 2.7 Ga continental magmatic arc built on the Superior proto-craton; Precambrian Research, v. 65, p. 115-153.

Winsky, P.A., Kusky, T.M., Percival, J.A., and Skulski, T.
1995: Archean unconformity in the Qalluviartuuq greenstone belt, Goudalie domain, northern Quebec; in Current Research 1995-C, Geological Survey of Canada, p. 131-140.

York, D.
1969: Least squares fitting of a straight line with correlated errors; Earth and Planetary Science Letters, v. 5, p. 320-324.

- 4 -

Geology and age of the Lac à la Perdrix fenite, southern Gatineau district, Quebec

D.D. Hogarth[1] and Otto van Breemen[2]

Hogarth, D.D. and van Breemen, O., 1996: Geology and age of the Lac à la Perdrix fenite, southern Gatineau district, Quebec; in Radiogenic Age and Isotopic Studies: Report 9; Geological Survey of Canada, Current Research 1995-F, p. 33-41.

Abstract: The Lac à la Perdrix fenite lies in the Central Metasedimentary Belt of the Grenville Province. This 30 m wide fenite, adjacent to a narrow calciocarbonatite sill, replaces diopside-oligoclase gneiss and is composed of magnesio-arfvedsonite, aegirine, microcline, albite, and fluorapatite. Near the contact with carbonatite, it contains appreciable monazite and barite whereas aegirine virtually disappears.

Fenitization probably took place early in the igneous stage of carbonatite development. A Pb/U monazite age of 1026 ± 2 Ma is thought to date fenite formation. Together with published data, this age shows that carbonatite intruded metamorphic rocks near the close of the Grenville Orogeny.

Résumé : La fénite de Lac à la Perdrix s'observe dans la ceinture métasédimentaire de la Province de Grenville. Cette fénite, mesurant 30 m de largeur et en position adjacente par rapport à un étroit filon-couche de calciocarbonatite, remplace un gneiss à diopside-oligoclase et se compose de magnésio-arfvedsonite, d'ægirine, de microcline, d'albite et de fluorapatite. Près du contact avec la carbonatite, la fénite contient de la monazite et de la barytine en quantité appréciable, tandis que l'ægirine disparaît pratiquement.

La fénitisation a probablement eu lieu au début de l'épisode igné durant lequel s'est formé la carbonatite. On pense qu'un âge Pb-U sur monazite de 1 026 ± 2 Ma correspond au moment de formation de la fénite. Conjugué aux données publiées, cet âge indique que la carbonatite a fait intrusion dans des roches métamorphiques vers la fin de l'orogenèse grenvillienne.

[1] Department of Geology, University of Ottawa, Ottawa, Ontario K1N 6N5
[2] Geological Survey of Canada, 601 Booth Street, Ottawa, Ontario K1A 0E8

INTRODUCTION

In the Grenville Province, the age and origin of layered and foliated rocks of carbonatite appearance and spatially related fenites have been debated since the beginning of this century. Carbonatite is used here in the broad sense defined by Heinrich (1966) as "a carbonate-rich rock of apparent magmatic derivation or descent". Such rocks and associated fenites are common north of Ottawa. Four Proterozoic occurrences were recognized in the Gatineau district: in a narrow 20 km long zone extending southwest from beyond Lac McGregor, through the Lac à la Perdrix area, to the Haycock iron mine (Fig. 1, localities 1, 2, and 3, respectively) as well as calciocarbonatites, magnesicarbonatites, and fenites near Meech Lake (Fig. 1, locality 4, Hogarth 1966; Hogarth and Rushforth, 1986). South of the Ottawa River, are found the Blackburn fluidized magnesiocarbonatites of Cretaceous age (Fig. 1, locality 6; Rushforth, 1985; Hogarth et al., 1988).

This paper focuses on the small Lac à la Perdrix fenite and carbonatite (locality 1381 in Fig. 2), which features a carbonatite-fenite contact, brecciated host rock, mineralized fractures in fenite, and alignment of xenoliths in carbonatite. At this outcrop, the grain size is sufficiently coarse to enable clear field observation and distinction of the most important phases, without a hand lens. The occurrence of fresh monazite provides a means of dating this fenite, and together with new petrological data may shed more light on the origin of these problematic rocks.

GEOLOGICAL SETTING

Lac à la Perdrix lies in the Mont Laurier terrane (Davidson, 1995) of the western Central Metasedimentary Belt in Quebec. No detailed geological map of the Lac à la Perdrix area is presently available but general features were described by D.D. Hogarth and J.M. Moore in Baird (1972) and geology of the area immediately to the south of Figure 2 was mapped and described by Hogarth (1981).

The area outlined in Figure 2 is underlain by calcite marble in the east, and mafic gneiss with subordinate biotite gneiss and feldspathic quartzite in the west. Although most mafic gneiss is amphibolite or diopside-oligoclase gneiss, assemblages scattered throughout the area, such as orthopyroxene-clinopyroxene-plagioclase with or without hornblende and biotite, are indicative of at least hornblende granulite metamorphic facies. Massive pegmatitic to slightly foliated granite, interlayered with basic gneiss, is common in the northwest. Gneiss, quartzite, and pegmatite are cut by carbonatite sills and replaced by fenite. Layers of this association (marble, gneiss, quartzite, pegmatite, fenite, and carbonatite) trend north-northeasterly and dip moderately to steeply, generally to the west and are plicated into tight- to isoclinal folds.

In the northern part of Figure 2, this association is intruded by post-tectonic diabase dykes that are vertical and east-trending, similar to the Grenville dyke swarm for which Kamo et al. (1995) obtained an age of 590+2/-1 Ma. Seemingly

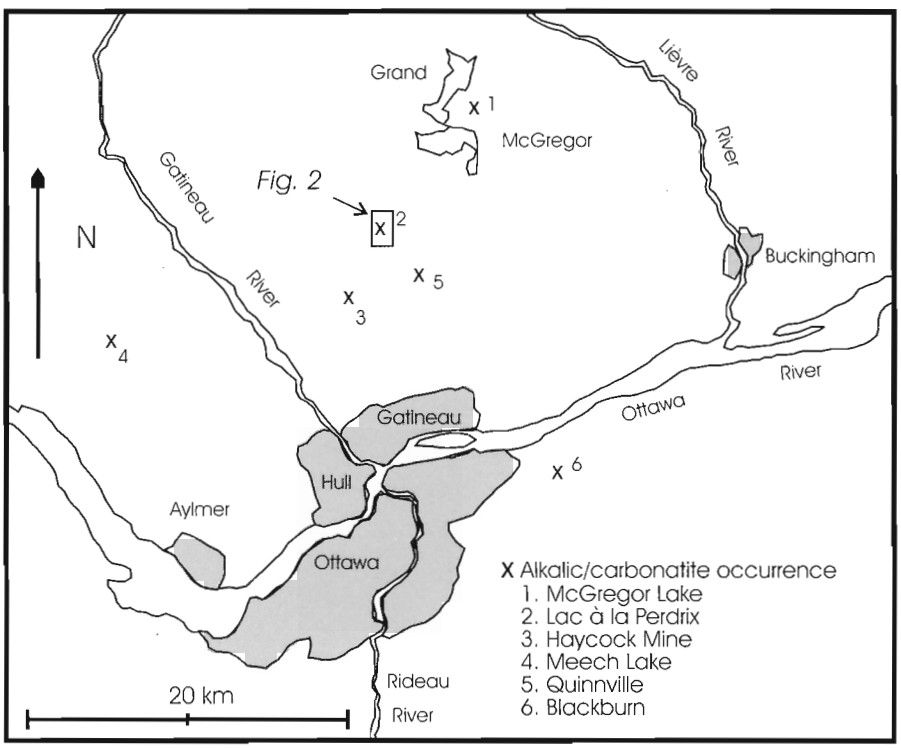

Figure 1. *Principal carbonatites in the National Capital area. Occurrences: 1) Lac McGregor, 2) Lac à la Perdrix, 3) Haycock mine, 4) Meech Lake, 5) Quinnville, 6) Blackburn quarries.*

post-tectonic, biotite-lamprophyre (minette) was noted at localities 1376 and 1377, but field relationships with the surrounding rocks are obscured by overburden. Although by no means conclusive, field evidence suggests that at Quinnville (Fig. 1) fenites are cut by a post-tectonic minette dyke giving a K/Ar-biotite age of 886 ± 25 Ma (Hogarth, 1981), which is probably a regional cooling age (see below). Overburden-filled west to west-northwest linear valleys appear to be underlain by faults of minor displacement that transect all rocks of the area (e.g. Fig. 2).

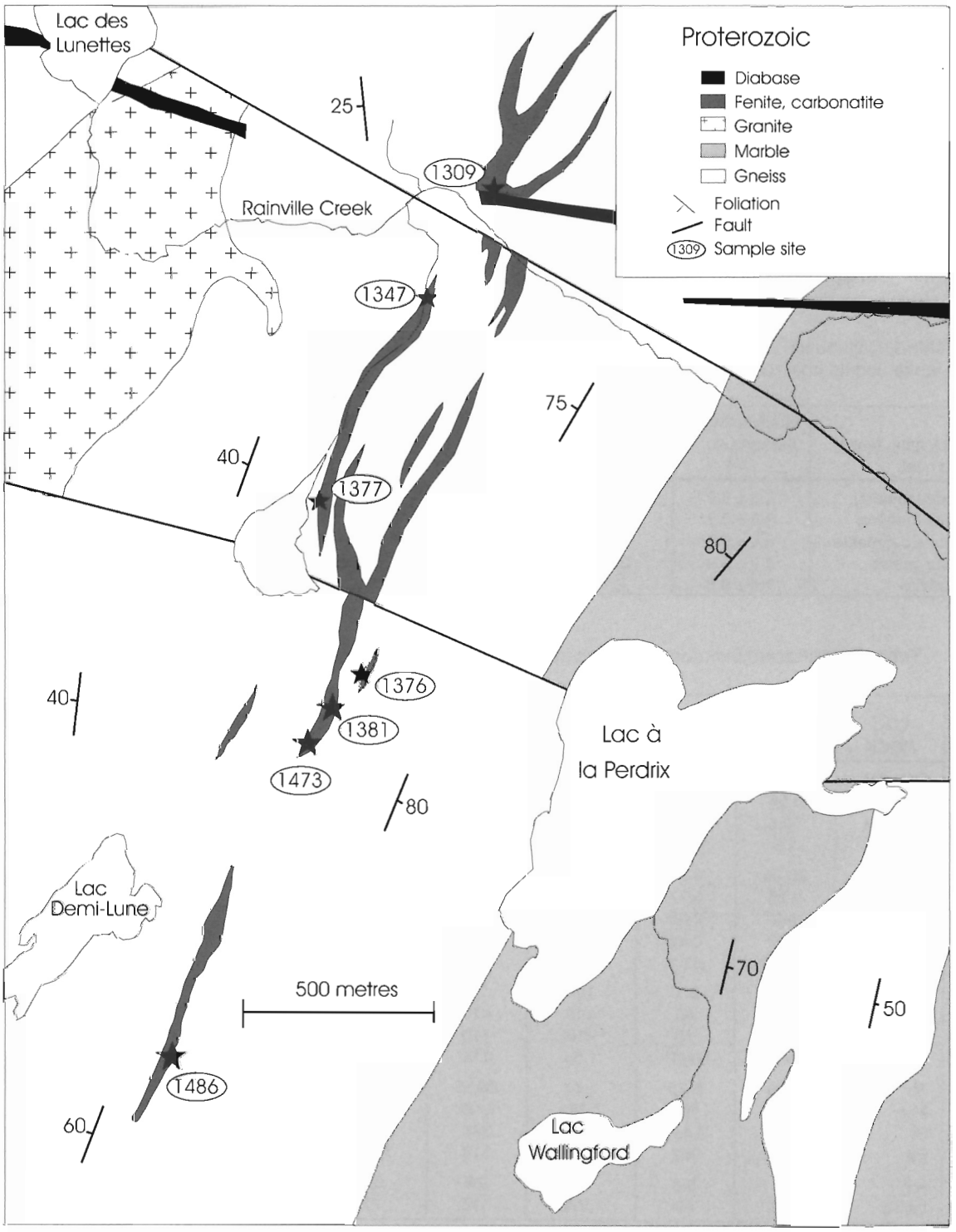

Figure 2. *Geology of the Lac à la Perdrix area Sample sites are those given text and tables.*

CARBONATITES AND FENITES

Near Lac à la Perdrix (area of Fig. 2) carbonatites (calciocarbonatites of Woolley and Kempe, 1989), are concordant, elongate, and small. Occurrence 1486, the largest, is 270 m long and 15 m (maximum) wide, but all associated fenites contain appreciable calcite. The average width of fenite surpasses that of carbonatite by at least 10 to 1.

This paper focuses on locality 1381 (Fig. 2), where a small carbonatite, barely 2 m wide, is exposed, wall-to-wall, in a shallow surface scraping. Layering, most apparent on surfaces of nearby blocks, is accentuated by trails of small, rounded, fenite xenoliths. The surrounding mafic gneiss is intensely fenitized with patches of dull green aegirine-augite and long, glistening, blue-black prisms of magnesio-arfvedsonite. The fenite is 25 to 35 m wide. Near its contact with carbonatite, barite and monazite become abundant but aegirine virtually disappears, where it contains microcline, albite, magnesio-arfvedsonite, calcite, barite, and monazite. The contact is strongly radioactive, owing to the mass effect of monazite, where a scintillation counter consistently registered total radioactivity at least five times above background (maximum 24; Table 1).

Table 1. Distribution of radioactivity across a fenite and its host rock.

Rock type, fenite and host	Radioactivity/ background (1σ)	No. of readings
fenite (contact)	9.2 ± 3.9	20
fenite (interior)	3.6 ± 0.8	23
granite pegmatite	3.6 ± 0.3	2
mafic gneiss	2.9 ± 0.9	23
quartzite	1.4 ± 0.6	2

The mineralogy and chemical composition of calciocarbonatite is dominated by calcite, amphibole, barite, and apatite. Calcite is coarse grained and contains appreciable strontium (0.3-0.4% SrO) and manganese (0.4-0.9% MnO). Pyroxene, approaching end-member aegirine ($NaFeSi_2O_6$), is present as green euhedral prisms (possibly phenocrysts). Other minerals, some possibly xenocrystic, are richterite (commonly with Na-rich rims), magnesio-arfvedsonite, fluorapatite, phlogopite, barite (some grains coexisting with celestite), allanite (some crystals rimmed with clinozoisite), andradite, euhedral end-member albite, and Ba-free microcline. Locally, magnetite and/or rutilated specularite fill breccias. Although reserves of iron ore proved to be insignificant, intense prospecting anticipated Canada's railroad boom of the 1880s; at location 1473 (formerly the Thomas Watson property) and location 1309, the "Rainville Creek iron occurrence" (formerly the James Grant property), carbonatites and fenites were later studied by Erdmer (1977).

The chemical composition of carbonatites in the Lac à la Perdrix area sets them apart from typical Grenville marble (Table 2; WALL is the mean composition of two samples collected just south of Lac Wallingford). Compared to local marble, the carbonatites have a lower content of Mg but higher contents of Fe, K, P, Zr, REEs, Sr, and Ba. Although the composition of carbonatites worldwide is extremely

Table 2. Abstracted bulk-rock analyses of carbonatites, fenites, and metasediments.

LOC ROCK	1309 carb	1309 fenite	1347 carb	1376 fenite	1381 carb	1381 fenite	WALL marble	HAY gneiss
SiO_2 (%)	4.88	56.25	5.77	48.11	20.62	26.75	4.19	50.55
Al_2O_3	0.56	2.06	0.69	4.76	4.26	3.5	0.46	17.31
Fe_2O_3tot	10.6	11.93	4.59	9.26	4.98	9.26	0.34	12.02
MgO	1.5	12.35	1.48	13.43	7.61	3.6	6.26	4.9
CaO	43.06	6.51	42.91	6.4	28.17	1.1	41.82	7.34
Na_2O	0.15	5.71	0.2	5.66	0.87	4.76	0	3.15
K_2O	0.3	2.03	0.38	2.91	2.19	0.56	0.22	1.87
P_2O_5	1.33	0.26	1.12	0.07	2.76	0.84	0.01	0
Total	62.38	97.1	57.14	90.6	71.46	50.37	53.3	97.14
Zr (ppm)	140	210	107	75	212	1,230	10	7.34
Nb	10	60	<10	<10	<10	<10	<10	<10
Cr	10	18	<10	<10	<10	<10	<10	49
U	0.4	0.62	1.84	0.56	2.44	1.3	n.a.	0.17
Th	2.68	3.75	7.65	83.55	9.15	125	n.a.	0.64
ΣLn	3,740	407	7,300	1,120	1,310	12,000	16	142
Sr	5,140	3,445	3,750	330	5,020	35,300	370	588
Ba	7,760	932	15,900	813	7,770	173,000	230	594
A.I.	1	5.6	1.1	2.6	0.9	2.4	0.5	0.4
La/Yb	197	40	1,770	118	77	25,000	19	5.7

Notes: Major and most trace elements detemined by XRF (Univ. of Ottawa); REE by DCP-AES (Univ. of Ottawa); Th by INAA (Ecole Polytechnique), U by INAA-DNC (Ecole Polytechnique). Abbreviations: A.I., agpaitic index (Na+K)/Al); carb, carbonatite; HAY, basic gneiss near Haycock Mine; ΣLn, sum of lanthanides; loc, locality; n.a., not analyzed; WALL, marble near Lac Wallingford.

variable (Woolley and Kempe, 1989), the compositions of local carbonatites fit much better those of calciocarbonatite, especially for the trace elements Zr, REEs, Sr, and Ba.

Fenites replace gneiss, quartzite, and granite pegmatite outwardly from carbonatite and, in some cases, without apparent carbonatite in the core. They are characterized by Na-rich amphiboles and pyroxenes, with amphiboles more sodic (magnesio-arfvedsonite; $Na^{\dagger}$ = 100 Na/(Na + K + Ca) = 82) than those in the associated carbonatite (richterite; $Na^{\dagger}$ 61). Amphiboles in local fenites and carbonatites (as well as fenites and carbonatites worldwide) are much more magnesian ($Mg^{\dagger}$ = 100 Mg/(Mg + Fe) = 71, 74; fenites and carbonatites, respectively) than the associated pyroxene ($Mg^{\dagger}$ = 17). Magnesio-arfvedsonite and aegirine-augite preferentially replace ferromagnesian minerals of the host rock, the composition of the metasome being controlled, in part, by that of the paleosome. Aegirine preferentially replaces quartz. Other characteristic minerals are neocrystallized phlogopite ($Mg^{\dagger}$ 87-93) and microcline (An 0.0, Ab 2.9, Or 97.1; BaO <0.5 %), albite (An 0.1, Ab 99.2, Or 0.7), allanite, ferrian rutile, specularite, monazite, apatite, calcite (SrO <0.1%), and barite.

In the Gatineau district, major mineral growth proceeded in four stages: 1) Oxidation of iron and brecciation of the host rock. 2) Replacement outward from breccia fractures, forming sodic amphiboles and sodic pyroxenes, of which magnesio-arfvedsonite and aegirine are the most common species. The sequence of formation of pyroxene and amphibole varies from location to location, even within an individual occurrence. 3) Growth of neocrystallized-microcline, appearance of end-member albite, introduction of calcite. 4) Continued replacement and crystal growth of pyriboles with consequent obliteration of foliation in the host rock. These stages appear to be universal in the development of sodic fenites (Heinrich, 1966; McKie, 1966).

The most important chemical feature of fenite results from replacement of aluminum-rich minerals (such as biotite, hornblende, and plagioclase) by aluminum-poor minerals (such as aegirine and magnesio-arfvedsonite). The rock then becomes depleted in Al as fenitization progresses and peralkalinity, here registered as agpaitic coefficient (A.I. = (Na + K)/Al), increases in response. Thus A.I. of basic gneiss HAY is only 0.4, but in fenites 1309, 1376, and 1381, probably derived from a similar rock, it varies from 2.4 to 5.6 (Table 2). Sample HAY was channelled across one metRE in an orthopyroxene-clinopyroxene-scapolite-plagioclase-ilmenite gneiss, near the Haycock mine.

Trace elements are also diagnostic. Characteristically, fenites contain considerable Sr, Ba, and REES and their unusually high values in the Lac à la Perdrix fenite (Table 1; far above the values in sample HAY) leaves little doubt that they were added during metasomatism.

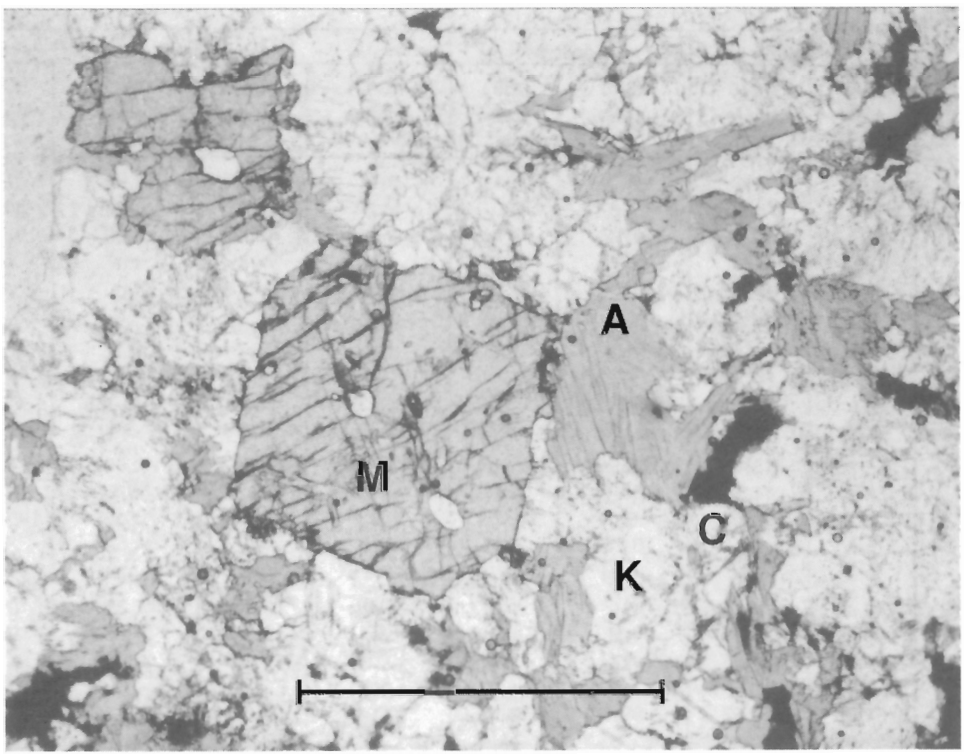

Figure 3. *Poikiloblastic monazite crystal (M), cut across the prism axis b, with magnesio-arfvedsonite (A), alizarin-stained calcite (C), and intermixed microcline and albite (K), in fenite 1381. Photomicrograph, plane-polarized light. Bar scale = 1 mm.*

MONAZITE, ALLANITE, AND APATITE

Prismatic apatite is present in all carbonatites and fenites examined in the region and it is Ce-rich fluorapatite containing barely detectable Cl. The very high Sr and low Mn contents suggest that this apatite is connected with carbonatite but not granite or regional skarn (Hogarth, 1989). Apatite from localities 1377 and 1381 has a patchy, back-scattered electron image, low-Ce content, and ragged outline; it may be hydrothermally altered. Monazite (Fig. 3) occurs with apatite in amphibole-fenite, at Lac à la Perdrix (occurrence 1381) and the Haycock mine (Hogarth and Lapointe, 1984; Hogarth et al., 1985); it has also been found with apatite in aegirine-fenite near the Haycock mine and in aegirine-calciocarbonatite north of Lac McGregor (Hogarth et al., 1985).

Rare-earth element minerals near Lac à la Perdrix are monazite-(Ce), fluorapatite, and allanite-(Ce) at locality 1376 (Table 3). Large (millimetric) crystals of monazite (Fig. 3) are elongated along the b axis, with well developed parting parallel to c (001). Small crystals are commonly pseudo-bipyramidal. The mineral is orange in hand specimen, pale green to colourless in transmitted light, and gives high-order interference colours under crossed polars. The last attribute suggests little or no radiation damage to the crystal structure. It is low in Ca (<0.05% CaO), Th (<1% ThO_2), and U (<0.1% UO_2) but, compared to monazite from other environments, relatively high in Sr (0.25-0.30% SrO); La/Nd is 2-3. This composition characterizes monazite from igneous carbonatite and fenite, but differs from monazite from hydrothermal carbonatite and regional skarn (Hogarth et al., 1991). Chondrite-normalized REE curves of these minerals in fenite 1381 (Fig. 4) show a steep slope downwards towards HREEs, in response to a strong bias of LREEs in carbonatites (Cullers and Graf, 1984). The illustration suggests that the LREE distribution is largely controlled by monazite.

Allanite prisms at locality 1376 are elongated parallel to the b axis and tend to radiate. They are pleochroic from orange-brown to grey and, under crossed polars, show high second-order colours. They have low concentrations of U and Th, features pertaining to allanite from igneous carbonatite and fenite (Hogarth et al., 1991). Allanite is also found in aegirine-magnetite-calciocarbonatite (occurrences 1309 and 1347). Coexisting allanite and monazite, apparently in equilibrium with apatite in amphibole-fenite at locality 1376, are normally considered an 'antagonistic' pair (Broska and Uhler, 1991, 1993). Monazite with allanite is, however, documented in fenite in the Vishnevye Mountains, Russia (Zhabin and Svyazhin, 1962) and in volcanic calciocarbonatite at Uyaynah, United Arab Emirates (Woolley et al., 1991).

Table 3. Allanite, monazite, and apatite compositions from carbonatite and fenite.

	Allanite		Monazite		Apatite			
Loc.	1347	1376	1376	1381	1309	1377	1381	1381
Rock	carb	fenite	fenite	fenite	carb	fenite	carb	fenite
n	2	2	3	6	6	3	3	3
SO_3	n.a	n.a	n.a	0.08	0.11	0.11	0.08	0.19
P_2O_5	n.a	n.a	29.87	30	41.54	42.31	42.53	40.85
SiO_2	32	32.11	0.12	0.14	0.02	0.02	0.03	0.13
TiO_2	0.03	0.02	0.03	0.03	n.a	n.a	n.a	n.a
ThO_2	<0.02	0.02	0.24	0.85	<0.02	n.a	n.a	n.a
UO_2	n.a	<0.02	0.03	0.08	<0.02	n.a	n.a	n.a
Al_2O_3	n.a	13	n.a	n.a	n.a	n.a	n.a	n.a
Fe_2O_3	—	14.78	—	—	—	—	—	—
FeO	n.a	6.72	<0.02	<0.02	<0.02	<0.02	<0.02	<0.02
Y_2O_3	0.02	<0.02	<0.02	<0.02	<0.02	<0.02	<0.02	0.06
ΣLn_2O_3	19.73	15.46	68.96	67.34	2.04	0.78	0.38	4.21
CaO	n.a	14.54	0.07	0.04	48.92	53.8	50.84	49.27
MnO	n.a	0.27	<0.01	<0.01	0.03	0.06	0.06	0.03
SrO	n.a	n.a	0.28	0.24	5.26	1.08	4.62	2.65
PbO	n.a	n.a	n.a	0.12	n.a	n.a	n.a	n.a
Na_2O	n.a	n.a	n.a	n.a	0.43	0.43	0.38	0.52
F	n.a	n.a	n.a	n.a	3.51	3.32	3.63	2.61
Cl	n.a	n.a	n.a	n.a	0.01	0.02	0.03	<0.01
H_2O	—	1.6	n.a	n.a	0.1	0.22	0.08	0.5
Total	51.78	98.52	99.6	98.92	100.49	100.7	101.12	99.92
La/Yb	—	—	>1000	700	—	—	—	—
La/Nd	2.3	2.3	2.5	2.8	0.8	1.4	0.5	0.9
Sr/Mn	—	—	>20	>26	200	20	80	100
Th/U	—	—	8	10.6	—	—	—	—

Notes. All analyses by WDS - EMP; Fe_2O_3, FeO, H_2O derived by calculation, assuming stoichiometry; O = F, Cl subtracted in totals. Abbreviations: carb carbonatite, ΣLn sum of lanthanides, loc location, *n* number of analyses processed, n.a. not analyzed.

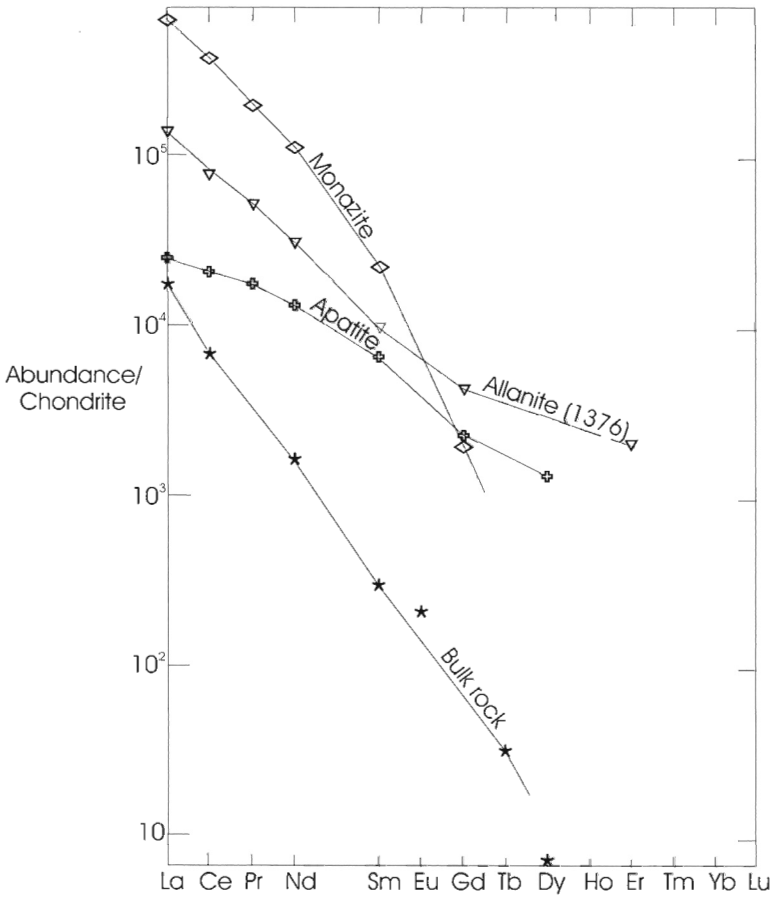

Figure 4.

Chondrite-normalized plot of bulk rock and minerals from fenite 1381, and allanite from nearby fenite 1376.

MODE AND TIME OF FENITE FORMATION

The carbonatites of the Gatineau district can be best explained in terms of deep-seated carbonatites, intruded as magma. Following the general model of Gittins (1989, p. 594-592), we infer that fenite was likely generated prior to carbonatite emplacement, when expelled alkali-rich, hydrothermal solutions reacted with wall rock; conversely, soda-pyroxenes and soda-amphiboles were generated in the carbonatite magma as a result of contamination by fenite xenoliths that were scraped from the walls and then digested or partially digested (general model of Le Bas, 1989, p. 438-440). Fenites, with an association of soda amphibole, soda pyroxene, and Ca-free albite, are generally regarded to have formed at low to moderate temperatures. Thus the range of 450-500°C proposed by Currie and Ferguson (1971) for emplacement of an almost identical mineral assemblage at Callander Bay, Ontario, was probably not exceeded at Lac à la Perdrix.

Previous geochronology on the carbonatites were obtained by the K-Ar method on micas. Phlogopite from fenite in the Haycock mine gave 862 ± 31 Ma (Wanless et al., 1974), whilst on the other side of the Gatineau River, reversely pleochroic phlogopite from two carbonate selvages, near Meech Lake gave an average age of 904 ± 25 Ma (Hogarth, 1966). These ages postdate tectonic events in the Grenville Province, which were terminated by 1000 Ma (Davidson, 1995), and can be attributed to slow regional cooling through ca. 280 ± 40°C (Harrison et al., 1985). It is likely that the granulite facies metamorphism documented in the mineralogy of the local gneisses corresponds to peak metamorphism 80 km to the northeast, within the Mont Laurier terrane (Corriveau et al., 1994), dated at about 1185 Ma (Boggs et al., 1994). Elsewhere, in the Central Metasedimentary Belt of Ontario, middle amphibolite assemblages formed as late as 1030 Ma (Corfu and Easton, 1995).

The Lac à la Perdrix locality was chosen because of accessibility and abundance of good quality, crystalline monazite. Three single grains of monazite were analyzed following methods described in Parrish et al. (1987). Uranium concentrations are low for monazite (250 ppm). Data points for three single grains cluster on concordia, or slightly above, with overlapping uncertainties (2 sigma). The close grouping of monazite ages appears to rule out an inherited radiogenic Pb component. (Table 4) Concordant analyses A and C yield an average Pb/U age of 1026 ± 2 Ma (Fig. 5). As fenitization occurred after peak metamorphism and as the closure temperature of U-Pb in monazite is estimated at about 700°C (Heaman and Parrish, 1991), this age is assigned to carbonatite emplacement and concomittant fenitization.

Previously dated carbonatites and fenites near the western margin of the Central Metasedimentary Belt of Ontario are in the range 1070 Ma to 1038 Ma (Lumbers et al., 1991; U-Pb zircon, no details of isotopic data nor localities are presented). The latter age range corresponds to a 1080 Ma to 1050 Ma period of northwest thrusting along the western boundary of

Table 4. U-Pb zircon isotopic data

F[1]	Wt. (ug)	U (ppm)	Pb[2] (ppm)	$^{206}Pb/^{204}Pb$[3] (meas.)	Pb_c[4] (pg)	^{208}Pb[2] (mole %)	$^{206}Pb/^{238}U$[5] (± 1σ, %)	$^{207}Pb/^{238}U$[5] (± 1σ, %)	$^{207}Pb/^{206}Pb$[5] (± 1σ, %)	^{206}Pb/U Age (± 2σ, Ma)	^{207}Pb/U Age (± 2σ, Ma)	Pb/Pb Age[6] (± 2σ, Ma)
Fenite, Lac à la Perdrix												
A	10	258	335	1,207	30	87.6	0.17256 ±.09	1.747 ±.15	0.07341 ±.11	1026.2 ±1.7	1025.9 ±2.0	1025.2 ±4.5
B	20	252	416	1,288	38	90.3	0.17236 ±.09	1.740 ±.15	0.07322 ±.10	1025.1 ±1.7	1023.5 ±1.9	1020.2 ±3.9
C	10	236	315	1,068	26	88	0.17260 ±.10	1.747 ±.18	0.07340 ±.14	1026.4 ±1.8	1025.9 ±2.4	1024.9 ±5.6

[1] Single crystal
[2] radiogenic Pb
[3] measured ratio, corrected for spike and fractionation;
[4] total common Pb in analysis corrected for fractionation and spike
[5] corrected for blank Pb and U, common Pb
[6] $^{207}Pb/^{206}Pb$ model age.

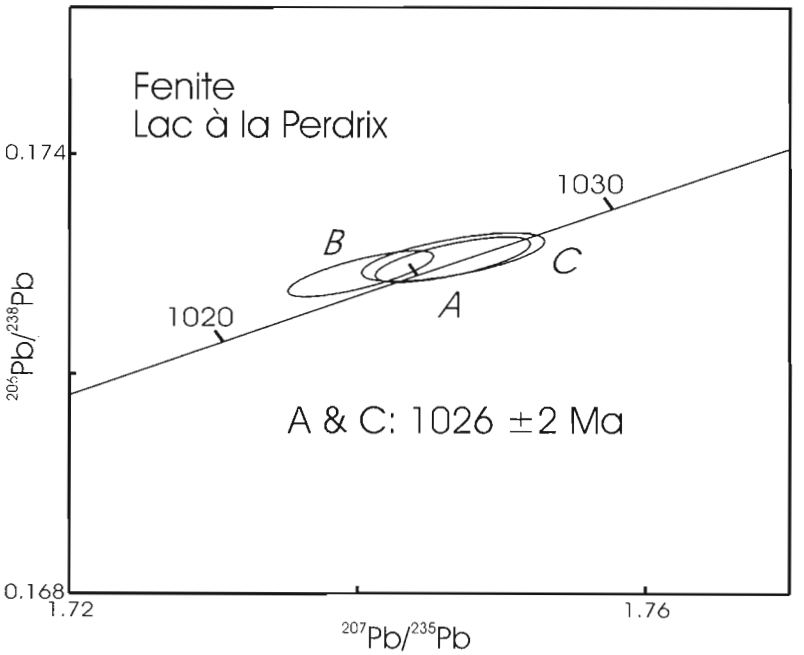

Figure 5.

U-Pb Concordia plot of monazite data.

the Central Metasedimentary Belt (McEachern and van Breemen, 1993). The carbonatite and fenite at Lac à la Perdrix thus appear to have formed late in the tectonic development of the region and the Grenville orogen.

ACKNOWLEDGMENTS

Some of the microprobe analyses were made by Peter Roeder (Queens University) and Peter Jones (Carleton University). Bulk rock constituents were mainly determined by Ron Hartree (University of Ottawa), but REEs, U, and Th were determined by Greg Kennedy (Ecole Polytechnique). Fieldwork was conducted in 1985 and 1986 with the able assistance of Michelle Veshais and Robert Thériault, and with the helpful support of NSERC. The manuscript benefitted from critical readings by A. Davidson and B. Bingen.

REFERENCES

Baird, D.M.
1972: Geology of the National Capital area; Guidebook to excursions B23-B27; 24th International Geological Congress, Montreal, 32 p.

Boggs, K., van Breemen, O., Corriveau, L., and Sawyer, E.W.
1994: New insights on metamorphism in the Central Metasedimentary Belt of Quebec, Grenville Province; Mineralogical Magazine, v. 58A, p. 105-106.

Broska, I. and Uhler, P.
1991: Regional typology of zircon and its relationship to allanite (monazite antagonism) on an example of Hercynian granitoids of the Western Carpathians; Geologicky Sbornik (CSK), v. 42, p. 271-277.
1993: Allanite-monazite antagonism and its importance for solving petrogenesis problems of granitoids (on an example of the Western Carpathian Mts.); in Rare Earth Minerals: Chemistry, Origin and Ore Deposits, (IGCP) projects 282, 234; Mineralogical Society of Great Britain and The Natural History Museum, p. 18-20.

Corfu, F. and Easton, R. M.
1995: U-Pb geochronology of the Mazinaw Terrane, an imbricate segment of the Central Metasedimentary Belt, Grenville Province, Ontario; Canadian Journal of Earth Sciences, v. 32, p. 959-976.

Corriveau, L., Morin, D., and Madore, L.
1994: Géologie et cibles d'exploration de la partie centre est de la ceinture métasédimentaire du Québec, Province de Grenville; dans Recherches en cours 1994-C; Commission géologique du Canada, p. 355-365.

Cullers, R.L. and Graf, J.L.
1984: Rare earth elements in igneous rocks of the continental crust: predominantly basic and ultrabasic rocks; in Developments in Geochemistry, Volume 2: Rare Earth Element Geochemistry; (ed.) P. Henderson; Elsevier, Amsterdam, p. 237-274.

Currie, K.L. and Ferguson, J.
1971: A study of fenitization around the alkaline carbonatite complex at Callander Bay, Ontario, Canada; Canadian Journal of Earth Sciences, v. 8, p. 498-517.

Davidson, A.
1995: A review of the Grenville orogen in its North American type area; AGSO Journal of Australian Geology and Geophysics, v. 16, (no. 1/2), p. 3-24.

Erdmer, P.
1977: Geology of the Rainville Creek iron occurrence; BSc. thesis, University of Ottawa, Ottawa, Ontario, 62 p.

Gittins, J.
1989: The origin and evolution of carbonatite magmas; in Carbonatites: Genesis and Evolution, (ed.) K. Bell; Unwin Hyman, London, p. 580-600.

Harrison, T.M., Duncan, I., and McDougall, I.
1985: Diffusion of 40Ar in biotite: temperature, pressure and compositional effects; Geochimica et Cosmochimica Acta, v. 49, p. 2461-2468.

Heaman, L. and Parrish, R.
1991: U-Pb geochronology of accessory minerals, Chapter 3; in Short course on applications of radiogenic isotope systems to problems in geology, (ed.) L. Heaman and J.N. Ludden; short course handbook, Toronto: Mineralogical Association of Canada; p. 59-102.

Heinrich, E.W.
1966: The geology of Carbonatites; Rand McNally and Company, Chicago, 607 p.

Hogarth, D.D.
1966: Intrusive carbonate rock near Ottawa, Canada; International Mineralogical Association, IMA volume, p. 45-53.
1981: Partie ouest de la région de Quinnville, rapport intérimaire; Ministère de l'Energie et des Ressources (Québec), DPV-816, 28 p. + map.
1989: Pyrochlore, apatite and amphibole: distinctive minerals in carbonatite; in Carbonatites; (ed.) K. Bell; Unwin Hyman, London, p. 105-148.

Hogarth, D.D. and Lapointe, P.
1984: Amphibole and pyroxene development in fenite from Cantley, Quebec; Canadian Mineralogist, v. 22, p. 281-295.

Hogarth, D.D. and Rushforth, P.
1986: Carbomotes and femotes near Ottawa, Ontario and Gatineau, Quebec; in Guidebook to Field Trip 9B; Geological Association of Canada-Mineralogical Association of Canada-Canadian Geophysical Union Joint Annual Meeting, Ottawa, 22 p.

Hogarth, D.D., Hartree, R., Loop, J., and Solberg, T.N.
1985: Rare-earth element minerals in four carbonatites near Gatineau, Quebec; American Mineralogist, v. 70, p. 1135-1142.

Hogarth, D.D., Jones, P., and Roeder, P.
1991: The composition of monazite and allanite from four geological environments; in Program with Abstracts, Geological Association of Canada-Mineralogical Association of Canada joint Annual Meeting, 16, Toronto, p. A 57.

Hogarth, D.D., Rushforth, P., and McCorkell, R.H.
1988: The Blackburn carbonatites, near Ottawa, Ontario: dykes with fluidized emplacement; Canadian Mineralogist, v. 26, p. 377-390.

Kamo, S.L., Krogh, T.E., and Kumarapeli, P.S.
1995: Age of the Grenville dyke swarm, Ontario-Quebec: implications for the timing of Iapetan rifting: Canadian Journal of Earth Sciences, v. 32, p. 273-280.

LeBas, M.J.
1989: Diversification of carbonatite; in Carbonatites: Genesis and Evolution, (ed.) K. Bell; Unwin Hyman, London, p. 428-447.

Lumbers, S.B., Heaman, L.M., Vertolli, V.M., and Wu, T.W.
1991: Nature and timing of Middle Proterozoic magmatism in the Central Metasedimentary Belt, Grenville Province, Ontario; in Mid-Proterozoic Laurentia-Baltica, (ed.) T. Rivers, C.F. Gower and B. Ryan; Geological Association of Canada, Special Paper, p. 243-276.

McEachern, S.J. and van Breemen, O.
1993: Age of deformation within the Central Metasedimentary Belt boundary thrust zone, southwest Grenville Orogen: constraints on the collision of the Mid-Proterozoic Elzevir terrane; Canadian Journal of Earth Sciences, v. 30, p. 1155-1165.

McKie, D.
1966: Fenitization; in Carbonatites, (ed.) O.E. Tuttle and J. Gittins; Interscience Publishers, New York, p. 261-294.

Parrish, R.R., Roddick, J.C., Loveridge, W.D., and Sullivan, R.W.
1987: Uranium-lead analytical techniques at the Geochronology Laboratory, Geological Survey of Canada; in Radiogenic Age and Isotopic Studies: Report 1; Geological Survey of Canada, Paper 87-2, p. 3-7.

Rushforth, P.
1985: A petrological study of some intrusive carbonatite dikes, near Blackburn Hamlet, Ontario; BSc. thesis; University of Ottawa, Ottawa, Ontario, 51 p.

Wanless, R.K., Stevens, R.D., Lachance, G.R., and Delabio, R.N.
1974: Age determinations and geological studies. K-Ar isotopic ages, report 11; Geological Survey of Canada, Paper 73-2, 139 p.

Woolley, A.R. and Kempe, D.R.C.
1989: Carbonatites: nomenclature, average chemical compositions, and element distribution; in Carbonatites: Genesis and Evolution; (ed.) K. Bell; Unwin Hyman, London, p. 1-14.

Woolley, A.R., Barr, M.W.C., Din, V.K., Jones, G.C., and Wall, F.
1991: Extrusive carbonatites from the Uyaynah area, United Arab Emirates; Journal of Petrology, v. 32, p. 1143-1167.

Zhabin, A.G. and Svyazhin, N.V.
1962: Concentrically zoned aggregates of rare-earth element minerals in the Vishnevye Gory alkaline complex; Trudy, Institut Mineralogii, Geokhimii i Kristallokhimii Redkikh Elementov, Akademiya Nauk SSSR (In Russian), no. 9, p. 55-56.

- 5 -

Preliminary chronostratigraphy of the Tetagouche and Fournier groups in northern New Brunswick[1]

R.W. Sullivan[2] and C.R. van Staal[3]

Sullivan, R.W. and van Staal, C.R., 1996: Preliminary chronostratigraphy of the Tetagouche and Fournier groups in northern New Brunswick; in Radiogenic Age and Isotopic Studies: Report 9; Geological Survey of Canada, Current Research 1995-F, p. 43-56.

Abstract: Seven U-Pb zircon ages of volcanic rocks from northern New Brunswick are reported and a preliminary stratigraphy of the middle Ordovician Tetagouche and Fournier groups is presented. Deposition of the Tetagouche Group started with calcareous rocks of the Vallée Lourdes Formation in the Late Arenig (>470 Ma). Quartz- and feldspar-phyric felsic volcanic rocks of the immediately overlying Nepisiquit Falls Formation yielded U-Pb zircon ages between ca. 471 and 469 Ma. These volcanic rocks are time stratigraphic equivalents of the feldspar-phyric dacites of the Spruce Lake Formation, which yielded a U-Pb zircon age of ca. 470 Ma, and tholeiitic and alkalic pillow basalts of the structurally overlying Canoe Landing Lake Formation. The final phase of rhyolitic to dacitic volcanism is marked by the emplacement of distinct quartz- and feldspar-phyric dacitic porphyries at ca. 465 Ma, thus limiting silicic volcanism to the Late Arenig and Ilanvirn. During the Ilandeilo and Caradoc (ca. 464-457 Ma) volcanic activity in the Tetagouche Group was characterized by extrusion of alkali basalts and minor comendites, interlayered with dark shales and siltstones of the Boucher Brook Formation. Oceanic crust of the Fournier Group was also formed during this period.

Résumé : Le présent rapport fait état de sept datations U-Pb sur zircon de volcanites de la partie nord du Nouveau-Brunswick de même que d'une stratigraphie provisoire des groupes de Tetagouche et de Fournier de l'Ordovicien moyen. La sédimentation du Groupe de Tetagouche a débuté par le dépôt des roches calcaires de la Formation de Vallée Lourdes durant l'Arénigien tardif (> 470 Ma). Les volcanites felsiques à phénocristaux de quartz et de feldspath de la Formation de Nepisiquit Falls sus-jacente ont livré des âges U-Pb sur zircon variant entre environ 471 et 469 Ma. Ces volcanites sont des équivalents chronostratigraphiques des dacites à phénocristaux de feldspath de la Formation de Spruce Lake (datation U-Pb sur zircon à environ 470 Ma) ainsi que des basaltes coussinés tholéiitiques et alcalins de la Formation de Canoe Landing Lake, structuralement sus-jacente. La phase finale du volcanisme rhyolitique à dacitique est marquée par la mise en place, à environ 465 Ma, de porphyres dacitiques distincts à phénocristaux de quartz et de feldspath, ce qui limite le volcanisme silicique à l'Arénigien tardif et au Llanvirnien. Durant le Llandeilien et le Caradocien (environ 464-457 Ma), l'activité volcanique dans le Groupe de Tetagouche s'est traduite par l'extrusion de basaltes alcalins et d'un peu de comendites, interstratifiés avec des shales et des siltstones sombres de la Formation de Boucher Brook. La formation de croûte océanique associée au Groupe de Fournier remonte également à cette période.

[1] Contribution to Canada-New Brunswick Cooperation Agreement on Mineral Development (1990-1995), a subsidiary agreement under the Canada-New Brunswick Economic and Regional Development Agreement.

[2] Geological Survey of Canada, retired.

[3] Geological Survey of Canada, 601 Booth Street, Ottawa, Ontario K1A 0E8

INTRODUCTION

The Middle Ordovician, volcanic-dominated Tetagouche and Fournier groups of northern New Brunswick are exposed principally in the northern Miramichi Highlands and the Elmtree-Belledune Inlier (Fig. 1, 2). They represent the remnants of a back-arc basin that was closed during the Late Ordovician to Late Silurian (van Staal et al., 1990; van Staal et al., 1991; Winchester et al., 1992). The Tetagouche and Fournier groups were internally imbricated and folded into tight to isoclinal folds during the closure of the back-arc basin; hence the present distribution of the rock units represents a complexly folded tectonostratigraphy of volcanic and sedimentary rocks (van Staal, 1994a). Analysis of the chronostratigraphy of the formations present in the Tetagouche and Fournier groups is therefore of vital importance to the structural analysis and understanding the internal geometry of the volcanic-dominated units, assuming that chemically distinct volcanic suites formed within a specific period (van Staal et al., 1991). Furthermore both the Tetagouche and Fournier groups are host to numerous syngenetic massive sulphide deposits that occur in several stratigraphic settings (van Staal et al., 1992). Understanding the chronostratigraphies of the Tetagouche and Fournier groups is therefore important for massive sulphide exploration and ore genetical studies.

This paper presents the available U-Pb ages of volcanic rocks and a preliminary working stratigraphy for the Tetagouche and Fournier groups (van Staal and Fyffe, 1991). However as each volcanic formation in the Tetagouche Group appears to contain an internal chemical stratigraphy (Rogers, 1994, 1995), this paper is best considered a progress report that may be modified by future age determinations.

ANALYTICAL METHODS

Zircon was concentrated from crushed rock samples by conventional Wilfley table, heavy liquid, and Frantz magnetic separation techniques. Zircons were strongly air abraded to improve concordancy (Krogh, 1982). Chemistry, mass analyses, and data reduction procedures are similar those outlined in Parrish et al. (1987). Analytical blanks were typically 0 to 5 pg and 0 to 25 pg for U and Pb, respectively. Analytical data are presented in Table 1 and displayed on concordia diagrams in Figures 4 to 10. All quoted age errors are at the 2σ (95% confidence interval).

TETAGOUCHE GROUP

General stratigraphy

The base of the Tetagouche Group is well exposed at Little Falls in the Tetagouche River (Fig. 1). A black shale mélange in the underlying Miramichi Group is unconformably overlain by conglomerate and calcareous psammites and pelites of the Vallée Lourdes Formation (Fig. 3; van Staal and Fyffe, 1991; Rice and van Staal, 1992). The Vallée Lourdes Formation yielded middle Arenig to early Llanvirn conodonts and middle to late Arenig brachiopods (Nowlan, 1981; Neuman, 1984). The Vallée Lourdes Formation thus is best interpreted as having a middle to late Arenig age. These fossils are important as they impose upper and lower time constraints on the underlying sedimentary Miramchi Group and overlying volcanic rocks of the Tetagouche Group, respectively. Although the base of the Tetagouche Group is rarely exposed elsewhere, Vallée Lourdes Formation rocks occur locally in several places (van Staal et al., in press). Regional relationships suggest that the dark shales and siltstones of the Patrick Brook Formation that overlie the Vallée Lourdes Formation at Little Falls, interfinger stratigraphically with the calcareous rocks of the latter formation. Conglomerate beds intersected in a drill hole east of the Brunswick No. 12 mine (J. Peter, pers. comm., 1995) at the Patrick Brook Formation-Miramichi Group contact are consistent with such an interpretation, as they suggest that the Vallée Lourdes Formation was only locally deposited. At Little Falls and elsewhere, the Patrick Brook Formation is conformably overlain by and interfingers with tuffaceous sediments and quartz- and feldspar-phyric dacite and rhyolite of the Nepisiguit Falls Formation (van Staal et al., 1992; Rice and van Staal, 1992).

In the western part of the northern Miramichi Highlands, near the hinge of the Tetagouche antiform, volcanic rocks similar to those of the Nepisiguit Falls Formation occur as small lenses interlayered with sanidine-phyric dacite and rhyolite of the Spruce Lake Formation (formally referred to as Caribou Mine Formation by Rogers, 1994, 1995), suggesting that these two formations are coeval. This suggestion is consistent with the observation that both the Nepisiguit Falls and the Spruce Lake formations are host to several massive sulphide deposits and iron-formation. However, the banded iron-formation, typically associated with the massive sulphides in the Nepisiguit Falls Formation, is generally rare and where present, jasperitic in nature in the Spruce Lake Formation, suggesting that depositional conditions varied in the Tetagouche basin both in space and time. Both the Nepisiguit Falls and Spruce Lake formations contain several chemically distinct porphyritic silicic volcanic rocks (Rogers, 1995), commonly referred to as porphyries. Each porphyry probably formed at different times. The porphyries of the Spruce Lake Formation are interlayered with pillowed tholeiitic basalts of the Forty Mile Brook suite (van Staal et al., 1991), indicating that this formation was deposited subaqueously. A feldspar-phyric dacitic tuff that closely resembles the Orvan Brook porphyry (Rogers, 1994, 1995) is interlayered with the alkali pillow basalts and comendites of the Canoe Landing Lake Formation suggesting that the Spruce Lake and Canoe Landing Lake formations are coeval. This dacite has yielded an age of 470+4/-2 Ma (Sullivan and van Staal, 1993).

The Nepisiguit Falls Formation is stratigraphically overlain by the Flat Landing Brook Formation, which comprises aphyric or sparsely feldspar-phyric rhyolites, pyroclastic rocks, tholeiitic basalts, and minor shales (van Staal and Fyffe, 1991; van Staal et al., 1991; 1992). A U-Pb zircon age determination on an aphyric rhyolite yielded a date of 466 ± 5 Ma (Sullivan and van Staal, 1990). The Flat Landing Brook rhyolites have been intruded by and/or are interlayered with chemically distinct quartz-feldspar phyric dacite porphyries (Rogers, 1994,1995), which do not seem to intrude

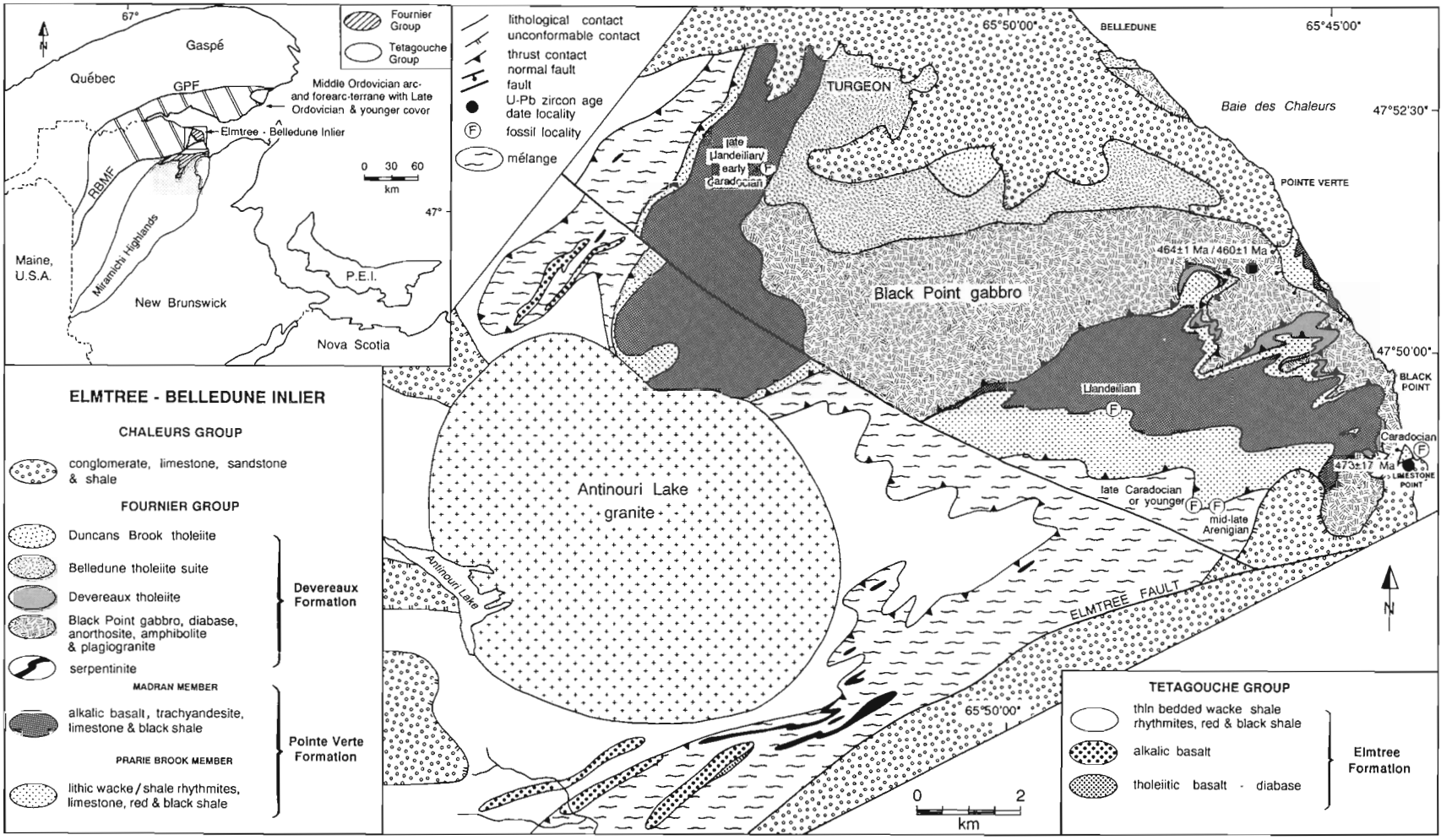

Figure 1. *Geological map of the northern Miramichi Highlands with the location of the dated samples. Geology modified from van Staal (1994a).*

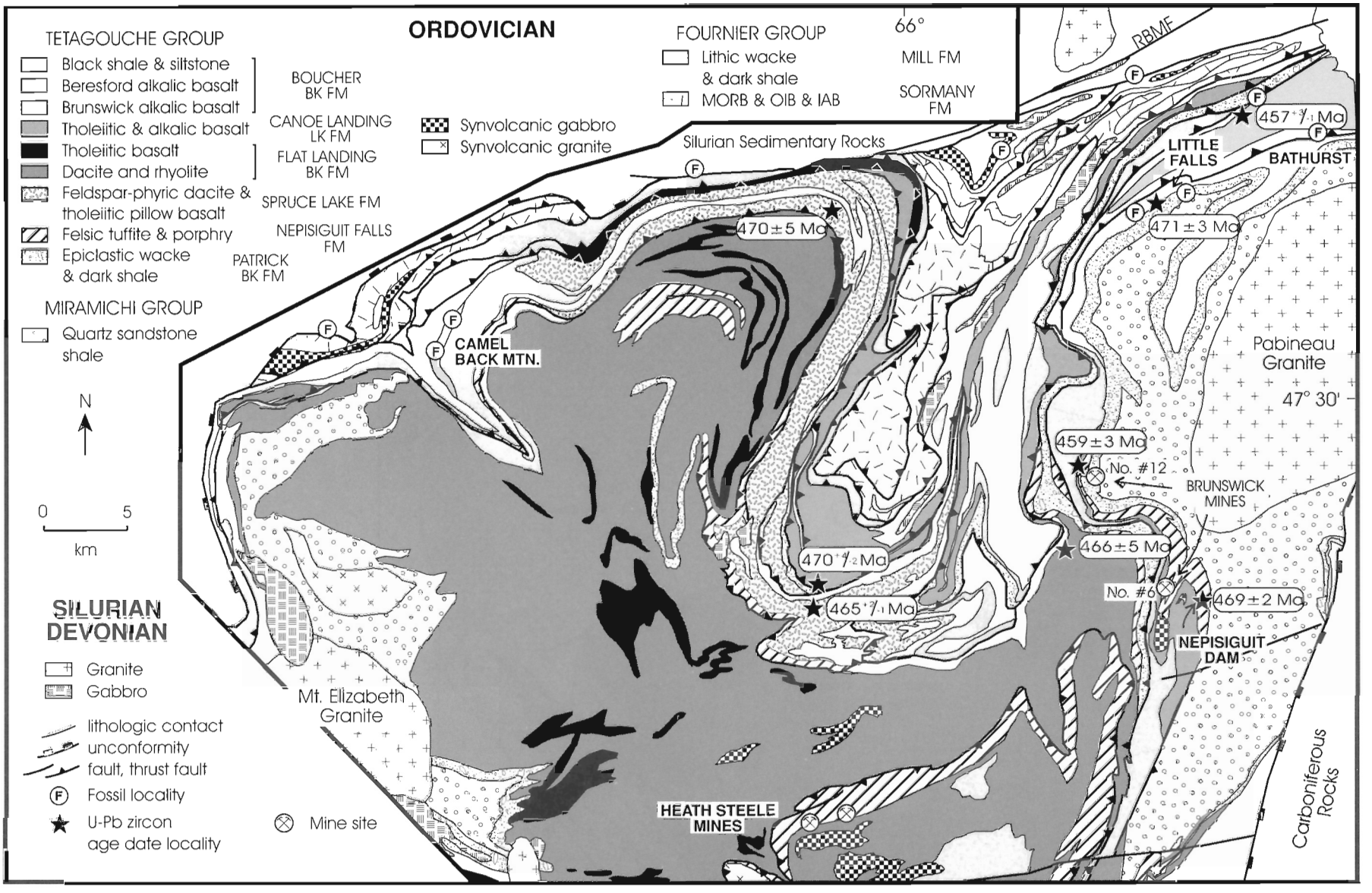

Figure 2. *Geology of the Elmtree-Belledune inlier, modified from Winchester et al. (1992).*

Table 1. U-Pb zircon isotopic data.

Sample & Fraction	Wt. µg[a]	U ppm	Pb* ppm	$^{206}Pb/^{204}Pb$[b]	Pb[c] pg	$^{208}Pb/^{206}Pb$[d]	$^{206}Pb/^{238}U$[d]	$^{207}Pb/^{235}U$[d]	Cor.[e] Coef.	$^{207}Pb/^{206}Pb$[d]	$^{207}Pb/^{206}Pb$ age (Ma)
Nepisiguit Falls Formation (NFFm)											
1. Quartz and feldspar augen schist VL-631 (47°36'80"N, 65°49'60"W)											
A,+105	54	205	28	5618	17	0.103	0.13644±.09%	1.5477±.10%	0.94	0.08227±.03%	1252.0±1.3
B,-105+74,3:1	41	167	18	5559	8	0.091	0.10610±.09%	1.0891±.10%	0.95	0.07444±.03%	1053.5±1.3
C,-105+74,3:1	28	187	24	2599	16	0.107	0.12649±.10%	1.2991±.11%	0.94	0.07449±.04%	1054.7±1.6
E,±105+62,5:1	5	87	7	162	15	0.127	0.07578±.33%	0.5869±1.2%	0.62	0.05618±1.0%	459.3±45.1
F,±105+62,5:1	10	351	31	1560	12	0.158	0.08318±.10%	0.7083±.15%	0.71	0.06176±.11%	665.8±4.6
2. Quartz and feldspar augen schist VL-307 (47°24'45"N, 65°47'50"W)											
A,-105+74,euh	40	269	25	2842	23	0.079	0.09537±.10%	0.8907±.13%	0.83	0.06774±.07%	860.5±3.0
B,-105+74,acic.	28	233	18	1416	22	0.107	0.07550±.20%	0.5855±.26%	0.70	0.05625±.19%	462.1±8.3
C,-74+62,acic.	21	246	19	638	40	0.119	0.07554±.30%	0.5850±.46%	0.58	0.05617±.37%	459.0±16.5
D,-74+62,3:1	48	257	24	2877	26	0.087	0.09521±.16%	0.9112±.18%	0.84	0.06941±.10%	910.9±4.0
E,-62,2:1	30	311	26	1810	28	0.078	0.08639±.11%	0.7567±.15%	0.76	0.06353±.10%	726.0±4.1
F,-105+62,acic.	137	241	19	6926	23	0.116	0.07618±.09%	0.5966±.10%	0.91	0.05680±.04%	483.9±1.9
H,-105+62,≥4:1	77	275	21	4506	23	0.109	0.07762±.09%	0.6246±.11%	0.90	0.05836±.05%	543.3±2.2
Spruce Lake Formation											
3. Feldspar-phyric dacite VL-644 (47°37'00"N, 66°06'02"W)											
A,+74,2:1,W,F	14	169	19	392	39	0.245	0.09871±.16%	1.0048±.33%	0.68	0.07383±.25%	1036.8±10.1
B,≥4:1,acic.	15	193	16	80	223	0.216	0.07555±.59%	0.5848±2.4%	0.67	0.05614±2.0%	458.0±90.7
C,-74,2:1	16	195	17	1293	11	0.220	0.07809±.09%	0.6227±.18%	0.69	0.05783±.13%	523.4±5.8
D,-74,≥4:1,acic	3	265	25	153	30	0.273	0.08206±.33%	0.6919±1.6%	0.58	0.06115±1.4%	644.5±62.3
Flat Landing Brook Formation (FLBFm)											
4. Quartz and feldspar-phyric rhyolite VL-638 (47°24'14"N, 66°05'40"W)											
A,+105	29	96	9	548	29	0.184	0.08858±.15%	0.7881±.24%	0.68	0.06453±.18%	759.2±7.4
B,+105	44	92	9	1677	15	0.168	0.09366±.09%	0.8658±.11%	0.88	0.06705±.05%	839.3±2.2
C,-105+74,≥4:1	17	100	8	693	12	0.178	0.07475±.12%	0.5782±.38%	0.60	0.05610±.32%	456.3±14.2
D,-105+74,2:1	22	86	8	902	11	0.206	0.08516±.11%	0.7343±.22%	0.57	0.06254±.18%	692.7±7.9
E,-74+62,5:1	22	115	9	1245	9	0.186	0.07487±.11%	0.5834±.23%	0.59	0.05652±.18%	472.7±8.1
F,-62,5:1,W,F	14	98	8	505	13	0.192	0.07481±.17%	0.5806±.53%	0.54	0.05629±.46%	463.8±20.4
Boucher Brook Formation											
5. Quartz and feldspar-phyric comendite dike VL-691 (47°28'20"N, 65°53'25"W)											
A,+74,3:1W	55	223	19	5695	11	0.186	0.08023±.09%	0.6572±.10%	0.95	0.05941±.03%	582.1±1.4
B,+74,3:1F	45	561	46	7325	17	0.207	0.07596±.09%	0.6002±.10%	0.94	0.05731±.04%	503.5±1.6
C,-62+37,E	25	321	26	4734	8	0.186	0.07470±.09%	0.5806±.10%	0.92	0.05637±.04%	467.0±1.8
D,-62+37,4:1	19	320	25	2872	10	0.188	0.07425±.09%	0.5769±.11%	0.92	0.05636±.04%	466.4±1.9
E,-74,5:1	10	188	15	127	79	0.195	0.07379±.33%	0.5716±1.4%	0.66	0.05618±1.2%	459.5±52.5
F,-74,E	7	364	29	450	27	0.181	0.07456±.14%	0.5803±.51%	0.57	0.05644±.45%	469.9±19.86
6. Aphanitic trachyandesite VL-637 (47°38'58"N, 65°47'53"W)											
B,+105,euh,W	9	304	31	488	32	0.239	0.09142±.27%	0.8292±.29%	0.90	0.06578±.13%	799.5±5.3
C,+105,F	16	516	45	549	72	0.331	0.07347±.12%	0.5694±.21%	0.73	0.05621±.15%	460.6±6.6
D,+105,F	11	546	60	1069	33	0.270	0.09461±.09%	0.8949±.12%	0.84	0.06860±.07%	886.7±2.8
E,residuals	12	494	42	596	47	0.294	0.07399±.12%	0.5744±.48%	0.59	0.05630±.42%	464.1±18.8
FOURNIER GROUP, Pointe Verte Formation											
7. Aphanitic tuffaceous rhyolite VL-646 (47°49'00"N, 65°43'43"W)											
A,-74,euh	19	186	22	935	27	0.163	0.11072±.09%	1.1314±.11%	0.87	0.07412±.06%	1044.7±2.3
B,-74,euh	21	143	21	706	37	0.179	0.13735±.12%	1.3912±.15%	0.76	0.07346±.10%	1026.6±4.0
C,±74,acic.	21	90	11	215	65	0.215	0.10980±.15%	1.0317±.37%	0.67	0.06815±.29%	873.0±12.0
D,+74,3:1,S	3	125	23	455	10	0.136	0.17343±.17%	1.7498±.20%	0.67	0.07317±.15%	1018.8±6.2
E,+74,2:1,S	4	369	97	2603	8	0.126	0.25144±.10%	3.1864±.11%	0.92	0.09191±.04%	1465.5±1.7
F,-62+37,euh	10	173	19	420	27	0.192	0.10092±.21%	0.9176±.57%	0.49	0.06594±.51%	804.6±21.2

Errors are 1 std. error of mean in % except $^{207}Pb/^{206}Pb$ age errors which are 2σ in million years.
Pb* = radiogenic Pb.
[a] Sample weight error of ± 1 µg in concentration uncertainty, all fractions were abraded, 3:1=L:B, W=whole zircons, F=zircon fragments, E=equant, Acic. = acicular, Euh = euhedral, S = single grain
[b] Corrected for fractionation and spike Pb
[c] Total common Pb in analysis in picograms
[d] Corrected for blank Pb and U, and common Pb
[e] Correlation Coefficient of errors in $^{206}Pb/^{238}U$ and $^{207}Pb/^{235}U$.

the alkali basalts and interlayered dark shales and siltstones of the overlying Boucher Brook Formation; hence they are considered to represent the last stage of volcanic activity contained within the Flat Landing Brook Formation.

The Flat Landing Brook, Spruce Lake, and Canoe Landing Lake formations are overlain by the Boucher Brook Formation, which therefore can be considered as a regional cover sequence to the volcanic-dominated formations of the lower part of the Tetagouche Group. The Boucher Brook Formation mainly consists of dark shales and siltstones interlayered with chert, alkali basalt, and associated red shale. Dark shale and siltstone also occur in the Patrick Brook Formation but chert, alkali basalt, and red shale are absent in the latter (van Staal et al., 1992).

Nepisiguit Falls Formation

The Nepisiguit Falls Formation comprises fine grained tuffaceous sediments, commonly containing quartz and feldspar phenoclasts, and quartz- and feldspar-phyric dacite to rhyolite porphyries. These silicic volcanic rocks are capped locally by iron-formation and massive sulphides. Because of the locally intense deformation, the porphyritic silicic volcanic and tuffaceous rocks are commonly referred to as quartz-feldspar augen schists (e.g. see Lentz and Goodfellow, 1993). Quartz-feldspar augen schists also occur locally in the Patrick Brook Formation, but black shale typical of the latter is absent in the Nepisiguit Falls Formation (van Staal et al., 1992). The porphyries represent at least in part pyroclastic flow deposits (e.g. Lentz and Goodfellow, 1993), but some may also represent shallow level intrusions. Two quartz-feldspar augen schists of the Nepisiguit Falls Formation were sampled for age dating (VL-307 and VL-631).

Quartz-feldspar augen schist: sample 1 (VL-631)

This sample is a relatively coarse grained rock taken from a large outcrop opposite the entrance to the Tetagouche Falls park (Fig. 2), west of Bathurst. This quartz-feldspar augen schist is bedded and locally some grading has been preserved. The augen schist consists mainly of juvenile pyroclastic fragments and over 60% by volume angular to moderately rounded phenoclasts of quartz and feldspar, indicating that they represent reworked silicic pyroclastic rocks, probably deposited distal from their source. These tuffaceous sandstones have been described by Rice and van Staal (1992) and are informally referred to as the Little Falls member of the Nepisiguit Falls Formation by Langton and McCutcheon (1993). They are separated by a few metres of dark shale and

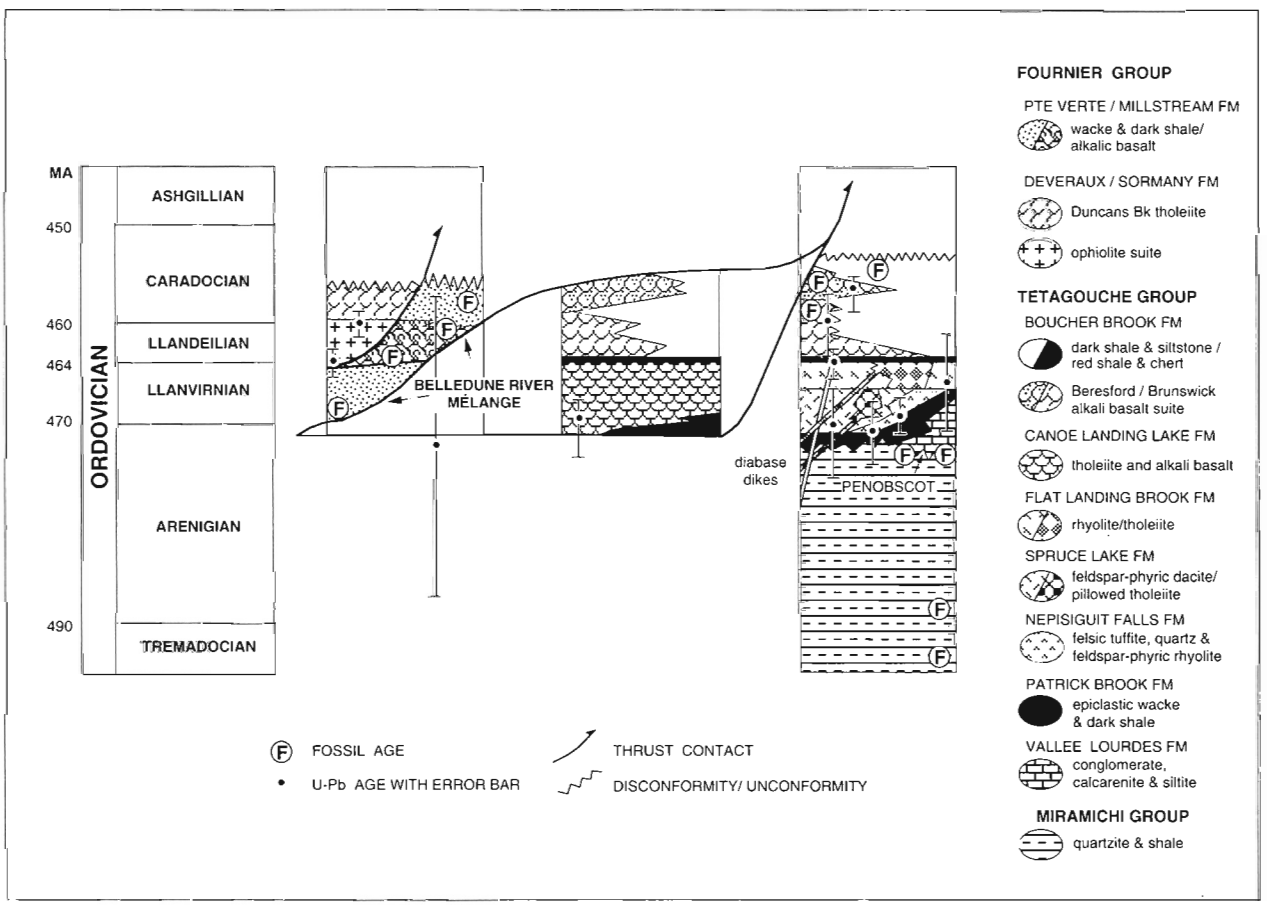

Figure 3. *Schematic tectonostratigraphy of the Tetagouche and Fournier groups with all U-Pb zircon ages determined by Sullivan and van Staal.*

siltstone of the Patrick Brook Formation from the calcarenites of the Vallée Lourdes Formation containing middle to late Arenig conodonts and brachiopods.

The zircon population consists of a variety of types including clear euhedral, prismatic, and acicular zircon. Some of the crystals have elongated terminations which appear multifaceted, with some showing distinct, and others more nebulous cores. Another type are clear and anhedral (rounded). Some zircons show a clear inner domain with a pink outer domain. Five zircon fractions A, B, C, E, and F were analyzed and gave a scattered linear trend that is interpreted as resulting from a mixture of inherited and magmatic zircons (Fig. 4).

The age of 471 ± 3 Ma is based on concordant fraction E which was picked from the most acicular (L:B ≥5:1) needle-like zircons and is interpreted to be essentially free of any inherited component. Fraction E ($^{206}Pb/^{238}U$ and $^{207}Pb/^{235}U$ ages are 471 ± 3 and 469 ± 9 Ma respectively) plots slightly above concordia but its error ellipse substantially overlaps the curve and was used to estimate the age and error (Fig. 4 inset). Regressing fraction E with other fractions, in pairs, yields upper intercept ages ranging from 1365 to 1680 Ma, which indicate a variety of ages of the inherited zircons.

Quartz-feldspar augen schist: sample 2 (VL-307)

The quartz-feldspar augen schist is a coarse grained tuffaceous rock taken from the base of the dam of the Nepisiguit Falls type locality (Fig. 2), near the stratigraphic top of the Nepisiguit Falls Formation, part of the Grand Falls member of Langton and McCutcheon, (1993). The quartz-feldspar augen schist is similar in composition to sample VL-631 of the Little Falls member. In contrast to the augen schists of the Little Falls member, those of the Grand Falls member are interbedded with layers of massive rhyolite of the Mt. Moser porphyry (Rogers, 1994,1995). These porphyritic rhyolites have been interpreted by Lentz and Goodfellow (1993) as subaqueous pyroclastic flow deposits. Although we agree at least in part with this interpretation, some of the coarse grained porphyritic rhyolites have very sharp contacts and appear to cut bedding at a very small angle, and may represent subvolcanic intrusions. The similarity in rare-earth element patterns between the tuffaceous rocks and the porphyritic rhyolites (McCutcheon et al., 1989) suggests that both rock types are related and derived from the same magmatic source; hence this sample is interpreted to give a representative age for the Mt. Moser porphyry.

The zircon population is characterized by rounded, dusty, purple and light tan grains, a few of which were pitted (possibly detrital), and clear, colourless euhedral zircons ranging from more equant prismatic (L:B up to 2:1) to acicular (L:B ≥4:1). These latter zircons are considered primary igneous but distinct cores were visible in some of the larger zircons. Bulbous caverns and longitudinal cavities were also observed. Seven zircon fractions A to F and H were analyzed from the clearest euhedral equant and acicular type. This yielded a linear trend that is interpreted as a mixing line (Fig. 5).

The interpreted age of 469 ± 2 Ma is based on concordant fractions B and C (essentially duplicate results) which contained acicular (L:B about 5:1) zircons that are considered to be essentially free of any inherited component. The other five fractions A, D, E, H, F (more equi-dimensional) have older ages and clearly contain inheritance. The age is estimated from the average of the four U-Pb ages of B and C, and the error estimated graphically from the concordia plot (Fig. 5 inset). The age of 469 ± 2 Ma is consistent, within error, by lower intercept (LI) regression results of the other fractions. Regression of five fractions A, D, E, H, and F only yields LI = 468 ± 8 Ma. The regression of all seven data gives LI = 469 ± 6 Ma and an upper intercept (UI) of 1580 ± 80 Ma.

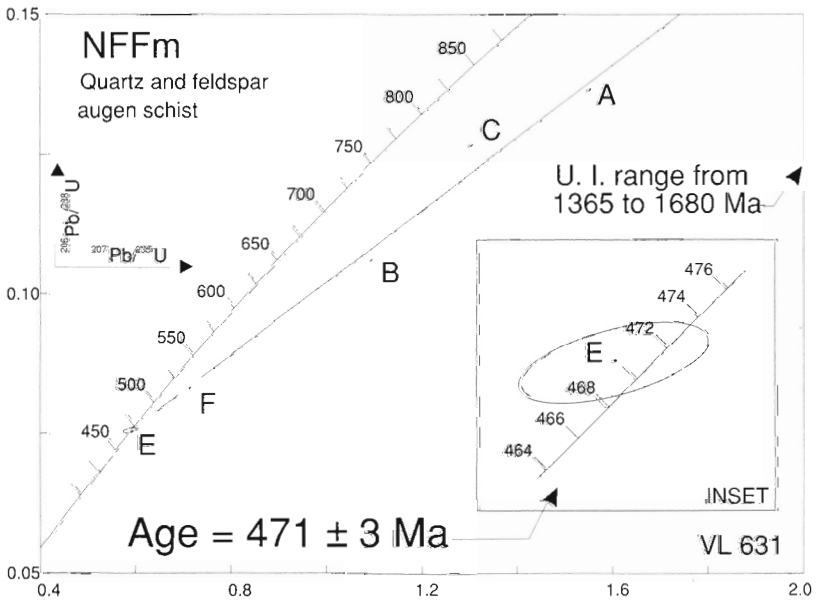

Figure 4.

U-Pb concordia diagram for sample 1, quartz and feldspar augen schist, from the Nepisiguit Falls Formation (NFFm). The upper intercept age range is generated by regressing fraction E with the other fractions in pairs.

Geological interpretation

The U-Pb zircon ages of the tuffaceous rocks of the Little Falls and Grand Falls members overlap in error and suggest an age of ca. 470 Ma for the bulk of the Nepisiguit Falls Formation. Although the Nepisiguit Falls Formation may contain three chemically distinct porphyries, the 469 ± 2 Ma of sample VL-307 may provide a minimum age if the interpretation by Rogers (1994, 1995) that the Mt. Moser porphyry is the youngest porphyritic rhyolite in the Nepisiguit Falls Formation is valid. The proximity of the Tetagouche Falls augen schist with respect to the underlying fossiliferous Vallée Lourdes Formation indicates that the Nepisiguit Falls Formation is late Arenig or early Llanvirn in age. This is consistent with the ca. 470 Ma age deduced for the Arenig-Llanvirn boundary by Tucker et al. (1990) on basis of U-Pb zircon dating of the Ordovician stratotypes in Britain.

Spruce Lake Formation

The Spruce Lake Formation contains three related feldspar-phyric dacitic porphyries, that are chemically, petrographically, and texturally distinct from the other felsic volcanic rocks in the Tetagouche Group (Rogers, 1994, 1995). The porphyries were initially included in the Flat Landing Brook Formation by van Staal and Fyffe (1991) although they were recognized as distinct and considered coeval with the Nepisiguit Falls Formation (dacite unit of Flat Landing Brook Formation in Fig. 3 of van Staal, 1994a). Rogers (1994, 1995) interpreted the dacitic porphyries mainly as shallow level sills and cryptodomes emplaced in dark shales of the Patrick Brook Formation, although lava flows and pyroclastic rocks also occur. The porphyries and associated sediments occur in closely associated thrust sheets emplaced on top of the Flat Landing Brook Formation (Fig. 1) during D_1 deformation (van Staal, 1994a). The relationship to the other Tetagouche Group volcanics is largely obscure as the thrust sheets are bounded by shear zones on all sides (tectonic horses of van Staal et al., 1990). However, they are locally interlayered with porphyritic volcanic rocks like those of the Nepisiguit Falls Formation, contain massive sulphide deposits and appear to have been intruded by quartz- and feldspar-phyric dacitic porphyries like those in the Flat Landing Brook Formation; hence they have been interpreted as coeval with eruption of volcanic rocks of the Nepisiguit Falls Formation.

Feldspar porphyry: sample 3 (VL-644)

This sample forms part of the Orvan Brook porphyry. The relative age relationships among the three porphyry suites in the Spruce Lake Formation are uncertain at this stage because of the very large D_1 strains imposed on the rocks.

The zircon population consists primarily of clear, colourless euhedral, prismatic and acicular crystals and crystal fragments with minor bubble inclusions. Evidence of possible resorption was visible, as were obvious cores in a few zircons. There was a minor amount of dark, well rounded, and pitted zircon. Four fractions A, B, C, and D define a linear trend (Fig. 6) that is interpreted as a mixing line.

The age of 470 ± 5 Ma is interpreted from concordant fraction B, picked from acicular (L:B ≥4:1) zircons and interpreted to be essentially free of inheritance. The other fractions are interpreted to contain inherited zircon components. The age and error were estimated graphically from the intersection of the error ellipse with the concordia curve (Fig. 6). Various regressions with the other fractions indicate somewhat higher ages. Regression of the three most concordant fractions B, C, D gives 476+4/-7 Ma. It is possible that

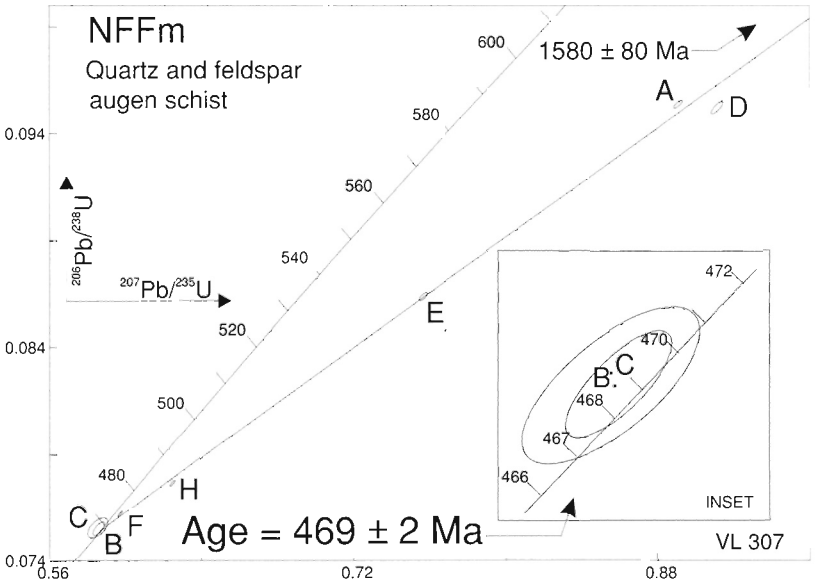

Figure 5.

U-Pb concordia diagram for sample 2, quartz and feldspar augen schist, from the Nepisiguit Falls Formation (NFFm). The upper intercept result of 1580 ± 80 Ma is from a regression of all seven fractions.

fraction B, even though concordant, may have suffered Pb loss and, as such, may be indicating an age that is somewhat too young. Fraction B contained the best fine, acicular zircons and was strongly abraded, so that, although a somewhat older age can not be ruled out, 470 Ma with realistic error of ±5 Ma is considered the best estimate of the age.

Geological interpretation

The U-Pb zircon age of 470 ± 5 Ma is consistent with the 470 Ma age deduced for the proposed time stratigraphic correlation with the Nepisiguit Falls Formation. Furthermore, it is similar in age to the 470+4/-2 Ma age of the narrow band of porphyritic dacitic tuff in the structurally overlying Canoe Landing Lake alkali basalt (Sullivan and van Staal, 1993).

Flat Landing Brook Formation

The Flat Landing Brook Formation is dominated by a suite of chemically related aphyric to sparsely feldspar-phyric dacites and rhyolites (Taylor Brook rhyolites) and pyroclastic rocks (Grant Lake pyroclastics, Rogers, 1994, 1995). Locally the felsic volcanic rocks are interlayered with tholeiitic basalts (van Staal et al., 1991), red shales, tuffaceous greenish-grey shales, and siltstones, and intruded by or interlayered with chemically distinct dacite porphyry (Rogers, 1994, 1995; O_{FP} on maps by van Staal, 1994b,c,d).

A spherulitic Taylor Brook rhyolite has given a U-Pb zircon age of 466 ± 5 Ma (Sullivan and van Staal, 1990), which is consistent with the field observation that the Flat Landing Brook Formation is younger than the stratigraphically underlying Nepisiguit Falls Formation (Lentz and van Staal, 1995). The Flat Landing Brook Formation is overlain by alkalic pillow basalts and shales of the Boucher Brook Formation. Fossils have not been found at the base of the Boucher Brook Formation; hence the upper age limit of the Flat Landing Brook Formation is not well defined.

Quartz-feldspar porphyry: sample 4 (VL-638)

This sample occurs as a narrow (2-3 m) band in the dacites of the Spruce Lake Formation south of Canoe Landing Lake (Fig. 2). This porphyry petrographically resembles the Wildcat porphyry of Rogers (1995), which cuts other chemically distinct quartz-feldspar porphyries that appear to have intruded the rhyolites and pyroclastics of the Flat Landing Brook Formation elsewhere (Rogers, 1994). Hence, it provides an upper age limit to the felsic volcanism of the Flat Landing Brook formation since similar porphyries appear absent in the overlying Boucher Brook Formation.

The zircon population contains clear to somewhat mottled, euhedral, prismatic, and acicular crystals. Some have rod- and bulbous-shaped inclusions. There was little visible evidence of cores. Six fractions A, B, C, D, E, and F were analyzed and gave a linear trend that is interpreted as a mixing line (Fig. 7).

An interpreted age of 465+2/-1 Ma is based on the concordant fractions C, E, and F. These are all acicular with L:B ≥4:1. The age and error were estimated graphically from the mean of the U-Pb ages with a minimum age given by the 464 Ma minimum of the $^{206}Pb/^{238}U$ ages of these three fractions (Fig. 7 inset). Regression of all six data gives LI = 465 ± 3 Ma and UI = 1520 ± 20 Ma (MSWD = 1.8).

Geological interpretation

The U-Pb zircon age of 465 +2/-1 Ma for the quartz- and feldspar-phyric porphyry is significant for the following reasons: (1) It signals the end of non-alkalic felsic volcanism and thus constraints the upper age of the Flat Landing Brook Formation and lower age of the Boucher Brook Formation; (2) The analyzed Devils Elbow Brook porphyry and the feldspar-phyric dacites of the Spruce Lake Formation it intrudes structurally underlie the Canoe Landing Lake alkali basalts, containing an interlayered porphyritic dacite that

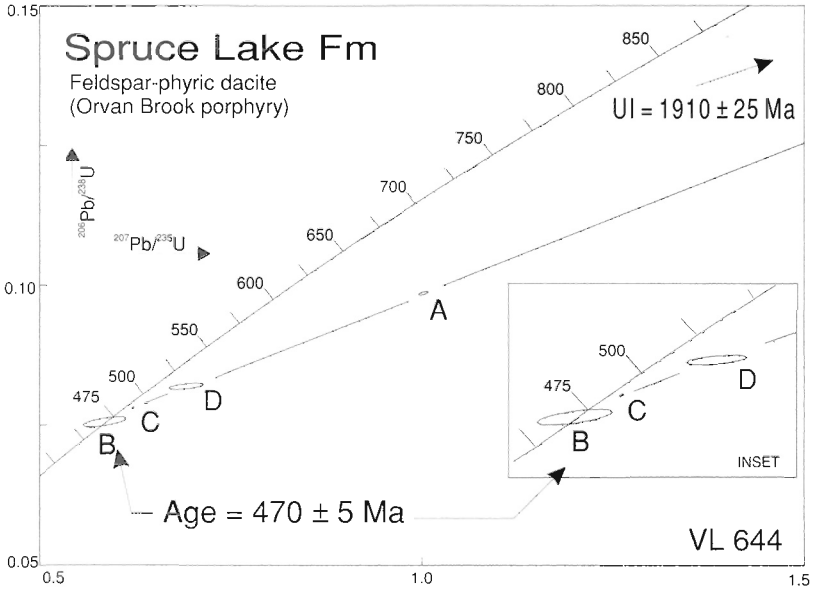

Figure 6.

U-Pb concordia diagram for sample 3, feldspar-phyric dacite, from the Spruce Lake Formation. The upper intercept result of 1910 ± 25 Ma is from a regression of the four fractions.

yielded a U-Pb zircon age of 470+4/-2 Ma (Sullivan and van Staal, 1993). This relationship requires a thrust somewhere in the highly deformed dark shales and siltstones, which separate the two volcanic formations (van Staal, 1994a,b).

Boucher Brook Formation

The Boucher Brook Formation consist mainly of dark shales and siltstones interlayered with alkalic basalts and intimately associated red cherts and red shales. The alkalic basalts, which locally contain differentiates of trachyandesite and comendite, either as flows, tuff layers, or dykes, comprise two main suites: the Brunswick alkali basalts and the Beresford alkali basalts (van Staal et al., 1991), both of which yielded fossil ages from interlayered limestone pods. Conodonts in limestone interlayered with alkali basalt and comendite of the stratigraphically upper part of the Brunswick suite on the western flank of the Camel Back Mountain, near the stratigraphic contact with the overlying Beresford suite (van Staal, 1994d) indicate an early Caradoc age (*Prioniodus variabilis* subzone of the A. tvaerensis zone, Nowlan, 1981). Conodonts in nearby limestone interlayered with the overlying Beresford suite alkali basalts indicate a middle Caradoc age (*Prioniodus alobatus* subzone of the *A. tvaerensis* zone, Nowlan, 1981). The alkalic basalts are overlain by Late Caradoc black shale of the *Dicranograptus clingani* zone (Riva and Malo, 1988) in Bathurst. Two felsic differentiates, one of each alkali basalt suite have been sampled for age dating.

Brunswick alkali basalt suite: sample 5 (VL-691)

A composite dyke ranging in composition from quartz- and feldspar-phyric comendite in the core to alkali basalt in the rim cuts the Nepisiguit Falls Formation in the footwall and Flat Landing Brook Formation in the hanging wall of the Brunswick No. 12 mine. The petrography of the dyke was described by Lentz and van Staal (1995), who considered the dyke to be a feeder to the overlying Brunswick alkali basalt suite volcanic rocks. The comendite core of the dyke from the west ore zone of the 850 m level in Brunswick No. 12 mine was selected for age dating. Extrusive comenditic volcanic rocks generally occur near the stratigraphic top of the Brunswick alkali basalt suite; hence this dyke is interpreted to provide age information concerning the upper part of the Brunswick alkali basalt suite.

The zircon population ranged from clear, colourless euhedral zircon, relatively free of internal features to those containing varying amounts of bleb-like bubble inclusions and rounded cavities. Equant, L:B ≥3:1, acicular, L:B ≥5:1, and flat platy zircon types were present. The acicular zircons were generally less clear. Cores were visible primarily in the coloured, more translucent zircons. Large, cored zircons were also observed in thin section. Twins were observed as were new zircon growths on the ends of presumably older crystals. Rounded and pitted (detrital) crystals were noted. The sample also contained abundant barite.

Six carefully selected zircon fractions A, B, C, D, E, and F were analyzed and form a linear trend between ca. 460 and ca. 1280 Ma, indicating that inheritance is involved (Fig. 8). The data set is quite linear, although fraction C (discussed below) falls somewhat above the general trend.

Fraction E consisted of fine acicular (L:B ≥5:1) crystals that were deliberately broken prior to abrasion and then picked again. This was done to test the idea that breaking the zircons would release any "core" and that with very selective picking, one might obtain a more concordant analysis. The procedure worked but because of sample loss, a relatively high error resulted. This most acicular fraction E, noted to have no visible core material, is concordant at 459 Ma but has a larger error ellipse resulting from a large common lead correction.

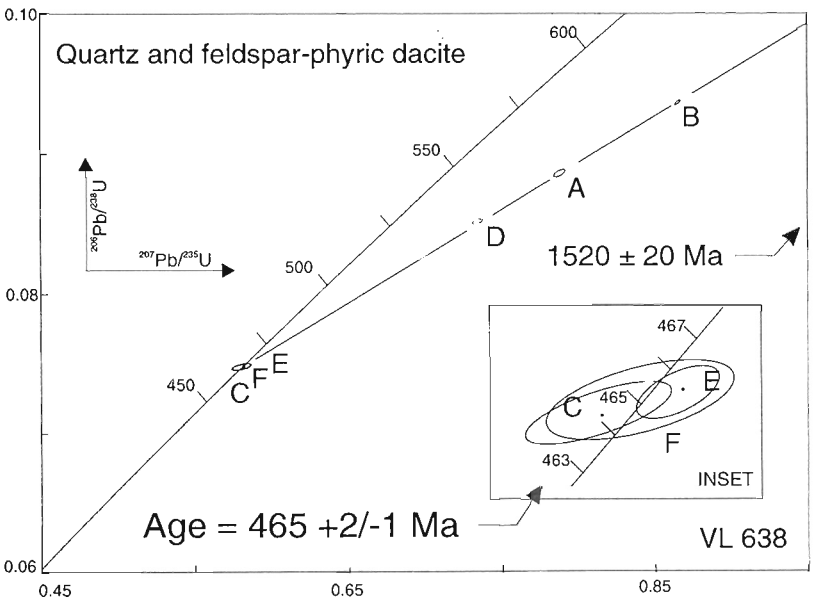

Figure 7.

U-Pb concordia diagram for sample 4, quartz- and feldspar-phyric dacite. The upper intercept result of 1520 ± 20 Ma is from a regression of the six fractions.

The interpreted age of 459 ± 3 Ma is based primarily on acicular fraction E but also on regression results which are consistent with this age. Regression of all 6 fractions gives LI = 461 ± 2 Ma and UI = 1280 ± 30 Ma (MSWD = 6.3). Regression of 5 fractions, excluding C, gives 459 ± 1 Ma (MSWD = 0.22). Regression of the two most discordant points A and B gives a lower intercept age of 459 ± 2 Ma.

Fraction C plots above the general linear trend but a linear trend also exists between fractions C and D, and possibly also E and F (Fig. 8). This indicates that Pb loss as well as inheritance may be involved. Fractions C and D have $^{207}Pb/^{206}Pb$ ages of 467.0 ± 1.8 and 466.4 ± 1.9 respectively, which may be closer to the actual age. Regressions of fractions C, D, E, and F forced through the origin gave ages of 466.7 ± 1.3 Ma. Thus, invoking Pb loss, an alternative interpretation is an age of 467 ± 2 Ma.

The preferred interpretation is that the dyke is 459 ± 3 Ma because fraction E contained the most acicular zircon, and because of the consistency of the other fraction regressions. This age is also consistent with the geological field evidence. An older age of ca. 467 Ma, however, can not be ruled out.

Geological interpretation

The interpreted age of 459 ± 3 Ma indicates that the Brunswick suite has a probable age range between 464 Ma and ca. 459 Ma. However, since the possibility of lead loss in the zircons can not be ruled out, the comendite could be as old as ca. 467 Ma. The interpreted 459 Ma age of the comendite correlates with the lowest subzone of the *A. tvaerensis* zone (Nowlan, 1981), and hence the base of the Caradoc. This is in good agreement with the results of Tucker et al. (1990), who placed the Caradoc-Llandeilo boundary at ca. 461 Ma.

Beresford suite: sample 6 (VL-637)

The Beresford suite contains locally two mappable basalt units (van Staal et al., 1991). These basalts are best preserved in an antiformal structure north of the town of Bathurst. Except for a very narrow strip of rocks along the southern limb of this structure, the pillowed basalts show a consistent younging towards the north (van Staal et al., 1988). A felsic trachyandesite (van Staal et al., 1991) interlayered with the youngest alkali basalt unit along the northern limb of this structure was collected for dating.

The zircon population consisted partly of euhedral to anhedral crystals, but was characterized by abundant massive crystal fragments that were relatively free of internal features. This habit may reflect the way they crystallized and the alkaline chemistry of the trachyte, or they could be broken larger zircons. The sample also contained clear euhedral zircon crystals, stubby to acicular L:B ≥5:1, fine- to coarse-grained, and often platy. Some of the larger euhedral zircon crystals have mottled interiors. There is a trace amount of rounded and pitted, possibly detrital, zircon. The sample also contained abundant euhedral apatite.

Four fractions B, C, D, and E were analyzed and produced a scattered linear trend that is interpreted as a mixing line (Fig. 9). A regression of all four fractions gives lower intercept = 457 ± 10 Ma. A regression of fractions C, F, and forced through the origin gives an upper intercept age of 461 ± 6 Ma. Fractions C and E are both concordant which makes interpretation somewhat problematic.

The preferred interpretation is an age of 457 ± 1 Ma based solely on concordant and analytically superior fraction C. The error being estimated graphically from the intersection of the error ellipse with concordia (Fig. 9 inset). The calculated ages for C are $^{206}Pb/^{238}U$ age = 457 ± 1, $^{207}Pb/^{235}U$ age = 458 ± 2, and $^{207}Pb/^{206}Pb$ age = 461 ± 7 Ma.

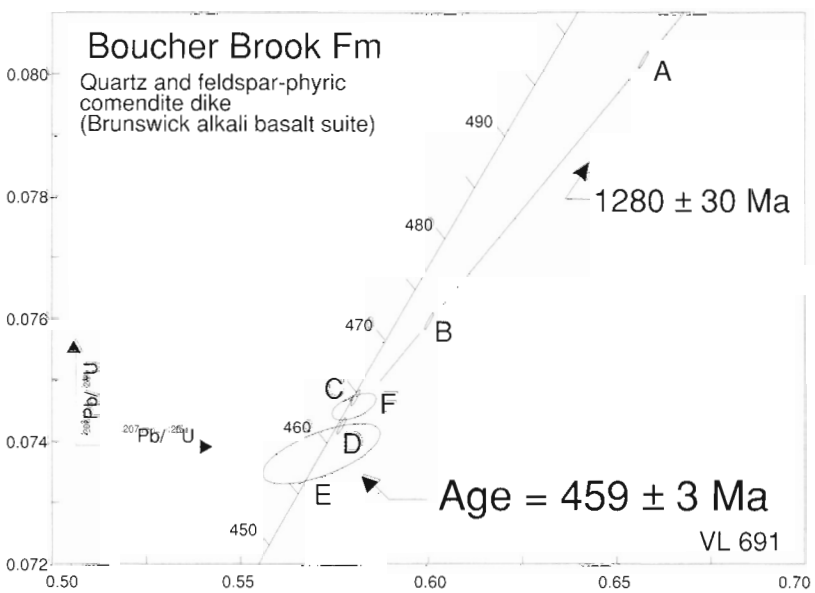

Figure 8.

U-Pb concordia diagram for sample 5, quartz- and feldspar-phyric comendite dyke from the Brunswick alkali basalt suite of the Boucher Brook Formation. The interpreted age of 459 ± 3 Ma based on fraction E is preferred, however, an alternative interpretation based on Pb loss indicates the age may be ca. 467 Ma (see text).

Fraction E is also concordant and appears to be slightly older, but with much larger errors. Inheritance is involved as evidenced from fractions B and D. Fractions C and E were both picked from large, clear, massive zircon fragments. Fraction C was selected after abrasion from the best, small grains, whereas E was selected from the larger grains. As such, fraction E may have had a small inherited zircon component that could explain its somewhat older age.

Another possibility is that fraction C has suffered recent Pb loss and that fraction E, at ca. 460 Ma, may be closer to the actual age. In this case, with age and error estimated graphically, an age of 460 ± 1 Ma is indicated.

The best age estimate is from the analytically superior fraction C at 457 ± 1 Ma but with a more conservative error of +3/-1 Ma assigned to reflect the interpretation that Pb loss is involved. Thus, 457+3/-1 Ma is the prefered age with assigned error.

Geological interpretation

The 457+3/-1 Ma age for the upper part of the Beresford suite dates the end of volcanic activity in the Tetagouche Group and correlates with the upper part of the *A. tvaerensis* zone, Nowlan (1981). This age is in good agreement with the 457 Ma U-Pb zircon date obtained by Tucker et al., (1990) for an ashbed occurring at the base of the *A. superbus* zone (conodont zone immediately above the *A. tvaerensis* zone) Gelli-grin limestone in Wales (Rhodes, 1953).

FOURNIER GROUP

The Fournier Group is best exposed in the Elmtree-Belledune Inlier north of Bathurst. The Fournier Group represents the ensimatic part of the Tetagouche back-arc basin. It was internally imbricated and emplaced above the Tetagouche Group during closure of the back-arc basin (van Staal et al., 1990). The highest thrust sheet contains the ophiolitic Deveraux Formation with a 464 ± 1 Ma age on gabbro and 460 ± 1 Ma on off-axis plagiogranite (Sullivan et al., 1990; Winchester et al., 1992). The Deveraux Formation structurally overlies the Pointe Verte Formation, that comprises lithic wackes, shales, and pillowed alkali basalts. Fossils indicate that the Pointe Verte Formation ranges in age between middle to late Arenig and the middle Caradoc (van Staal and Fyffe, 1991).

Felsic ash bed: sample 7 (VL-646)

A thick, aphanitic felsic ash bed, in the turbiditic lithic wackes, immediately north of Limestone Point was selected for age dating. Palynomorphs recovered from these rocks indicated a Caradoc age (A. Achab, written comm. to J. Langton, 1991).

The zircon population consists primarily of clear, colourless prismatic (L:B ≤3:1) crystals with lesser amounts of acicular (L:B = 4:1) types. The best zircon was in the finer -62, +37 µm size range. Four multi-grain fractions A, B, C, and F, and two single grain fractions D and E were analyzed and display a scattered linear trend when plotted (Fig. 10) which indicates that inheritance is involved.

The very discordant and scattered data preclude a low error estimate of the lower intercept regression age. The multi-grain analyses appear to be complex ≥3 component mixtures. Fraction A plots somewhat to the right of the general trend. An estimate of the age is taken from a regression of the three most concordant fractions A, C, and F which give a lower intercept of 473 ± 17 Ma and upper intercept age of 1209 ± 18 Ma. Single grain D plots slightly above the curve but is essentially concordant with $^{206}Pb/^{238}U$ age = 1031 ± 3 Ma. Single grain E is somewhat discordant but its

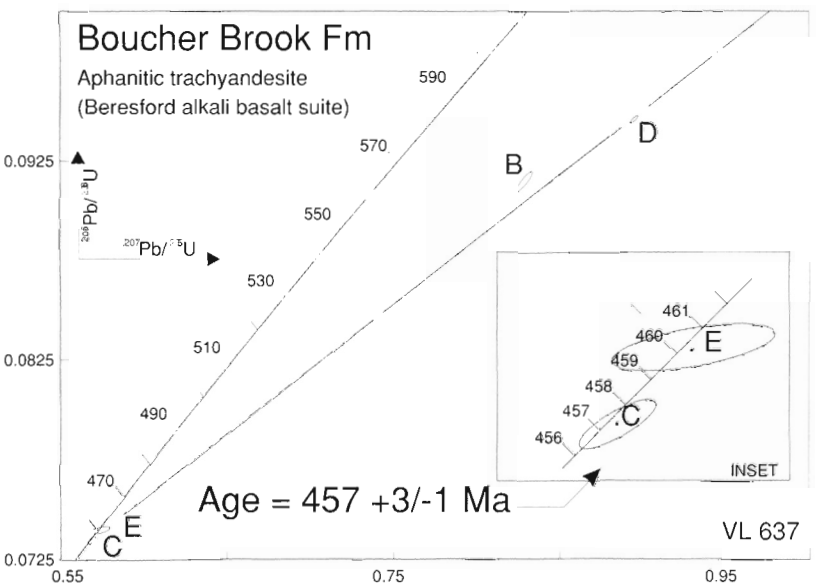

Figure 9.

U-Pb concordia diagram for sample 6, aphanitic trachyandesite from the Beresford alkaki basalt suite of the Boucher Brook Formation. The interpretated age and assigned error is based on fractions C and E.

$^{207}Pb/^{206}Pb$ age points to an age of 1467 ± 3 Ma. A lower intercept age of 473 ± 17 Ma is the best estimate available from this data set.

Geological implications

The lower intercept age of 473 ± 17 Ma confirms that the ashbed is Lower or Middle Ordovician in age, compatible with the fossil evidence. However, the large error covers the whole Middle Ordovician and part of the Lower Ordovician; hence it does not constitute a test or refinement of the inferred Caradoc age of this particular part of the Pointe Verte Formation on the basis of palynomorphs.

Significant is the presence of near concordant zircon xenocrysts. Single grains D with $^{206}Pb/^{238}U$ age of 1031 Ma, and E with $^{207}Pb/^{206}Pb$ age of 1467 Ma, suggests proximity of a basement that contains rocks of early and late Mesoproterozoic age. Basement of this age has been shown to be present beneath the Tetagouche Group (Roddick and Bevier, 1995, van Staal et al., in press).

CONCLUSIONS AND GEOLOGICAL IMPLICATIONS

The U-Pb zircon dates of the Tetagouche Group show a relatively simple volcanic stratigraphy. The non-alkalic felsic volcanic rocks seem to range in age between 471 and 465 Ma, which corresponds closely with the time period of the Llanvirn as determined by Tucker et al. (1990). Despite the overlap in error between most dated samples, the Nepisiguit Falls Formation volcanic rocks (ca. 470 Ma) are older than those in the Flat Landing Brook Formation (ca. 466 Ma), in accordance with the field relationships. The deposition of iron-formation and massive sulphides between these two chemically distinct volcanic sequences represent a period of relative volcanic quiescence, consistent with the lack of measured ages spanning the period between 469 and 466 Ma. The Spruce Lake Formation volcanic rocks (ca. 470 Ma) appear coeval with deposition of the Nepisiguit Falls Formation volcanic rocks, yet interfingering between the two types of volcanic rocks in the field is rare, suggesting the presence of several geographically separated volcanic centres juxtaposed by deformation.

The volcanic rocks in the Nepisiguit Falls and Spruce Lake formations are all time equivalents to the structurally overlying, relatively primitive tholeiitic and alkalic pillow basalts of the Canoe Landing Lake Formation (ca. 470 Ma, Sullivan and van Staal, 1993). However, basaltic feeder dykes with the appropriate composition have never been observed in the structurally underlying felsic volcanic rocks or sediments, supporting the interpretation that it is allochthonous and far travelled (van Staal et al., 1991). Probably the Canoe Landing Lake basalts and the underlying felsic volcanic rocks formed in widely separated parts of the Tetagouche back-arc basin. The structurally higher Canoe Landing Lake Formation probably formed closer to the oceanic side of the Tetagouche basin, perhaps representing transitional crust. Dark shales and greenish-grey siltstones, locally interfingering stratigraphically with the Canoe Landing Lake basalts, but generally occurring below the base of the Canoe Landing Lake Formation (van Staal, 1994b), are therefore mapped as Patrick Brook Formation. The Patrick Brook Formation also underlies and interfingers locally with the volcanic rocks of the Nepisiguit Falls and Spruce Lake formations (Fig. 3), indicating that the Tetagouche basin was dominated by reduced anoxic conditions for most of its lifespan (471-455 Ma), interrupted locally by more oxidizing conditions during short periods in the Llanvirn and Llandeilo as a result of volcanism. This is indicated by the intimate spatial association of oxide facies iron-formation, jasperite, and red shale with felsic and mafic volcanic rocks.

During the Llandeilo volcanic activity was characterized by extrusion of the Brunswick alkali basalts, minor comendites, and dark shales and siltstones in the Tetagouche Group, while oceanic crust was formed in the Fournier Group.

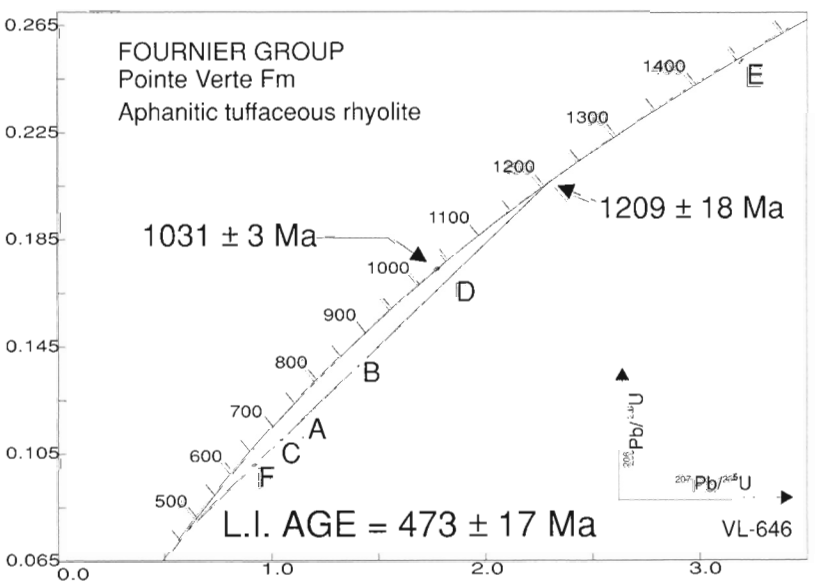

Figure 10.

U-Pb concordia diagram for sample 7, aphanitic tuffaceous rhyolite, from the Pointe Verte Formation of the Fournier Group. A lower intercept age of 473 ± 17 Ma from a regression of the three most concordant fractions B, C, and F only is the best estimate available from this data set. The upper intercept age of 1209 ± 18 Ma is from the same regression. Fractions D and E are single grains. Fraction D is essentially concordant with a $^{206}Pb/^{238}U$ age = 1031 ± 3 Ma. Fraction E has a $^{207}Pb/^{206}Pb$ age of 1467 ± 3 Ma.

Peralkaline volcanism in the Tetagouche basin waned in the early to middle Caradoc, while sedimentation, characterized mainly by black shale and cherts, records starved anoxic conditions.

ACKNOWLEDGMENTS

The authors gratefully acknowledge help with sample collection and discussions with Neil Rogers, Steve McCutcheon, Jan Peter, Dave Lentz, John Langton, Jim Mortensen, and Randy Parrish. Neil Rogers, Steve McCutcheon, and Randy Parrish critically reviewed the paper. We also thank the staff of the Geochronology Laboratory for assistance in generating the U-Pb data. This paper is, in part, a product of the Canada-New Brunswick Cooperation agreement on mineral development.

REFERENCES

Krogh, T.E.
1982: Improved accuracy of U-Pb zircon ages by the creation of more concordant systems using an air abrasion technique; Geochimica et Cosmochimica Acta, v. 46, p. 637-649.

Langton, J.P. and McCutcheon, S.R.
1993: Brunswick Project, NTS 21P/5 west, 21 P/4 west, Gloucester County, New Brunswick; in Current Research, (ed.) S.A. Abbott; New Brunswick Department of Natural Resources and Energy, Mineral Resources Division, Information Circular 93-1, p. 31-51.

Lentz, D.R. and Goodfellow, W.D.
1993: Petrology and mass-balance constraints on the origin of quartz-augen schist associated with the Brunswick massive sulphide deposits, Bathurst, New Brunswick; Canadian Mineralogist, v. 31, p. 877-903.

Lentz, D.R. and van Staal, C.R.
1995: Predeformational syngenesis at the Brunswick No. 12, Pb-Zn-Cu deposit, Bathurst, New Brunswick: evidence from the composite porphyry dike; Economic Geology, v. 90, p. 453-463.

McCutcheon, S.R., Brewer, A., and Belland, M.
1989: Brunswick project, Gloucester County, New Brunswick; in: Project Summaries for 1989, 14th Annual Review of Activities, (ed.) S.A. Abbott; New Brunswick Department of Natural Resources and Energy, Minerals, p. 110-118.

Neuman, R.B.
1984: Geology and paleobiology of islands in the Ordovician Iapetus Ocean: review and implications; Geological Society of America Bulletin, v. 94, p. 1188-1201.

Nowlan, G.S.
1981: Some Ordovician conodont faunules from the Miramichi Anticlinorium, New Brunswick; Geological Survey of Canada, Bulletin 345, 35 p.

Parrish, R.R., Roddick, J.C., Loveridge, W.D., and Sullivan, R.W.
1987: Uranium-lead analytical techniques at the geochronology laboratory, Geological Survey of Canada; in Radiogenic Age and Isotopic Studies: Report 1; Geological Survey of Canada, Paper 87-2, p. 3-7.

Rhodes, F.H.T.
1953: Some British Lower Paleozoic conodont faunas; Philosophical transactions of the Royal Society, v. 237, p. 261-334

Rice, R.J. and van Staal, C.R.
1992: Sedimentological studies in the Ordovician Miramichi, Tetagouche and Fournier groups, Bathurst Camp and Belledune-Elmtree Inlier, northern New Brunswick; in Current Research, Part D; Geological Survey of Canada, Paper 92-1D, p. 257-264.

Riva, J. and Malo, M.
1988: Age and correlation of the Honorat Group, southern Gaspé Peninsula; Canadian Journal of Earth Sciences, v. 25, p.1618-1628.

Roddick, J.C. and Bevier, M.L.
1995: U-Pb dating of granites with inherited zircon: conventional and ion microprobe results from two Paleozoic plutons, Canadian Appalachians; Chemical Geology, v. 119, p. 307-329.

Rogers, N.
1994: The geology and geochemistry of the felsic volcanic rocks of the Acadians Range Complex, Tetagouche Group, New Brunswick; PhD. thesis, Keele University, U.K., 420 p.
1995: The petrological variations of the Ordovician felsic volcanic rocks of the Tetagouche Group, New Brunswick; in Current Research 1995-E; Geological Survey of Canada, p. 279-286.

Sullivan, R.W. and van Staal, C.R.
1990: Age of a metarhyolite from the Tetagouche Group, Bathurst, New Brunswick, from U-Pb isochron analyses of zircons enriched in common Pb; in Radiogenic Age and Isotopic Studies: Report 3, Geological Survey of Canada, Paper 89-2, p. 109-117.
1993: U-Pb age of the Canoe Landing Lake Formation, Tetagouche Group, New Brunswick; in Radiogenic Age and Isotopic Studies: Report 7; Geological Survey of Canada, Paper 93-2, p. 39-43.

Sullivan, R.W., van Staal, C.R., and Langton, J.P.
1990: U-Pb zircon ages of plagiogranite and gabbro from the ophiolitic Deveraux Formation, Fournier Group, northeastern New Brunswick; in Radiogenic Age and Isotopic Studies: Report 3, Geological Survey of Canada, Paper 89-2, p. 119-122.

Tucker, R.D., Krogh, T.E., Ross, R.J., Jr., and Williams, S.H.
1990: Time-scale calibration by high precision U-Pb zircon dating of interstratified volcanic ashes in the Ordovician and Lower Silurian stratotypes of Britain; Earth and Planetary Science Letters, v. 100, p. 51-58.

van Staal, C.R.
1994a: The Brunswick subduction complex in the Canadian Appalachians: record of the Late Ordovician to Late Silurian collision between Laurentia and the Gander margin of Avalon; Tectonics, v. 13, p. 946-962.
1994b: Geology, Canoe Landing Lake, New Brunswick; Geological Survey of Canada, Map 1827A, scale 1:20 000.
1994c: Geology, Wildcat Brook, New Brunswick; Geological Survey of Canada, Map 1803A, scale 1:20 000.
1994d: Geology, Caribou Mines, New Brunswick; Geological Survey of Canada, Map 1826A, scale 1:20 000.

van Staal, C.R. and Fyffe, L.R.
1991: Dunnage and Gander Zones, New Brunswick: Canadian Appalachian Region; New Brunswick Natural Resources and Energy, Geoscience Report 91-2, 39 p.

van Staal, C.R., Fyffe, L.R., Langton, J.P., and McCutcheon, S.R.
1992: The Ordovician Tetagouche Group, Bathurst Camp, northern New Brunswick, Canada: history, tectonic setting and distribution of massive-sulphide deposits, exploration and mining geology; Journal of the Geological Society of the CIM, v. 1, p. 93-103.

van Staal, C.R., Ravenhurst, C., Winchester, J.A., Roddick, J.C., and Langton, J.P.
1990: Post-Taconic blueschist suture in the northern Appalachians of northern New Brunswick, Canada; Geology, v. 18, no. 10, p. 1073-1077.

van Staal, C.R., Sullivan, R.W., and Whalen, J.B.
in press: Provenance and tectonic history of the Gander Zone in the Caledonian/Appalachian Orogen: implications for the origin and assembly of Avalon; in Avalonian and Related Terranes of the Circum-North Atlantic, Geological Society of America, Special Paper.

van Staal, C.R., Winchester, J.A., and Bedard, J.H.
1991: Geochemical variations in Ordovician volcanic rocks of the northern Miramichi Highlands and their tectonic significance; Canadian Journal of Earth Sciences, v. 28, p. 1031-1049.

van Staal, C.R., Winchester, J.A., and Cullen, R.
1988: Geology and structure of the Bathurst-Millstream River area, New Brunswick: evidence for D1-related thrusting and folding; in Current Research, Part B; Geological Survey of Canada, Paper 88-1B, p. 135-148.

Winchester, J.A., van Staal, C.R., and Langton, J.P.
1992: The Ordovician volcanics of the Elmtree-Belledune Inlier and their relationship with volcanics of the northern Miramichi Highlands, New Brunswick; Canadian Journal of Earth Sciences, v. 29, p. 1430-1447.

- 6 -

A compilation of ^{40}Ar-^{39}Ar and K-Ar ages: Report 25

P.A. Hunt[1] and J.C. Roddick[2]

Hunt, P.A. and Roddick, J.C., 1996: A compilation of ^{40}Ar-^{39}Ar and K-Ar ages: Report 25; in Radiogenic Age and Isotopic Studies: Report 9; Geological Survey of Canada, Current Research 1995-F, p. 57-74.

Abstract: Twenty-three ^{40}Ar-^{39}Ar age determinations (including two potassium-argon analyses) carried out by the Geological Survey of Canada are reported. Each age determination is accompanied by a description of the rock and mineral concentrate used; brief interpretative comments regarding the geological significance of each age are also provided where possible. The experimental procedures employed are described in outline. An index of all Geological Survey of Canada K-Ar age determinations published in this format has been prepared using NTS quadrangles as the primary reference.

Résumé : Les auteurs présentent les résultats de vingt-trois datations ^{40}Ar-^{39}Ar (incluant deux analyses par la méthode K-Ar) réalisées par des scientifiques de la Commission géologique du Canada. Chaque datation est accompagnée d'une description de la roche et du concentré minéral utilisés; lorsque cela est possible, on présente aussi de brefs commentaires sur l'importance géologique de chaque âge déterminé. Le protocole expérimental est décrit dans les grandes lignes. Un index de toutes les datations K-Ar que la Commission géologique du Canada a publiées dans la série *Radiogenic age and isotope studies* a été préparé avec, comme référence principale, les numéros du SNRC.

[1] Geological Survey of Canada, 601 Booth Street, Ottawa, Ontario, K1A 0E8
[2] Deceased, February 1995

INTRODUCTION

This compilation of ^{40}Ar-^{39}Ar ages determined in the Geochronological Laboratories of the Geological Survey of Canada is the latest in a series of reports, the last of which was published in 1994 (Hunt and Roddick, 1994). In this new contribution twenty-three determinations are reported. As in the last report, a number of analyses (2) using the K-Ar technique are reported. An explanation of ^{40}Ar-^{39}Ar procedures used and general interpretation of the data are given below. The format of this compilation is similar to the previous reports, with data ordered by province or territory and subdivided by map sheet number. In addition to the GSC numbers, laboratory numbers (AAxxx and K-Ar xxxx) are included for internal reference.

EXPERIMENTAL PROCEDURES

Conventional K-Ar

The data compiled here represent analyses carried out between 1993 and 1994. Potassium, for conventional analyses, was analyzed by atomic absorption spectrometry on duplicate dissolutions of the samples. Conventional argon extractions were carried out using a radio frequency vacuum furnace with a multi-sample loading system capable of holding six samples. The extraction system is on-line to a modified A.E.I. MS-10 with a 0.18 tesla permanent magnet. An atmospheric Ar aliquot system is also incorporated to provide routine monitoring of mass spectrometer mass discrimination. Details of computer acquisition and processing of data are given in Roddick and Souther (1987). Decay constants recommended by Steiger and Jäger (1977) are used in the age calculations and errors are quoted at the 2 sigma level.

^{40}Ar-^{39}Ar analyses

The Geochronology Laboratory is replacing the conventional K-Ar dating with the ^{40}Ar-^{39}Ar step heating technique for most samples. In this technique a sample is irradiated in a nuclear reactor to convert some K atoms to ^{39}Ar. The ^{39}Ar is used as a measure of the K in the sample and a sample's age is determined by the measurement of the ^{40}Ar-^{39}Ar isotopic ratio (corrected for interfering isotopes and atmospheric Ar). By step-wise heating of a sample in a vacuum furnace ages can be calculated for Ar fractions released at incrementally higher temperatures. In general, ages determined from the higher temperature steps represent Ar released from more retentive sites in a mineral. For further analytical details see Roddick (1990) and for an explanation of the principles of the technique see McDougall and Harrison (1988) or Hanes (1991).

The analyses reported here consist of three heating steps, with the temperature of the first step selected to liberate most of the atmospheric argon but a minimum of the radiogenic argon from the sample. This step contains very little radiogenic Ar and usually is not reported. The next temperature step is selected to release about 50% of the radiogenic argon from the sample. A final fusion step releases any remaining Ar. The analyses are therefore essentially two age measurements and permit a comparative test of the consistency of the ages of argon released from a sample. If the ages of the two fractions are in agreement, it is assumed that a reliable age can be assigned to the sample. Should the ages differ then it is likely that there has been a disturbance to the K-Ar system in the sample.

The results are presented in a format similar to the K-Ar reports but with an additional section detailing the ages of the steps and the preferred age of the sample. The first age given represents the weighted mean age of all three gas fractions, weighted and summed according to the amounts of ^{39}Ar in each fraction, and is indicated as an integrated age with 2σ uncertainty limits. The error limit on the age includes uncertainty in irradiation calibration of the amount of K converted to ^{39}Ar (J factor, typically $\pm$ 0.5 - 1.0% 2σ) which must be considered when comparing the ages of different samples. The integrated age is equivalent to a conventional K-Ar age and, in samples that are not subject to recoil Ar loss (see McDougall and Harrison, 1988), is the age which would be determined by that technique. The per cent atmospheric argon in the sample is given for this integrated age. The ages of the last two steps are given separately, along with their 2σ uncertainties and proportions of sample argon, as percentages of ^{39}Ar, in the fractions. The uncertainties of these ages do not include irradiation calibration error since it does not contribute to uncertainties between heating steps on a single sample. If these two ages agree within their error limits the preferred age is a weighted mean of these fractions weighted by the amounts of ^{39}Ar in the fractions. The error estimate for this age also includes uncertainty in the irradiation calibration. This is termed the plateau age. If these two ages do not agree then one of the steps may be designated as the preferred age. In many cases of known complex geological history the age of highest temperature gas fraction may be the best estimate of the age as the lower temperature release may record a partial ^{40}Ar loss induced by the most recent geological reheating of the sample. In some cases excess argon is present in the initial Ar released and in this case the highest temperature step is also the best estimate of the age of a sample. Some explanation of the reason for the preferred age is given in the geological discussion of a sample.

The potassium concentration of the sample is also given. This is determined from calibration of the mass spectrometer as a precise manometer, the conversion factor for ^{39}Ar production, and the weight of the sample. The precision of this K concentration is one to four per cent and is limited mainly by errors associated with weighing of the small (4 to 30 mg) samples used for analyses.

The complete series of reports including the present one is given in the Appendix.

ACKNOWLEDGMENTS

We would like to thank Fred Quigg for the argon extractions and Diane Bellerive for the potassium analyses.

REFERENCES

Hanes, J.A.
1991: K-Ar and $^{40}Ar/^{39}Ar$ Geochronology: methods and applications; in Applications of Radiogenic Isotope Systems to Problems in Geology, (ed.) L. Heaman and J.N. Ludden; Mineralogical Association of Canada, v. 19, p. 27-58.

Hunt, P.A. and Roddick, J.C.
1994: A compilation of K-Ar and ^{40}Ar-^{39}Ar ages: Report 24; in Radiogenic Age and Isotopic Studies: Report 8; Geological Survey of Canada, Current Research 1994-F, p. 125-155.

McDougall, I. and Harrison, T.M.
1988: Geochronology and Thermochronology by the $^{40}Ar/^{39}Ar$ Method; Oxford University Press, Oxford, 272 p.

Roddick, J.C.
1990: $^{40}Ar/^{39}Ar$ evidence for the age of the New Quebec Crater, northern Quebec; in Radiogenic Age and Isotopic studies: Report 3; Geological Survey of Canada, Paper 89-2, p. 7-16.

Roddick, J.C. and Souther, J.G.
1987: Geochronology of Neogene volcanic rocks in the northern Garibaldi Belt, B.C.; in Radiogenic Age and Isotopic Studies: Report 1; Geological Survey of Canada, Paper 87-2, p. 25-32.

Steiger, R.H. and Jäger, E.
1977: Subcommission on Geochronology: convention on the use of decay constants in geo- and cosmo-chronology; Earth and Planetary Science Letters, v. 36, p. 359-362.

BRITISH COLUMBIA
(GSC 95-1 TO GSC 95-14)

GSC 95-1 Whole rock
45.1 ± 0.5 Ma, integrated ^{40}Ar-^{39}Ar

Wt % K = 3.43
K-Ar 4524 % Atmos. Ar = 10.5

(AA529) Ages of three heating steps (% gas):
45.3 ± 0.1 Ma (55%), 44.5 ± 0.5 Ma (19%), 44.8 ± 0.2 Ma (15%)
Preferred age: integrated ^{40}Ar-^{39}Ar age of 45.1 ± 0.5 Ma

(93B/12) From a dacite.
From a road outcrop, 0.8 km east of Clisbako Canyon, B.C.; 52°43′20.9"N, 123°33′13.1"W; UTM zone 10, 462607E, 5841329N; sample HHB933710. Collected and interpretated by P. Metcalfe.

For interpretation see GSC 95-4.

GSC 95-2 Whole rock
47.7 ± 0.5 Ma, integrated ^{40}Ar-^{39}Ar

Wt % K = 3.25
K-Ar 4525 % Atmos. Ar = 9.9

(AA530) Ages of two heating steps (% gas):
48.5 ± 0.1 Ma (23%), 47.6 ± 0.2 Ma (10%)
Preferred age: 33% gas plateau age of 48.2 ± 0.5 Ma

(93B/13) From a dacite.
From a roadside outcrop, 3.5 km south of the main Michelle Creek logging road, B.C.; 52°48′2.7"N, 123°43′2.6"W; UTM zone 10, 451645E, 5851368N; sample HHB933306; Collected and interpretated by P. Metcalfe.

For interpretation see GSC 95-4.

GSC 95-3 Whole rock
44.0 ± 0.4 Ma, integrated ^{40}Ar-^{39}Ar

Wt % K = 3.41
K-Ar 4526 % Atmos. Ar = 8.74

(AA531) Ages of three heating steps (% gas):
44.2 ± 0.1 Ma (64%), 41.2 ± 0.4 Ma (7%), 43.4 ± 0.2 Ma (8%)
Preferred age: integrated ^{40}Ar-^{39}Ar age of 44.0 ± 0.4 Ma

(93B/13) From a dacite.
On the west side of Little Mountain, roadside quarry, B.C.; 52°50′6.9"N, 123°54′48.1"W; UTM zone 10, 438469E, 5854119 N; sample HHB933501. Collected and interpretated by P. Metcalfe.

For interpretation see GSC 95-4.

GSC 95-4 Whole rock
48.3 ± 0.5 Ma, integrated ^{40}Ar-^{39}Ar

Wt % K = 2.68
K-Ar 4527 % Atmos. Ar = 8.33

(AA532) Ages of two heating steps (% gas):
48.0 ± 0.3 Ma (13%), 47.6 ± 0.5 Ma (4%)
Preferred age: 17% gas plateau age of 47.9 ± 0.6 Ma

(93C/16) From a dacite.
From the summit of Toil Mountain, B.C., 52°48′26.2"N, 124° 8′14.3"W; UTM zone 10, 423334E 5851224N; sample HHB933005. Collected and interpretated by P. Metcalfe.

The four samples analyzed from the Clisbako River area (GSC 95- 1, 2, 3, 4) are Eocene in age and have previously been assigned to the Ootsa Lake Group. All four samples are dacites and contain augite and plagioclase phenocrysts, with minor hornblende. Geophysical studies, satellite imagery, and

chemical coherence of the Clisbako volcanic area indicates that it is the root of an Eocene volcano with a late phase of intense pyroclastic activity. The four samples are interpreted as representing volcanic events prior to this eruption and indicate a period of activity extending from at least 48.2 Ma to 44.0 Ma.

GSC 95-5 Hornblende
119.8 ± 1.2 Ma, integrated ^{40}Ar-^{39}Ar

Wt % K = 0.750
K-Ar 4502 % Atmos. Ar = 17.9

(AA456) Ages of two heating steps (% gas):
120.4 ± 0.2 Ma (78%), 120.5 ± 0.7 Ma (20%)
Preferred age: 98% gas plateau age of 120.4 ± 1.2 Ma

(102P/9E) From a diorite.
From the sea cliffs on the exposed western side of Calvert Island, B.C., about 6 km south of the west end of Owikeno Traverse; 51°35.49′N, 128°8.34′W; UTM zone 9, 559650E, 5715750N; sample RD67.30235. Collected by W.W. Hutchison and interpreted by J.A. Roddick.

This sample is a dark, homogeneous, coarse grained, hornblende-rich diorite. A faint foliation can be seen trending northeast and dipping steeply to the southeast (050/75), oblique to the regional trend. The outcrop is cut by a swarm of basalt dykes trending west-northwest and dipping steeply to the north. The diorite is thought to represent a cleaner phase of the dioritic complex that underlies much of the eastern part of the island south of the apparently younger Calvert Island Pluton.

This is the westernmost dated rock between latitudes 51° and 52°N, and at 120.4 Ma, also the oldest. The Early Cretaceous (Aptian) age on hornblende is about equivalent to the 117 Ma biotite date obtained from a granite on Price Island, about 110 km to the northwest (see GSC 80-26 in Stevens et al., 1982).

For further interpretation see *Summary of ages from the Owikeno Traverse* after GSC 95-14.

GSC 95-6 Biotite
104.2 ± 1.0 Ma, integrated ^{40}Ar-^{39}Ar

Wt % K = 6.82
K-Ar 4505 % Atmos. Ar = 27.3

(AA459) Ages of two heating steps (% gas):
110.2 ± 0.2 Ma (74%), 112.1 ± 1.1 Ma (11%)
Preferred age: 85% gas plateau age of 110.5 ± 1.1 Ma

(102P/9E) From a leucocratic granite.
From the west side of the northern part of Calvert Island, opposite Surf Islands, on the west coast of B.C.; 51°39.90′ N, 128°8.41′W; UTM zone 9, 559470E, 5723920N; sample RD67.30245. Collected by W.W. Hutchison and interpreted by J.A. Roddick.

This sample is from the Pruth Bay Granite, a highly evolved pluton on the west coast. It consists of a leucocratic biotite granite with a highly variable texture that ranges from aplitic to coarse grained. It has well defined jointing, some close (5-30 cm) and some wide (2-70 m). The granite is inclusion-free and in most places massive. It is free of basalt dykes which cut the diorite to the south.

For interpretation see GSC 95-8.

GSC 95-7 Hornblende
110.1 ± 1.2 Ma, integrated ^{40}Ar-^{39}Ar

Wt % K = 0.589
K-Ar 4504 % Atmos. Ar = 43.0

(AA458) Ages of two heating steps (% gas):
110.0 ± 0.4 Ma (84%), 111.9 ± 1.0 Ma (15%)
Preferred age: 99% gas plateau age of 110.3 ± 1.1 Ma

(102P/9E) From a massive quartz monzodiorite.
From the north shore of Calvert Island, B.C., south side of Kwakshua Channel, about 8 km from west coast of the island; 51°39.07′N, 128°1.64′W; UTM zone 9, 567290E, 5722475N; sample RD67.50455. Collected by M. Lasserre and interpreted by J.A. Roddick.

This sample comes from near the western margin of Calvert Island Pluton. The rock is a clean, high-contrast, quartz monzodiorite, with abundant mafic minerals (40% in places), which probably accounts for the high density (2.86). The outcrop is marked by irregularly distributed amphibolitic inclusions, some elongate, some made nebulitic by feldspathic metasomatism.

For interpretation see GSC 95-8.

GSC 95-8 Hornblende
109.3 ± 1.3 Ma, integrated ^{40}Ar-^{39}Ar

Wt % K = 0.513
K-Ar 4503 % Atmos. Ar = 25.7

(AA457) Ages of two heating steps (% gas):
110.5 ± 0.3 Ma (77%), 109.7 ± 1.9 Ma (21%)
Preferred age: 98% gas plateau age of 110.3 ± 1.2 Ma

(92M/12) From a moderately foliated, mafic tonalite.
From the north shore of Calvert Island, B.C., 1.5 km west of Wedgborough Point, about 12 km from west coast of the island; 51°38.88′N, 127°58.10′W; UTM zone 9,

571382E, 5722170N; sample RD67.50575. Collected by M. Lasserre and interpreted by J.A. Roddick.

This sample comes from within 200 m of the eastern margin of Calvert Island Pluton. The rock is a homogeneous, rather dark tonalite containing about 2% amphibolitic inclusions with hornblende and biotite in about equal abundance which form, together, about 25% of the rock. The sample is moderately foliated (325/55), roughly parallel with the pluton margin and the regional trend.

The essentially identical dates of 110 Ma from GSC 95-6, 7, and 8 for hornblende and biotite suggests that the Pruth Granite is possibly a phase of the Calvert Island Pluton. With rapid cooling, the hornblende of the Calvert Island Pluton closed at about the same time as the biotite of the Pruth Granite. On this data alone it is not possible to distinguish between progressive west to east uplift and sequential intrusion.

For further interpretation see *Summary of ages from the Owikeno Traverse* after GSC 95-14.

GSC 95-9 Hornblende
107.8 ± 1.1 Ma, integrated ^{40}Ar-^{39}Ar

Wt % K = 0.6085
K-Ar 4501 % Atmos. Ar = 15.7

(AA455) Ages of two heating steps (% gas):
108.6 ± 0.3 Ma (81%), 109.5 ± 0.7 Ma (18%)
Preferred age: 99% gas plateau age of 108.7 ± 1.1 Ma

(92M/12) From a moderately foliated tonalite.
From the west shore of the B.C. mainland (east side of Fitz Hugh Sound), about 18 km from the west coast; 51°41.34′N, 127°52.81′W; UTM zone 9, 577414E, 5726821N; sample RD67.50371. Collected by M. Lasserre and interpreted by J.A. Roddick.

This sample was collected from near the western margin of Fish Egg Pluton. The actual contact, however, lies somewhere in adjacent Fitz Hugh Sound. The outcrop is formed by clean, coarse grained tonalite with north-trending, near-vertical moderate foliation.

This date was expected to confirm an eastward younging, even within the pluton, that was suggested by previous dates on biotite (103.7 Ma (see GSC 93-11 in Hunt and Roddick, 1993) from the central part of the pluton, and 96.6 Ma (GSC 93-13, Hunt and Roddick, 1993) from the eastern margin. This hornblende date of about 108 Ma, however, is within the error limits of the hornblende date (about 107 Ma, see GSC 93-12, Hunt and Roddick, 1993) obtained from the east side of the pluton. Taken at face value, the results suggest that progressive west to east unroofing of the pluton is reflected in the biotite dates but not in the hornblende dates. A biotite date from the west side and a hornblende date from the central part of the pluton are needed to resolve the matter.

GSC 95-10 Hornblende
78.2 ± 1.1 Ma, integrated ^{40}Ar-^{39}Ar

Wt % K = 0.478
K-Ar 4521 % Atmos. Ar = 20.9

(AA524) Ages of two heating steps (% gas):
77.8 ± 0.1 Ma (83%), 78.8 ± 1.0 Ma (16%)
Preferred age: 99% gas plateau age of 78.0 ± 0.8 Ma

(92M/10) From a mafic-rich, low-contrast diorite.
From a ridge 4 km north of the Machmell River, 9 km east of Owikeno Lake, about 96 km east of the B.C. mainland coast; 51°38.70′N, 126°30.52′W; UTM zone 9, 672377E, 5724283N; sample RD67.50758. Collected by M. Lasserre and interpreted by J.A. Roddick.

This sample is from a dark, low contrast diorite which is cut by synplutonic dykes and a feldspathic stockwork. Although included within the granitoid gneiss map unit, the rock is not foliated. On the basis of its density (2.92) the rock could be classified as a hornblende gabbro. The thin section shows 25-30% mafic minerals, dominated by decussate, irregular-shaped clusters of hornblende.

For interpretation see *Summary of ages from the Owikeno Traverse* after GSC 95-14.

GSC 95-11 Hornblende
85.4 ± 2.0 Ma, integrated ^{40}Ar-^{39}Ar

Wt % K = 0.715
K-Ar 4520 % Atmos. Ar = 19.6

(AA523) Ages of two heating steps (% gas):
84.1 ± 0.4 Ma (85%), 70.2 ± 1.3 Ma (14%)
Preferred age: step 3 age of 70.2 ± 1.5 Ma with 14% gas

(92M/9) From a mafic, strongly foliated quartz diorite.
From a ridge 3 km west of Ankitree Creek, 16 km east of Owikeno Lake, about 103 km east of the B.C. mainland coast; 51°40.45′N, 126°25.33′W; UTM zone 9, 678243E, 5727732N; sample RD67.50728. Collected by M. Lasserre and interpreted by J.A. Roddick.

The sample is from an unnamed quartz diorite pluton lying west of Machmell Pluton and in most places separated from it by the granitoid gneiss map unit. The rock has a prominent vertical foliation, striking northeasterly (065), across the regional trend. Aplitic veining and epidote are common. Mafic minerals are abundant, forming about 30% of the rock and in thin section are about evenly divided between hornblende and biotite. In this sample the ages of the two heating steps do not agree, excess argon was present in the initial Ar

released and so in this case the highest temperature step (step 3) is assumed to be the best estimate of the age of sample.

For interpretation see *Summary of ages from the Owikeno Traverse* after GSC 95-14.

GSC 95-12 Hornblende
75.8 ± 1.4 Ma, integrated ^{40}Ar-^{39}Ar

Wt % K = 0.979
K-Ar 4523 % Atmos. Ar = 27.6

(AA526) Ages of two heating steps (% gas):
74.6 ± 0.4 Ma (85%), 74.8 ± 0.7 (14%)
Preferred age: 99% gas plateau age of 74.6 ± 0.8 Ma

(92M/9) From a massive, high-contrast tonalite. From a ridge south of icefield, 6 km east of 'Ankitree Creek, about 112 km east of the mainland coast, B.C.; 51°40.46'N, 126°17.53'W; UTM zone 9, 687230E, 5728070N; sample RD82.12183. Collected and interpreted by J.A. Roddick.

This sample is a massive, homogeneous, high-contrast tonalite from the central part of Machmell Pluton. It is cut by epidote veins which are flanked by hydrothermally altered margins. Mafic minerals make up about 15% of the rock, with hornblende and biotite in about equal abundance.

For interpretation see *Summary of ages from the Owikeno Traverse* after GSC 95-14.

GSC 94-13 Hornblende
61.0 ± 0.7 Ma, integrated ^{40}Ar-^{39}Ar

Wt % K = 1.04
K-Ar 4522 % Atmos. Ar = 21.6

(AA525) Ages of three heating steps (% gas):
60.7 ± 5.4 Ma (3%), 61.1 ± 0.2 Ma (83%), 60.6 ± 0.9 Ma (13%)
Preferred age: integrated ^{40}Ar-^{39}Ar age of 61.0 ± 0.7 Ma

(92M/9) From a gneissic quartz diorite. From 2 km northeast of Mount Brager (within a kilometre of the eastern border of Rivers Inlet map area) B.C.; 51°44.22'N, 126°0.45'W; UTM zone 9, 706620E, 5735810N; sample RD82.12150. Collected and interpreted by J.A. Roddick.

This sample is from the granitoid gneiss map unit that forms a reentrant between Sheemahant and Page plutons. It contains about 15% screens of irregularly layered gneiss which consists of a dark, fine grained, salt and pepper amphibolite cut by a network of feldspathic (partly pegmatitic) veinlets. The gneissic foliation trends nearly due north and dips 70° west. The sample has the composition of quartz diorite, with about 12% mafic minerals. Hornblende and biotite are about equal in abundance.

This date is somewhat older than the 54 Ma and 58 Ma biotite ages from the Sheemahant Pluton (see GSC 80-45 in Stevens, et al., 1982, and GSC 93-10 in Hunt and Roddick, 1993), but the higher closure temperature of hornblende may account for the 61 Ma age. Interpretation is limited by the lack of a biotite date from this sample.

GSC 94-14 Biotite
76.6 ± 0.8 Ma, integrated ^{40}Ar-^{39}Ar

Wt % K = 7.25
K-Ar 4519 % Atmos. Ar = 15.7

(AA522) Ages of two heating steps (% gas):
76.8 ± 0.1 Ma (70%), 77.4 ± 0.2 Ma (28%)
Preferred age: 98% gas plateau age of 77.0 ± 0.8 Ma

(92N/13) From a homogeneous, massive tonalite. From Mount Waddington map area, about 1 km northeast of Wilderness Mountain, about 180 km east of the B.C. mainland coast; 51°56.76'N, 125°31.03'; UTM zone 10, 327000E, 5757800N; sample RD67.30956. Collected by W.W. Hutchison and interpreted by J.A. Roddick.

This sample is a tonalite from the Wilderness Mountain Pluton which borders the northwest end of Klinaklini Pluton. The outcrop is homogeneous, massive, with no inclusions visible. Thin section shows about 18% biotite. This body has yielded the most highly discordant biotite-hornblende dates in the Coast Mountains (see GSC 78-61,62 in Wanless et al., 1979, and GSC 80-23, 22 in Stevens et al., 1982). The former pair yielded 66 Ma biotite and 121 Ma hornblende, and the latter, 86 Ma biotite and 140 Ma hornblende. On the basis of further work by van der Heyden (1991), who named the body Wilderness Mountain Pluton, U-Pb dates were interpreted as Late Jurassic. This biotite date falls midway between the previous biotite dates, although the specimen was collected about 6 km to the northeast of the previously dated rocks. The specimen which yielded the 140 Ma hornblende came from a foliated quartz diorite-diorite that appears to be thrust northeasterly over the main mass of the pluton. Whether it is part of the pluton, or part of the more gneissic Atnarko Complex to the west is not definitely known. Interpretation remains difficult.

Summary of Ages from the Owikeno Traverse

The *Owikeno Traverse* is a closely sampled (roughly at 500 m intervals) traverse that extends across the Coast Plutonic Complex, from the west coast of Calvert Island (in Queens Sound map area, 102P/9E), across Rivers Inlet (92M) and Mount Waddington map areas (92N), and a short distance into

Anahim Lake map area (92C). In straight line segments the Owikeno Traverse consists of 11 km in 102P, 140 km in 92M, and 70 km in 92N, for a total of 221 km and about 400 stations.

At least one sample was collected at each station and for all homogeneous plutonic samples, specific gravity was measured. Except for gabbros and hornblendites, each plutonic sample was stained before estimates of the mineral abundances were made and the rock classified. The results of 232 chemical analyses from the traverse collection appear in Roddick (1983).

The Coast Mountains granitoid matrix in which the plutons are imbedded is very heterogeneous and difficult to map on any scale. It includes granitoid gneiss, layers of practically normal plutonic rock, dioritic complexes, elongate agmatites with narrow screens of amphibolite, and metavolcanic and metasedimentary rock (including crystalline limestone). In part it resembles the Central Gneiss Complex in the Douglas Channel map area to the north, but in this region it is not a well defined unit. Yet, the granitoid matrix underlies most of the area and, in spite of its complexity, dates from it may be more significant than those from the plutons.

The 10 ^{40}Ar-^{39}Ar age determinations in the current batch extend the dated part of the traverse with five new ages from the west end and five from the east end. The five new dates from the west end of the traverse extends the trend of east to west progressive cooling that was established previously (Hunt and Roddick, 1993, p. 132-136), and adds about 12 Ma to the oldest previous date. From west to east the major units dated are shown in Table 1.

Previous radiogenic dates for the major plutons include 57.5 Ma and 53.0 Ma biotites from the Sheemahant Pluton (see GSC 80-45 in Stevens et al., 1982, and GSC 93-10 in Hunt and Roddick, 1993); a hornblende-biotite pair from the Doos Creek Pluton (82, 85 Ma, respectively; see GSC 89-15, 16 in Hunt and Roddick, 1990); and a 77-67 Ma pair from Kwatna Pluton (see GSC 89-13, 14 in Hunt and Roddick, 1990).

By projecting the locations of those dates to the *Owikeno Traverse*, and treating the hornblende and biotite dates as separate data sets, Figure 1. charts the west to east sequences. The distances were calculated as perpendicular offsets from a line that trends 340 (the regional trend in that part of the world) and passes through the westernmost date (120.4 Ma) on Calvert Island (Table 2). Note that four date locations are off the line of the Owikeno Traverse, but they fit well when projected perpendicular to the axial trend of the Coast Plutonic Complex.

The hornblende sequence shows consistent younging eastward as far as the east side of Owikeno Pluton (biotite 74 Ma, hornblende 81 Ma; see GSC 93-24, 23 in Hunt and Roddick, 1993). The granitoid gneiss which confines the pluton on the east yielded a hornblende age of 100 Ma (see GSC 93-26, Hunt and Roddick, 1993). To the east the four hornblende ages from this study, 78-70-75-61 Ma (GSC 95-10, 11, 12, and 13) show a less consistent trend. The biotite sequence, while less consistent than the hornblende, also reflects a general west to east younging. The sequences may be interpreted as a gradual unroofing of the plutonic terrane from west to east. From other dates in other map areas in the Coast Plutonic Complex, the unroofing spanned a longer period of time, extending from the Late Jurassic to Late Eocene. Some of it seems episodic and some continuous. More data will probably indicate many exceptions to the overall trend and provide focal points for more detailed geological examinations.

Table 1. Major rock units dated from west to east along the Owikeno Traverse.

^{40}Ar-^{39}Ar ages from the Owikeno Traverse			
	Rock Units	Hornblende (Ma)	Biotite (Ma)
West to East	Calvert Island diorite	120.4	
	Pruth Bay Granite		110.5
	Calvert Island Pluton	110.3 (W side) 110.3 (E side)	
	Fish Egg Pluton	108.7 (W side) 106.5	103.7 (central) 96.6 (E side)
	Dioritic complex		99.4
	Granitoid gneiss	103.6 97.7 94.2	91.7 89.2 91.2
	Amback Pluton	87.4	85.4
	Owikeno Pluton	80.5	73.9
	Granitoid gneiss	100.0	80.6
	Unnamed pluton	70.2	
	Machmell Pluton	74.6	
	Granitoid gneiss	61.0	
	Sheemahant Pluton		57.5
	Wilderness Mountain Pluton		77.0

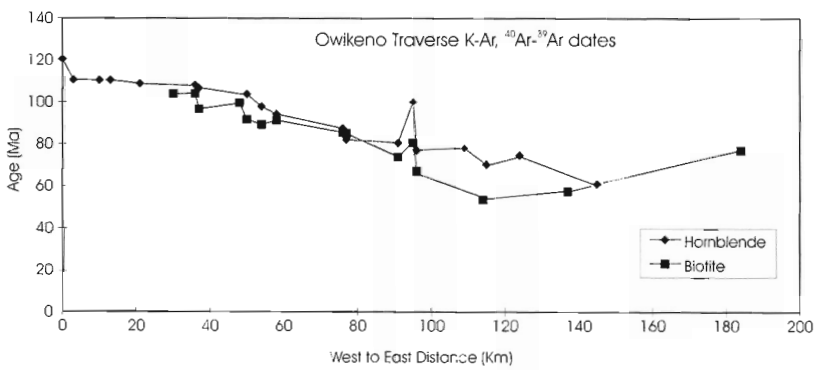

Figure 1.

Plot of age vs. west to east distance in km for hornblende and biotite ^{40}Ar-^{39}Ar and K-Ar ages for the Owikeno Traverse.

Table 2. Summary table of ^{40}Ar-^{39}Ar and K-Ar ages from rock units of the Coast Mt. Plutonic Complex.

Easting	Northing	Distance (km)	Hornblende (Ma)	Biotite (Ma)	Lab No.	Rock Unit	Distance from Traverse
559650	5715750	0.0002	120.4		GSC 95-5	Calvert Island diorite	
559470	5723920	2.70	110.5		GSC 95-6	Pruth Bay granite	
567290	5722475	9.52	110.3		GSC 95-7	Calvert Island Pluton	
571382	5722170	13.24	110.3		GSC 95-8	Calvert Island Pluton	
577414	5726821	20.52	108.7		GSC 95-9	Fish Egg Pluton	
586479	5730021	30.13		103.7	GSC 93-11	Fish Egg Pluton	
610680	5683022	36.29	108	104	GSC 76-17,18	Smith Inlet Pluton	45km S of OT
594563	5729358	37.47	106.5	96.6	GSC 93-12,13	Fish Egg Pluton	
605880	5728300	47.69		99.4	GSC 93-14	dioritic complex	
609171	5725375	49.75	103.6	91.7	GSC 93-16,15	granitoid gneiss	
612800	5726671	53.60	97.7	89.2	GSC 93-18,17	granitoid gneiss	
616972	5727588	57.83	94.2	91.2	GSC 93-20,19	granitoid gneiss	
636171	5728257	76.04	87.4	85.4	GSC 93-22,21	Amback Pluton	
643550	5712250	77.33	82	85	GSC 89-13,14	Doos Creek Pluton	13 km S of OT
652144	5727141	90.60	80.5	73.9	GSC 93-23,24	Owikeno Pluton	
656854	5726912	94.93	100	80.6	GSC 93-26,25	granitoid gneiss	
644600	5762250	95.87	77	67	GSC 89-15,16	Kwatna Pluton	35 km N of OT
672377	5724283	108.54	78		GSC 95-10	granitoid gneiss	
678243	5727732	115.25	70.2		GSC 95-11	unnamed Pluton	
667600	5753200	114.22		53.5	GSC 93-10	Sheemahant Pluton	30 km N of OT
687230	5728070	123.78	74.6		GSC 95-12	Machmell Pluton	
697010	5738540	136.61		57.5	GSC 80-45	Sheemahant Pluton	
706620	5735810	144.65	61		GSC 95-13	granitoid gneiss	
739000	5760800	183.74		77	GSC 95-14	Wilderness Mtn Pluton	

REFERENCES

Hunt, P.A. and Roddick, J.C.
1993: A compilation of K-Ar and ^{40}Ar-^{39}Ar ages: Report 23; in Radiogenic Age and Isotopic Studies: Report 1; Geological Survey of Canada, Paper 93-2, p. 127-154.

Roddick, J.A.
1983: Geophysical review and composition of the Coast Plutonic Complex south of latitude 55°N; in Circum-Pacific Plutonic Terranes, (ed.) J.A. Roddick; Geological Society of America, Memoir 159, p. 195-212.

Stevens, R.D., Delabio, R.N., and Lachance, G.R.
1982: Age determinations and geological studies; Geological Survey of Canada, Paper 81-2, 56 p.

van der Heyden, P.
1991: Preliminary U-Pb dates and field observations from the eastern Coast Belt near 52°N, British Columbia; in Current Research, Part A; Geological Survey of Canada, Paper 87-1A, p. 79-84.

Wanless, R.K., Stevens, R.D., Lachance, G.R., and Delabio, R.N.
1979: Age determinations and geological studies; Geological Survey of Canada, Paper 79-2, 67 p.

QUEBEC
GSC 95-15 TO GSC 95-18

GSC 95-15 Biotite
1028 ± 0.7 Ma, integrated ^{40}Ar-^{39}Ar

Wt.% K= 8.10
K-Ar 4492 % Atmos. Ar=0.85

(AA446) Ages of two heating steps (% gas):
1023 ± 1 Ma (37%), 1032 ± 1 Ma (62%)
Preferred age: step 3 age of 1032 ± 8 Ma with 62% gas

(31J/3) From a migmatitic metapelite.
From 1 km east of Lac du Camso, Quebec; 46°02.5′N, 75°25.5′W; UTM zone 18, 467400E, 5097950N; sample CQA3832. Collected and interpreted by K.J.E. Boggs.

This sample is from the melanosome of a strongly foliated, fine- to medium-grained, migmatitic metapelite (Corriveau et al., 1994; Corriveau and Jourdain, 1992). Leucosomes from this sample also have given a U-Pb zircon age of 1188 ± 1.2 Ma. The two step heating ages of this sample do

not agree within error and because of the known complex geological history the age of highest temperature gas fraction (step 3) is considered the best estimate of the age. This biotite age is also anomously old, nearly 50 Ma older than nearby biotite samples (see samples GSC 95-16 and GSC 95-17). This is most likely due to excess argon contained within the biotite of this sample. Extraneous argon is typical of Grenville biotite from Ontario (Cosca et al., 1991) to Labrador (Dallmeyer and Rivers, 1983).

See GSC 95-18 for references.

GSC 95-16 Biotite
932 ± 7 Ma, integrated ^{40}Ar-^{39}Ar

Wt% K = 7.36
K-Ar 4493 % Atmos. Ar = 1.2

(AA447) Ages of two heating steps (% gas):
963 ± 2 Ma (39%), 916 ± 1 Ma (60%)
Preferred age: step 3 age of 916 ± 1 Ma with 60% gas

(31 J/3) From migmatitic metapelite.
From 2 km east of Lac Fourchu, Quebec; 46°04.8′N, 75°18.1′W; UTM zone 18, 477200E, 5102800N, sample CQA3302. Collected and interpreted by K.J.E. Boggs.

This sample is from the melanosome of a strongly foliated, fine- to medium-grained, migmatitic metapelite (Corriveau et al., 1994; Corriveau and Jourdain, 1992). A U-Pb monazite from the melanosome of this sample has given a date of 1185 ± 3 Ma. This ^{40}Ar-^{39}Ar biotite age is interpreted as a cooling age through 300°C (Dodson and McClelland-Brown, 1985) following regional metamorphism. In this case where the step heating ages do not agree, the age of the highest temperature gas fraction (step 3) is considered the best estimate of the age.

Metamorphic cooling ages from this portion of the Central Metasedimentary Belt (CMB), Grenville Province, Quebec follow the same general pattern as those observed within the Central Metasedimentary Belt of Ontario (Cosca et al., 1992; Cosca et al., 1991). The belt yields a range of Precambrian cooling ages.

See GSC 95-18 for references.

GSC 95-17 Biotite
956 ± 8 Ma, integrated ^{40}Ar-^{39}Ar

Wt % K = 5.12
K-Ar 4494 % Atmos. Ar = 15.1

(AA448) Ages of two heating steps (% gas):
954 ± 1 Ma (64%), 967 ± 1 Ma (34%)
Preferred age: step 3 age of 967 ± 8 Ma with 34% gas

(31J/6) From a migmatitic metapelite.
From Highway 117, 1 km north of Lac Ganmon and Lacs Allard, Quebec; 46°26.7′N, 75°04.3′W; UTM zone 18, 494300E, 5148850N; sample CQA2039. Collected and interpreted by K.J.E. Boggs.

This sample is from the melanosome of a strongly foliated, fine- to medium-grained migmatitic metapelite (Corriveau et al., 1994; Corriveau and Jourdain, 1992). There are no U-Pb ages from nearby samples. In this case where the step heating ages do not agree, the age of the highest temperature gas fraction (step 3) is considered the best estimate of the age. This date possibly corresponds to cooling through 300°C (Dodson and McClelland-Brown, 1985) after extensive plutonism and shearing along the nearby Nominingue-Cheneville Shear Zone at c. 1165 Ma (Boggs et al., 1994). The Central Metasedimentary yields a range of Precambrian cooling ages.

See GSC 95-18 for references.

GSC 95-18 Biotite
1190 ± 9 Ma, integrated ^{40}Ar-^{39}Ar

Wt% K = 6.77
K-Ar 4495 % Atmos. Ar = 1.14

(AA449) Ages of two heating steps (% gas):
1199 ± 1 Ma (64%), 1191 ± 1 Ma (34%)
Preferred age: 98% gas plateau age of 1197 ± 9 Ma

(31J/6) From a migmatitic metapelite.
From east side of Lac Mountjoie, 1 km south of its northern end, Quebec; 46°18.5′N, 75°05.0′W; UTM zone 18, 491200E, 5128400N; sample CQA1280. Collected and interpreted by K.J.E. Boggs.

This sample is from the melanosome of a strongly foliated, fine- to medium-grained, migmatitic metapelite (Corriveau et al., 1994; Corriveau and Jourdain, 1992). A nearby U-Pb monazite has given an age of 1183 ± 3 Ma. This ^{40}Ar-^{39}Ar biotite age is anomously old, possibly due to extraneous argon incorporated into the biotite during peak metamorphism or shearing along the Nominingue-Cheneville Shear Zone at ca. 1165 Ma (Boggs et al., 1994). These abnormally old ^{40}Ar-^{39}Ar biotite ages are not uncommon throughout the Grenville from Ontario (Cosca et al., 1991) to Labrador (Dallmeyer and Rivers, 1983).

REFERENCES

Boggs, K.J.E., van Breemen, O., Corriveau, L., and Sawyer, E.W.
1994: New insights on metamorphism in the Central Metasedimentary Belt of Quebec, Grenville Province; Mineralogical Magazine, 58A, p. 105-106.

Corriveau, L. and Jourdain, V.
1992: Terrane characterization in the Central Metasedimentary Belt of the southern Grenville Orogen, Lac Nominingue map area, Quebec; in Current Research, Part C; Geological Survey of Canada, Paper 92-1C, p. 81-90.

Corriveau, L., Morin, D., et Madore, L.
1994: Géologie et cibles d'exploration de la partie centre est de la ceinture métasédimentaire du Québec, Province de Grenville; dans Recherches en cours 1994-C; Commission géologique du Canada, p. 355-365.

Cosca, M.A., Essene, E.J., Kunk, M.J., and Sutter, J.F.
1992: Differential unroofing within the CMB of the Grenville Orogen: Constraints from ^{40}Ar-^{39}Ar thermochronology; Contributions to Mineralogy and Petrology, v. 119, p. 211-255.

Cosca, M.A., Sutter, J.F., and Essene, E.J.
1991: Cooling and inferred uplift/erosion history of the Grenville Orogen, Ontario: Constraints from ^{40}Ar-^{39}Ar thermochronology; Tectonics, v. 10, p. 959-977.

Dallmeyer, R.D. and Rivers, T.
1983: Recognition of extraneous argon components through incremental-release ^{40}Ar-^{39}Ar analysis of biotite and hornblende across the Grenvillian metamorphic gradient in southwestern Labrador; Geochimica et Cosmochimica Acta, v. 47, p. 413-428.

Dodson, M.H. and McClelland-Brown, E.
1985: Isotopic and paleomagnetic evidence for rates of cooling, uplift and erosion; in The Chronology of the Geological Record, (ed.) N.J. Snelling; Memorandum of the Geological Society of London, v. 10, p. 315-325.

NOVA SCOTIA
GSC 95-19

GSC 95-19 Biotite
367.7 ± 3.3 Ma, integrated ^{40}Ar-^{39}Ar

Wt % K = 6.16
K-Ar 4506 % Atmos. Ar = 3.72

(AA460) Ages of two heating steps (% gas):
372.5 ± 0.4 Ma (75%), 368.9 ± 0.5 Ma (21%)
Preferred age: step 3 age of 368.9 ± 3.4 Ma with 21% gas

(11K/10) From a pelitic schist.
On the Pembroke Lake road, 2.8 km northeast of Margaree River, Nova Scotia; 46°34′57"N, 60°52′12"W; UTM zone 20, 663497E, 5160448N; sample CP93194. Collected and interpreted by K.L. Currie.

The sample was collected from a pelitic schist, with the assemblage biotite-muscovite-garnet, which forms a screen 4 m wide between migmatitic granite bodies with many pegmatite layers up to several centimetres thick. These migmatitic granites form part of the Belle Cote Road gneiss, for which a Silurian U-Pb zircon emplacement age of 429 Ma was obtained near this locality (Jamieson et al., 1986). The Belle Cote Road gneiss, 500 m to the west (but probably <100 m vertically) is thrust west over the Latest Devonian or Early Carboniferous Fisset Brook Volcanics along the Margaree Shear Zone (Lynch and Tremblay, 1994). This resulted in the formation of new biotite and muscovite in the shear zone. The two heating step ages do not agree within error so therefore the highest temperature gas fraction may be the best estimate of the age. This Ar-Ar age therefore suggests that (i) any screens or enclaves in the Belle Cote Road gneiss were metamorphosed sufficiently at ~370 Ma that no trace of pre-Acadian metamorphism persists (if any existed), and (ii) that traces of post-Acadian (Late Devonian-Carboniferous) metamorphism, if any, cannot be found outside major shear zones. The coincidence of the Ar-Ar date with U-Pb zircon dates for granitic plutons in this region (compare Jamieson et al., 1986) confirms that Acadian granite emplacement was accompanied by rapid uplift and unroofing, a conclusion previously reached on stratigraphic grounds.

REFERENCES

Jamieson, R.A., van Breemen, O., Sullivan, R.W., and Currie, K.L.
1986: The age of igneous and metamorphic events in the western Cape Breton Highlands, Nova Scotia; Canadian Journal of Earth Sciences, v. 23, p. 1891-1901.

Lynch, G. and Tremblay,C.
1994: Late Devonian-Carboniferous detachment faulting and extensional tectonics in western Cape Breton Island, Nova Scotia, Canada; Tectonophysics, v. 238, p. 231-245.

NEWFOUNDLAND
GSC 95-20 to GSC 95-23

GSC 95-20 Muscovite
383 ± 5 Ma
Wt % K = 8.19
Rad. Ar = 1.356×10^{-4} cm^3/g
K-Ar 4387 % Atmos. Ar= 0.7

(11O/10) From a muscovite-rich schistose granite.
Derived from Windowglass Hill Granite, 18 km northeast off Port Aux Basques, Trench along H Brook of the Isle Aux Morts River, Newfoundland; 47°47′00"N, 58°55′00"; UTM zone 21, 356500E 5291500N; sample BD137-91. Collected by B. Dubé and interpreted by B. Dubé and K. Lauzière.

See GSC 95-23 for interpretation.

GSC 95-21 Muscovite
381 ± 6 Ma

Wt % K = 8.14
Rad. Ar = 1.343×10^{-4} cm^3/g
K-Ar 4386 % Atmos. Ar = 0.9

(11O/10) From a muscovite-rich schistose granite. From the Windowglass Hill Granite, 18 km northeast of Port Aux Basques, Trench along H Brook of the Isle Aux Morts River, Newfoundland; 47°47′00"N, 58°55′00"; UTM zone 21, 356500E, 5291500N; sample BD135-91. Collected by B. Dubé and interpreted by B. Dubé and K. Lauzière.

See GSC 95-23 for interpretation.

GSC 95-22 Sericite
383 ± 4 Ma integrated ^{40}Ar-^{39}Ar

Wt% K= 8.17
K-AR 4410 % Atmos. Ar = 2.5

(AA341) Ages of two heating steps + % gas:
383 ± 1 Ma (62%), 382 ± 1 Ma (33%)
Preferred age: 95% gas plateau age of 383 ± 4 Ma

(11O/10) From a sericite-rich schist.
Derived from the Windowglass Hill Granite southwest coast of Newfoundland. Trench located on top of Windowglass Hill, on the west bank of the Isle Aux Morts River, Newfoundland; 47°44¢00"N, 58°52'00"W; UTM zone 21 352500E, 5288500N; sample BD115-91; Collected by B. Dubé and interpreted by B. Dubé and K. Lauzière.

See GSC 95-23 for interpretation.

GSC 95-23 Sericite
381 ± 3 Ma integrated ^{40}Ar-^{39}Ar

Wt % K = 7.74
K-AR 4409 % Atmos. Ar = 1.4

(AA340) Ages of two heating steps + % gas:
380 ± 1 Ma (53%), 381 ± 1 Ma (42%)
Preferred age: 95% gas plateau age of 381 ± 3 Ma

(11O/10) From a sericite-rich schist.
Derived from the Windowglass Hill Granite, southwest coast of Newfoundland. Trench located on top of Windowglass Hill, on the west bank of the Isle Aux Morts River, Newfoundland; 47°44′00"N, 58°52′00"W; UTM zone 21 352500E, 5288500N; sample BD113-91. Collected by B. Dubé and interpreted by B. Dubé and K. Lauzière.

The K-Ar samples GSC 95-20 and GSC 95-21 are from a muscovite-rich schist located within a trench along the H Brook showing of the Isle aux Morts River. The ^{40}Ar-^{39}Ar samples GSC 95-22 and GSC 95-23 are from a sericite-rich schist located within a trench on top of the Windowglass Hill Granite. The schist is derived from a mylonitized Windowglass Hill Granite (zircon dated at 424 Ma by Dubé et al., in press). Mineralization occurs in stockworks of galena-rich quartz veinlets. Several veinlets are perpendicular to both the strong planar S3b fabric as well as to the down dip L3 stretching lineation suggesting emplacement as extension veinlets during the reverse movement along the Cape Ray Fault Zone (Dubé et al., in press). The integrated ^{40}Ar-^{39}Ar and K-Ar results suggest either that the mineralization is the same age and possibly related to the late tectonic Strawberry granite (zircon, 384 ± 2 Ma) (Dubé et al., in press) or that the age of the sericite and muscovite was reset by this younger intrusion located near the dated samples. Results for the integrated ^{40}Ar-^{39}Ar indicate that the initial step of several per cent gas gave the same age as the next two heating steps suggesting no excess argon present. As the integrated age is the same for the two heating steps, this strongly suggest that these ages have not been reset (J.C. Roddick, pers. comm., 1994). However, structural field relationships indicate that the ductile structures host of the mineralization, are crosscut by the Isle aux Morts granite dated zircons at 386 Ma (Dubé et al., in press). Thus, the gold-bearing hosting structures are pre-emplacement of the Strawberry and/or Isle aux Morts intrusions. However, the mineralization could still have been emplaced in already developed older structures. Because of these conflicting relationships there is no unique interpretation of the age of the mineralizing event but to say that the mineralization is post-424 Ma and pre- to syn-384 Ma (Dubé and Lauzière, unpub. data).

REFERENCES

Dubé, B., Dunning, G., Lauzière, K., and Roddick, C.J.
in press: New insights into the Appalachian orogen from geology and geochronology along the Cape Ray Fault Zone, SW Newfoundland; Geological Society of America Bulletin.

APPENDIX

The numbers listed below refer to the individual sample determination numbers, e.g. (GSC) 62-189, published in the Geological Survey of Canada age reports listed below:

	Determinations		*Determinations*
GSC Paper 60-17, Report 1	59-1 to 59-98	GSC Paper 79-2, Report 14	78-1 to 78-230
GSC Paper 61-17, Report 2	60-1 to 60-152	GSC Paper 81-2, Report 15	80-1 to 80-208
GSC Paper 62-17, Report 3	61-1 to 61-204	GSC Paper 82-2, Report 16	81-1 to 81-226
GSC Paper 63-17, Report 4	62-1 to 62-190	GSC Paper 87-2, Report 17	87-1 to 87-245
GSC Paper 64-17, Report 5	63-1 to 63-184	GSC Paper 88-2, Report 18	88-1 to 88-105
GSC Paper 65-17, Report 6	64-1 to 64-165	GSC Paper 89-2, Report 19	89-1 to 89-135
GSC Paper 66-17, Report 7	65-1 to 65-153	GSC Paper 90-2, Report 20	90-1 to 90-113
GSC Paper 67A, Report 8	66-1 to 66-176	GSC Paper 91-2, Report 21	91-1 to 91-187
GSC Paper 69a, Report 9	67-1 to 67-146	GSC Paper 92-2, Report 22	92-1 to 92-100
GSC Paper 71-2, Report 10	70-1 to 70-156	GSC Paper 93-2, Report 23	93-1 to 93-73
GSC Paper 73-2, Report 11	72-1 to 72-163	GSC Current Research 1994-F, Report 24	94-1 to 94-62
GSC Paper 74-2, Report 12	73-1 to 73-198	GSC Current Research 1995-F, Report 25	95-1 to 95-23
GSC Paper 77-2, Report 13	76-1 to 76-248		

GSC Age Determinations Listed by N.T.S. Co-ordinates

1-M	62-189, 190; 63-136, 137; 66-170, 171; 70-145, 146, 147, 152
1-N	65-150; 70-156
2-C	70-155
2-D	59-94, 95, 96, 97, 98; 60-151, 152; 63-182; 65-142, 143; 66-172; 70-153, 154
2-E	62-187, 188; 63-168, 169, 170, 171, 183, 184; 64-159; 65-144, 145, 146, 147, 148, 149; 67-144; 70-151; 78-229, 230
2-F	70-148; 80-206
2-L	72-158, 159
2-M	66-173; 73-192, 193, 194
3-D	63-161
10-N	72-163
11-D	70-122, 123
11-E	66-156, 157, 158; 70-124, 125; 78-209; 87-14
11-F	62-168, 169; 78-211; 80-200; 87-14
11-J	78-212
11-K	66-159, 160, 161; 78-210; 80-199
11-K/10	95-19
11-L	65-133, 134, 135; 66-163; 70-128, 129, 130; 72-124, 125, 126; 76-231, 232, 233, 234, 235, 236, 237, 238, 239
11-N	78-206, 207, 208; 81-206, 207
11-O	61-202; 63-162; 65-138, 139, 140, 141; 66-168
11-O/10	94-57, 58; 95-20, 21, 22, 23
11-P	67-143
12-A	67-142; 70-120, 121; 72-160, 161; 73-197, 198; 81-212, 213, 214, 215, 216, 217
12-A/5	89-128, 129, 130
12-A/11	94-61
12-A/15	94-60
12-B	60-147; 61-199; 62-186; 63-166, 167; 81-218, 219
12-E	65-129; 66-153; 70-102, 103, 104, 105; 72-95
12-H	60-148; 61-203, 204; 70-143, 144, 149
12-I	60-149; 61-200, 201; 64-158; 66-169; 70-150; 72-153, 154, 155, 156, 157; 73-195, 196
12-L	60-133, 134, 143
12-M	78-202, 203, 204, 205
12-O	60-135
12-P	73-191
13-A/3	91-167, 168, 169, 170, 171, 172
13-C	66-167; 67-138
13-D	60-132
13-E	64-160; 70-133; 80-201
13-F	60-145; 67-136, 137
13-H	60-146; 67-141
13-I	70-138, 142; 72-140, 150
13-J	70-134, 135, 136, 137; 72-139; 78-228; 87-1, 2, 3, 4, 5
13-K	60-144; 61-196; 62-183, 184, 185; 63-178, 179; 72-141, 142, 143; 73-168, 169; 76-241, 242, 244, 247, 248; 81-208, 209, 211
13-L	61-197; 62-177; 63-148, 163, 177; 64-157; 65-151; 73-163, 164, 167; 76-240, 245
13-M	63-174; 64-162; 70-131, 132; 73-174; 76-243
13-M/3	87-19
13-M/6	87-6
13-M/11	87-7
13-M/14	87-8
13-N	62-178; 63-172; 73-176, 177, 178, 179, 183, 184; 76-246; 81-210
13-N/6	87-9
13-N/9	87-10
13-O	62-179, 180, 181, 182; 67-133, 134, 135; 70-140, 141; 72-144, 145, 146, 147, 148, 149, 151, 152; 73-180, 181, 185, 186, 187, 188, 189, 190
13-O/13	87-11
14-C	72-138; 73-182

Other publications containing geochronological data generated by the Geochronology Laboratory of the Geological Survey of Canada

Anderson, R.G. and McNicoll, V.J.
1995: A note on U-Pb dating of Middle Jurassic plutonic suites: Cumshewa Head pluton, southeastern Moresby Island, Queen Charlotte Islands, British Columbia; in Current Research 1995-A; Geological Survey of Canada, p. 91-96.

Bostock, H.H. and van Breemen, O.
1994: Ages of detrital and metamorphic zircons and monazites from a pre-Taltson magmatic zone basin at the western margin of Rae Province; Canadian Journal of Earth Sciences, v. 31, p. 1353-1364.

Emslie, R.F., Hamilton, M.A., and Thériault, R.J.
1994: Petrogenesis of a Mid-Proterozoic Anorthosite-Mangerite-Charnockite-Granite (AMCG) Complex: isotopic and chemical evidence form the Nain Plutonic Suite; The Journal of Geology, v. 103, p. 539-558.

Greig, C.J., McNicoll, V.J., Anderson, R.G., Daubeny, P.H., Harakal, J.E., and Runkle, D.
1995: New K-Ar and U-Pb dates for the Cambria Icefield area, northwestern British Columbia; in Current Research 1995-A; Geological Survey of Canada, p. 97-103.

Hamilton, M.A.
1994: Tholeiitic and weakly alkalic basaltic volcanism of the Mugford Group, northern Labrador: preliminary geochemical results; in Current Research 1994-C; Geological Survey of Canada, p. 333-342.

Hanmer, S., Parrish, R.R., Williams, M., and Kopf, C.
1994: Striding-Athabasca mylonite zone: complex Archean deep-crustal deformation in the East Athabasca mylonite triangle, northern Saskatchewan; Canadian Journal of Earth Sciences, v. 31, p. 1287-1300.

Hegner, E., Kroner, A., and Hunt, P.
1994: A precise U-Pb zircon age for the Archaean Pongola Supergroup volcanics in Swaziland; Journal of African Earth Sciences, v. 18, no. 4, p. 339-341.

Henderson, J.R., Kerswill, J.A., Henderson, M.N., Villeneuve, M., Petch, C.A., Dehls, J.F., and O'keefe, M.D.
1995: Geology, geochronology, and metallogeny of High Lake greenstone belt, Archean Slave Structural Province, Northwest Territories; in Current Research 1995-C; Geological Survey of Canada, p. 97-106.

Lynch, G.
1995: Geochemical polarity of the Early Cretaceous Gambier Group, southern Coast Belt, British Columbia; Canadian Journal of Earth Sciences, v. 32, p. 675-685.

McDonough, M.R., McNicoll, V.J., and Schetselaar, E.M.
1995: Age and kinematics of crustal shortening and escape in a two-sided oblique-slip collisional and magmatic orogen, Paleoproterozoic Taltson Magmatic Zone, northeastern Alberta; in 1995 Alberta Basement Transects Workshop, (ed.) G.M. Ross; Lithoprobe Report #47, Lithoprobe Secretariat, University of British Columbia, p. 265-309.

McDonough, M.R., Plint, H.E., McNicoll, V.J., and Grover, T.W.
1994: $^{40}Ar/^{39}Ar$ age constraints on shear zone evolution, southern Taltson Magmatic Zone, northeastern Alberta; in 1994 Alberta Basement Transects Workshop, (ed.) G.M. Ross; Lithoprobe Report #37, Lithoprobe Secretariat, University of British Columbia, p. 254-266.

McNicoll, V.J. and Brown, R.L.
1995: The Monashee décollement at Cariboo Alp, southern flank of the Monashee complex, southeastern British Columbia, Canada; Journal of Structural Geology, v. 17, p. 17-30.

McNicoll, V.J. and McDonough, M.R.
1995: The Waugh Lake basin: a 2.01-1.97 back-arc basin, southern Taltson Magmatic Zone, northeastern Alberta; in 1995 Alberta Basement Transects Workshop, (ed.) G.M. Ross; Lithoprobe Report #47, Lithoprobe Secretariat, University of British Columbia, p. 310-329.

McNicoll, V.J., Harrison, J.C., Trettin, H.P., and Thorsteinsson, R.
1995: Provenance of the Devonian clastic wedge of Arctic Canada: evidence provided by detrital zircon ages; in Stratigraphic Evolution of Foreland Basins, (ed.) S.L. Dorobek and G.M. Ross; Society of Economic Paleontologists and Mineralogists Special Publication 52, p. 77-93.

Murphy, D.C., van der Heyden, P., Parrish, R.R., Klepacki, D.W., McMillan, W., Struik, L.C., and Gabites, J.
1995: New geochronological constraints on Jurassic deformation of the western edge of North America, southeastern Canadian Cordillera; in Jurassic Magmatism and Tectonics of the North American Cordillera, (ed.) D.M. Miller and C. Busby; Boulder, Colorado, Geological Society of America Special Paper 299, p.159-171.

Mustard, P.S., Parrish, R.R., and McNicoll, V.
1995: Provenance of the Upper Cretaceous Nanaimo Group, British Columbia: evidence from U-Pb analyses of detrital zircons; in Stratigraphic Developments in Foreland Basins, (ed.) S.L. Dorobek and G.M. Ross; Society of Economic Paleontologists and Mineralogists Special Publication No. 52, p. 65-76.

O'Sullivan, P.B. and Parrish, R.R.
1995: The importance of apatite composition and single-grain ages when interpreting fission data from plutonic rocks: a case study from the Coast Ranges, British Columbia; Earth and Planetary Science Letters, v. 132, p. 213-224.

Percival, J.A., Skulski, T., Lin, S., and Card, K.D.
1995: Granite-greenstone terranes of the northern Goudalie domain, northeastern Superior Province, Quebec; in Current Research 1995-C; Geological Survey of Canada, p. 141-150.

Percival, J.A., Stern, R.A., Skulski, T., Card, K.D., Mortensen, J.K., and Bégin, N.J.
1994: Minto block, Superior province: missing link in deciphering assembly of the craton at 2.7 Ga; Geology, v. 22, p. 839-842.

Plint, H. and Parrish, R.R.
1994: U-Pb geochronometry in the Horseranch Range, northern Omineca Belt, British Columbia, Canada; Canadian Journal of Earth Sciences, v. 31, p. 341-350.

Stern, R.A., Syme, E.C., and Lucas, S.B.
1995: Geochemistry of 1.9 Ga MORB- and OIB-like basalts from the Amisk collage, Flin Flon Belt, Canada: evidence for an intra-oceanic origin; Geochimica et Cosmochimica Acta, v. 59, no. 15, p. 3131-3154.

Stern, R.A., Syme, E.C., Bailes, A.H., and Lucas, S.B.
1994: Paleoproterozoic (1.90-1.86 Ga) arc volcanism in the Flin Flon Belt, Trans-Hudson Orogen, Canada; Contributions to Mineralogy and Petrology, v. 119, p. 117-141.

Wiedenbeck, M., Allé, P., Corfu, F., Griffin, W.L., Meier, M., Oberli, F., von Quadt, A., Roddick, J.C., and Spiegel, W.
1995: Three natural zircon standards for U-Th-Pb, Lu-Hf, trace element and REE analyses; Geostandards Newsletter, v. 19, no. 1, p. 1-23.

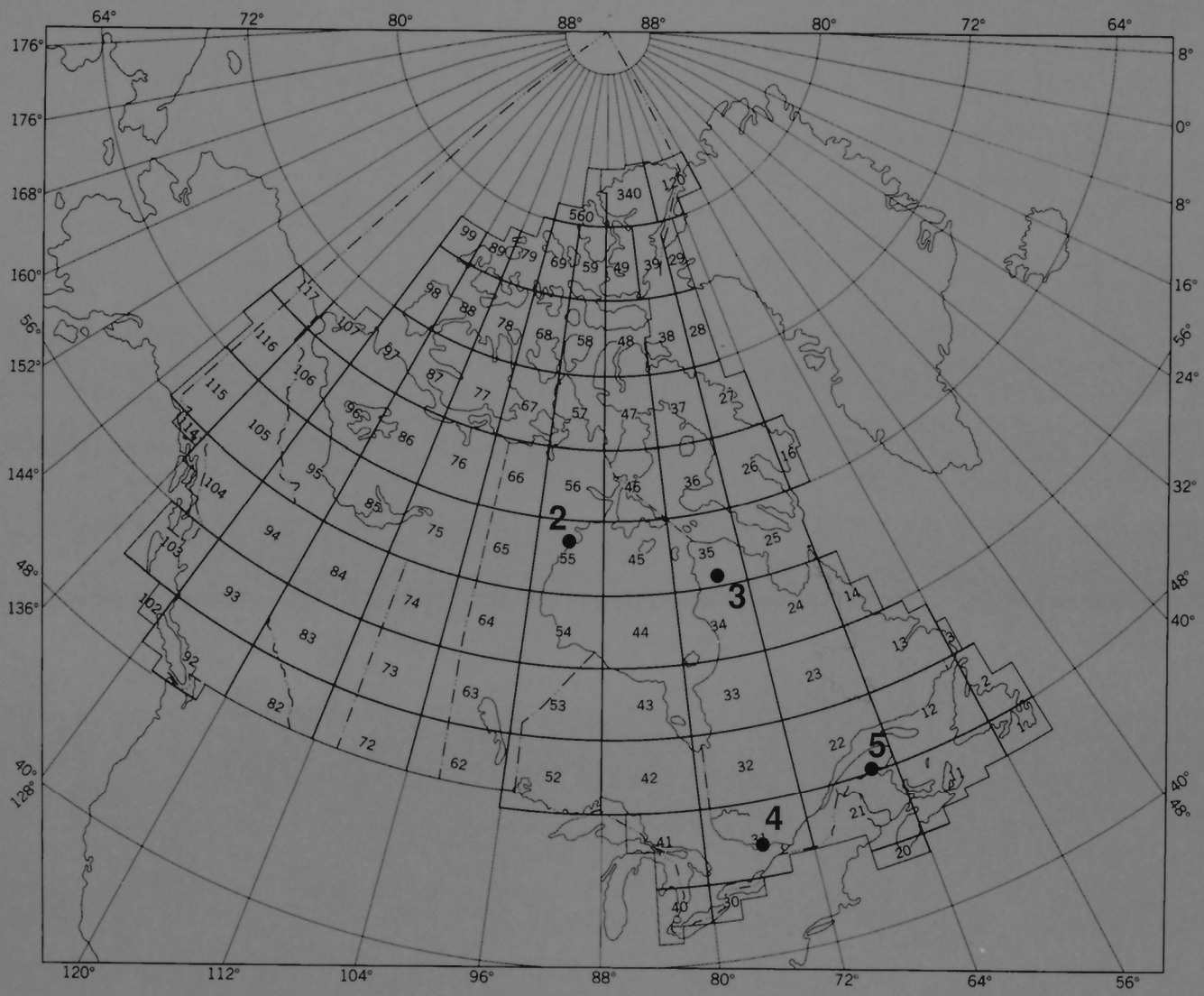

Locations on the map refer to reports in this volume
Les localités indiquées sur la carte correspondent aux rapports contenus dans le présent volume